A study in environmental chemistry: natural and anthropogenic radionuclides in sediment cores from the Norwegian Trench and the Vefsnfjord

by

Lena Helvik

Master of Science Thesis

Department of Chemistry

University of Bergen

Bergen, June 2019

SUMMARY

In this work the anthropogenic radionuclide ^{137}Cs and the naturally occurring radionuclides ^{226}Ra, ^{228}Ra, ^{210}Pb and ^{40}K have been studied in sediment cores from the Norwegian Trench and from the Vefsnfjord in Nordland.

Caesium-137 is a fission product, introduced to the environment by nuclear weapons tests in 1950s and -60s, discharges from reprocessing plants for spent nuclear fuel, and from accidents like the Chernobyl accident in 1986. Levels of ^{137}Cs in Norwegian marine areas are generally low, and the levels are routinely monitored. Investigations in selected Norwegian fjords have, however, shown elevated levels of ^{137}Cs in surface sediments and sediment profiles, compared to adjacent open marine areas. The Vefsnfjord, which is investigated in this work, is one of the fjords in Norway with the highest measured levels of ^{137}Cs. The contamination source is most likely the Chernobyl accident.

Potassium-40 is a naturally occurring radioactive isotope of potassium (isotopic abundance of 0.012%). radium-226 and lead-210 are members of the natural radioactive "uranium series", while radium-228 is member of the natural radioactive "thorium series". All four are found in various amounts in bedrock and the marine environment. However, it is well known that different industries, including the oil and gas industry, also discharge naturally occurring radionuclides to the marine environment.

In this thesis, local and regional variations of ^{137}Cs, ^{226}Ra, ^{228}Ra, ^{210}Pb and ^{40}K in the two study areas have been investigated. Such information is important when monitoring results are to be interpreted, as monitoring results often are thought to represent a large area. Results from analyses of the different radionuclides in sediment cores taken within an area of 30x30 cm were generally in good agreement with regards to activity concentration, both in the Norwegian Trench and in the Vefsnfjord. Some regional variations between the different sampling locations in the Vefsnfjord were, however, found.

The ^{137}Cs in the Norwegian Trench ranged from below the detection limit (<0.4) to 3.0 Bq/kg dry weight, while the levels found in the Vefsnfjord were in the range of 13 to 432 Bq/kg dry weight. The levels found in the Vefsnfjord show that still over 30 years after the Chernobyl accident, elevated levels of ^{137}Cs are found in sediments in the fjord. Levels of the other radionuclides studied in this work are comparable for the two study areas. Radium levels in sediment cores from the Norwegian Trench and the Vefnfjord ranged from 23 to 53

Bq/ kg d.w. and from 28 to 79 Bq/kg d.w. for ^{226}Ra and ^{228}Ra, respectively. ^{210}Pb levels ranged from 24 to 279 Bq/kg d.w., and ^{40}K levels ranged from 581 to 949 Bq/kg d.w.

The radionuclide levels found in the present study are generally in good agreement with results on radionuclide levels in adjacent areas. There are, however, few studies on radioactivity levels in the Vefsnfjord, and generally few studies on naturally occurring radionuclides in sediments to compare with. Also, often only surface samples have been analyzed, and thus comparison with sediment profiles could not be done.

All sediment cores were dated using the CRS ^{210}Pb-dating method, and sedimentation rates were determined using both ^{210}Pb and ^{137}Cs. The sedimentation rates found in the Norwegian Trench ranged from 0.07 to 0.12 cm/year, and the sedimentation rates from the Vefsnfjord ranged from 0.17 to 0.27 cm/year. The results are in fairly good agreement with results found in the literature.

Four cores from the Vefsnfjord were analysed for total organic carbon (TOC), total carbon (TC), and total sulphur (TS) (LECO analyses) at the Norwegian Geological Surveys (NGU). The content of TS ranged from 0.10 to 0.49 %, the content of TC ranged from 1.4 to 2.9 %, and the TOC content ranged from 1.0 to 2.0 %.

SAMMENDRAG

I denne masteroppgaven har den antropogene radionukliden ^{137}Cs og de naturlig forekomne radionuklidene ^{226}Ra, ^{228}Ra, ^{210}Pb og ^{40}K blitt studert i sedimentkjerner tatt fra Norskerenna og fra Vefsnfjorden i Nordland.

Caesium-137 er et fisjonsprodukt som har blitt introdusert til miljøet gjennom prøvesprengninger av kjernevåpen på 50- og 60-tallet, utslipp fra gjenvinningsstasjoner for brukt kjernebrensel, og ulykker som Tsjernobyl-ulykken i 1986. Nivåene av ^{137}Cs i norske havområder er for det meste lave, og blir rutinemessig kontrollert. Studier av noen fjorder i Norge har imidlertid avdekket forhøyede verdier av ^{137}Cs i sedimenter, både i overflateprøver og i kjerneprøver, sammenlignet med nærliggende havområder. Vefsnfjorden, som det er fokus på i denne oppgaven, er en av fjordene i Norge hvor det er målt høyest nivåer av ^{137}Cs. Tsjernobyl-ulykken er mest sannsynlig kilden til denne forurensningen.

Kalium-40 er en radioaktiv isotop av kalium, som finnes naturlig i miljøet (omtrent 0.012 % av alt kalium er kalium-40). Radium-226 og bly-210 er et nedbrytningsprodukt av den naturlig forekommende radionukliden uran-238, mens radium-228 er nedbrytningsprodukt av den naturlig forekommende radionukliden thorium-232. Alle finnes de i varierende mengder i berggrunnen, men ulik industri, som olje og gass industri, kan bidra til utslipp av naturlige radionuklider til marine miljø.

I denne oppgaven har lokal og regional variasjon i nivåer av ^{137}Cs ^{226}Ra, ^{228}Ra, ^{210}Pb og ^{40}K blitt undersøkt i Norskerenna og Vefsnfjorden. Informasjon om nivåene er viktig når overvåkningsresultater skal tolkes, da overvåkningsdata ofte antas å representere et større område. Nivåer av de ulike radionuklidene i sedimentkjerner tatt innenfor et område på 30x30 cm, stemte i de fleste tilfeller godt overens, både i Norskerenna og i Vefsnfjorden. Det ble imidlertid funnet noen variasjoner i nivåer av radionuklider mellom de ulike prøvetakningsstedene i Vefsnfjorden.

^{137}Cs nivåene i Norskerenna ble målt fra under deteksjonsgrensen (<0,4) til 3,0 Bq/kg tørrvekt, mens nivåene i Vefsnfjorden ble målt fra 13 til 432 Bq/kg tørrvekt. Nivåene i Vefsnfjorden viser at det fremdeles, over 30 år etter Tsjernobyl-ulykken, fins forhøyede verdier av ^{137}Cs i fjorden. Nivåer av de andre radionuklidene undersøkt i denne oppgaven var sammenlignbare for Norskerenna og Vefsnfjorden. Radiumnivåene målt i kjerneprøver fra Norskerenna og Vefsnfjorden varierte fra 23 til 53 Bq/kg tørrvekt, og fra 28 til 79 Bq/kg

tørrvekt, for henholdsvis ^{226}Ra og ^{228}Ra. ^{210}Pb-nivåene varierte fra 24 til 279 Bq/kg tørrvekt, og ^{40}K-nivåene fra 581 til 949 Bq/kg tørrvekt.

Nivåer av radionuklider i sedimentkjerner funnet i denne oppgaven stemmer generelt godt overens med resultater som er funnet fra tidligere studier på samme radionuklider, i samme, og nærliggende områder. Det er imidlertid få publiserte studier om radioaktivitet i Vefsnfjorden, og generelt få publiserte studier om naturlige radionuklider i sedimenter, å sammenligne resultatene i denne oppgaven med.

Alle sedimentkjernene i denne oppgaven ble datert ved hjelp av CRS ^{210}Pb-dateringsmetoden, i tillegg til at det ble bestemt sedimentasjonsrater ved hjelp av ^{210}Pb og ^{137}Cs. Sedimentasjonsratene fra kjernene i Norskerenna varierte fra 0,07 til 0,12 cm/år, mens sedimentasjonsratene fra kjernene i Vefsnfjorden varierte fra 0,17 til 0,27 cm/år. Resultatene funnet i denne oppgaven stemmer relativt godt overens med tidligere resultater fra litteraturen.

Fire kjerner fra Vefsnfjorden ble analysert for totalt organisk karbon (TOC), totalt karbon (TC), og totalt svovel (TS) (LECO-analyser) ved Norges Geologiske Undersøkelse (NGU). Innholdet av TS varierte fra 0,10 til 0,49%, innholdet av TC varierte fra 1,4 til 2,9% og TOC innholdet varierte fra 1,0 til 2,0%.

ACKNOWLEDGMENTS

This master thesis has been carried out as a collaboration between the University of Bergen (UiB), the Institute of Marine Research (IMR) and the Norwegian Radiation and Nuclear Safety Authority (DSA). I have been given exciting and unforgettable opportunities like taking a course in experimental radioecology at the Norwegian University of Life Sciences (NMBU) during the spring of 2018, participating on a research cruise with R/V "Kristine Bonnevie" in October 2018, and working with a very interesting project. For this I am very grateful!

I would like to thank my supervisors Dr. Hilde Elise Heldal (IMR), Associate Professor Svein Are Mjøs (UiB) and Dr. Hallvard Haanes (DSA). Thank you for excellent supervision throughout the project! Also, thanks once more to Hilde Elise, for always having time for me, for your good advices, comments and feedback. It has been truly invaluable!

All the analyses have been carried out at the Chemistry laboratory at IMR. I would like to thank the staff at the Chemistry laboratory, especially Andrey Volynkin and Penny Lee Liebig for all help and support. I am grateful to Penny for assisting me with sample preparation, and to Andrey for assisting with sample preparation, sample measurements, and analyses of the results. Thank you for always having time for me, and for patiently answering my numerous questions.

I would also like to thank Jon Rønning (IMR) for collecting the sediment samples from the Norwegian Trench in November 2017, Kjell Bakkeplass (IMR) for making maps, and Harald Fitje (IMR) for helping me make the polycarbonate discs for all my samples. Thanks are also due to Runhild Gjelsvik (DSA) for providing data on ^{137}Cs in soils, and Dr. Henning Jensen and the staff at NGU for performing LECO analyses on samples from the Vefsnfjord.

Last but not least, a big thanks to my family and friends, both for grammar-help, for your love and support, and for cheering me on during the project. I am so grateful to all of you.

Bergen, June 2019

Lena Helvik

CONTENTS

LIST OF ABBREVIATIONS & EXPLANATIONS

Activity concentration – also called specific activity, is the activity per quantity of a radionuclide (e.g. Bq/kg)

^{241}Am – Americium-241

Bq – Becquerel – Unit used to describe the activity of a radionuclide and indicates the number of disintegrations per second

^{40}Ca – Calcium-40

CIC – Constant Initial Concentration (method used to date sediment samples)

^{60}Co – Cobalt-60

CRS – Constant Rate of Supply (method used to date sediment samples)

$^{(134, 137)}$Cs – Caesium-134, -137

DSA – Norwegian Radiation and Nuclear Safety Authority (former NRPA - Norwegian Radiation Protection Authority)

D.w. – Dry weight

FWHM – Full Width Half Maximum

GBq – Giga becquerel – 10^9 becquerel

HPGe – High Purity Germanium

^{131}I – Iodine-131

IAEA – International Atomic Energy Agency

IMR – Institute of Marine Research

^{40}K – Potassium-40

K_d – Distribution coefficient

Kg – kilogram

MAREANO – Marine area database for Norwegian waters

mSv – Millisievert – Unit used to describe biological effect of ionizing radiation

NKS – Nordic Committee for Nuclear Safety Research

NPL – National Physical Laboratory

NSTF – North Sea Task Force

^{210}Pb – Lead-210

PBq – Peta becquerel = 10^{15} becquerel

^{210}Po – Polonium-210

$^{(238, 239, 240)}$Pu – Plutonium-238, -239, -240

PVC – Poly Vinyl Chloride

^{226}Ra – Radium-226

^{228}Ra – Radium-228

RAME – Radioactivity in the Marine Environment

^{222}Rn – Radon-222

^{90}Sr – Strontium-90

TBq – Tera becquerel = 10^{12} Bq

^{99}Tc – Techenetium-99

TC – Total Carbon

^{232}Th – Thorium-232

TOC – Total Organic Carbon

TS – Total Sulphur

$^{(235, 238)}$U – Uranium-235, -238

1. INTRODUCTION

1.1. Background and main objectives of the thesis

Radioactive contamination has been present in the marine environment for more than 70 years (chapter 2.2). The Institute of Marine Research (IMR) and the Norwegian Radiation and Nuclear Safety Authority (DSA) have monitored radioactive contamination in the Norwegian sea areas since the beginning of the 1990s. The purpose of the monitoring is to document time trends and geographical trends of radioactive contamination in seawater, sediments, fish and other marine species (Skjerdal et al., 2017). The monitoring is important for at least two reasons. Firstly, it is vital to document present levels in different Norwegian areas today, and secondly, to have a benchmark of the levels in case of a future nuclear accident.

The monitoring has shown that fjords in mid-Norway still have elevated levels of radioactive contamination, due to fallout from the Chernobyl accident in 1986 (chapter 2.2.2). One of the affected fjords is the Vefsnfjord (chapter 2.4.2), where levels of ^{137}Cs in surface sediments are two orders of magnitude higher than in open sea areas (e.g. Gäfvert et al, 2012., Skjerdal et al, 2015., Skjerdal et al, 2017). In the Norwegian Trench, which is a depression along the Norwegian coast (chapter 2.4.1), fine-grained sediments from the whole North Sea area settle. Therefore, the Norwegian Trench can act as a sink for radioactive contamination from sources close to the North Sea, like Sellafield and La Hauge (e.g. Dowdall & Lepland, 2012., NSTF, 1993). This thesis focuses on the two different marine areas; the Norwegian Trench and the Vefsnfjord.

The monitoring tends to focus on anthropogenic radionuclides. However, there are also natural radionuclides in the marine environment (chapter 2.3). Elevated levels of these radionuclides may occur in some areas as a result of e.g. operations by the oil and gas industry (chapter 2.3.2). In this study, the naturally occurring radionuclides ^{226}Ra, ^{228}Ra, ^{210}Pb, as well as ^{40}K will be investigated. ^{210}Pb and ^{226}Ra results will also be used to date the sediment cores (chapter 2.6). During the last years, the analytical methods for analysing these radionuclides have been improved at IMR.

Within the monitoring program (RAME), surface-samples are often the only sediment samples taken, thus no information on the vertical distribution is obtained. When sediment cores are collected, it is common to collect only one single core within a large area. Few studies investigate local variations within an area. To assume a homogenous distribution if there is none, will lead to inaccurate estimates of the radioactive content in an area. Also, in

case of a sudden nuclear accident, it is essential to establish methods on how to take representative samples, about sample preparation, and how to present the results.

The main objectives of this thesis are:

- Study local variations of ^{137}Cs, ^{226}Ra, ^{228}Ra, ^{210}Pb and ^{40}K within a box corer (30*30*40 cm) in samples collected from the Norwegian Trench and the Vefsnfjord (Figure 3.1).
- Study regional variations of ^{137}Cs, ^{226}Ra, ^{228}Ra, ^{210}Pb and ^{40}K in four different locations in a gradient from the outermost to the innermost in the Vefsnfjord (Figure 3.3).

2. THEORY

2.1. The studied radionuclides

2.1.1. Caesium-137

Caesium is an alkali metal with atomic number 55. The element has similar physical and chemical properties as the other alkali metals. It has oxidation number +1 in chemical compounds, and is present as cations (Cs^+) in water solutions (Kofstad & Pedersen, 2018).

There are several artificially made radioactive isotopes of caesium, among them ^{137}Cs. ^{137}Cs is a fission product from ^{235}U and ^{239}Pu and has a half-life of 30.08 years (Dreher et al., 2015). ^{134}Cs is another important radioactive isotope of caesium. It has a half-life of 2.06 years (Dreher et al., 2015), and has, along with ^{137}Cs, been among the main radioisotopes responsible for radiation exposure in humans after the Chernobyl accident (OECD, 2002).

As a positively charged ion, caesium tends to bind to particles and sediments, especially clay and organic colloids. The surface of small soil particles most often has a negative charge which make them attract positively charged ions. To what extent this happens, depends on the properties of the sediment and the chemical element. Changes in pH, temperature or salinity in the environment can cause remobilisation of caesium, e.g. from the sediments to seawater (chapter 2.2.4) (Harbitz & Skuterud, 1999).

Physical, geochemical and biological processes influence on the behaviour, transport and fate of radionuclides in the marine environment. Parameters describing these processes are used in models that assess the impact of radionuclide discharges. The distribution coefficient (K_d) (equation 1) is such a parameter. It describes the relationship between radionuclide concentration in solid phase or sediments, and in seawater or freshwater, and can give information on whether a certain radionuclide is mobile, or retained in sediments (IAEA, 2004). The higher the K_d, the more of the radionuclide will be found in the sediments relative to the water masses (Rudjord et al., 1999). In Table 1, recommended K_d values from IAEA (2004) of Cs, Ra and Pb is listed.

$$K_d = \frac{Concentration\ in\ sediments\ \left(\frac{kg}{kg}\text{or}\frac{Bq}{kg\ d.w.}\right)}{Concentration\ in\ water\ \left(\frac{kg}{kg}\text{or}\frac{Bq}{kg}\right)} \quad (1)$$

Table 1: K_d-values obtained from IAEA, 2014.

	K_d- values		
Radionuclide	**Open ocean**	**Coastal and continental shelf environments**	**Bottom sediments consisting of pelagic clay**
Cs	$2.0*10^3$	$4.0*10^3$	$2.0*10^4$
Ra	$4.0*10^3$	$2.0*10^3$	$3.6*10^4$
Pb	$1.7*10^7$	$1.0*10^5$	$2.0*10^7$

The K_d values indicate that caesium is slightly more retained in sediments along the coast and continental shelf areas than in open ocean areas, and that caesium is more retained in clay sediments. However, the K_d values are simplifications of the reality, where equilibrium between the phases is assumed, which may not be the case. Many factors can affect the K_d value, such as different sites and environments. The distribution of radionuclides between water and sediment or soil is a time dependent function, and thus literature data on K_d suffers from large variability (Skipperud et al., 2000). This is because the mobility of a radionuclide in a water-sediment system will depend on the strength of sorption to the sediment, the reversibility of the sorption mechanism and the kinetics of these processes. These factors are again dependent on the physical and chemical properties of the radionuclide, the water and the sediment (Rudjord et al., 1999). Still, the values can work as indicators for whereas the radionuclides are mobile or retained in sediments.

^{137}Cs behaves conservatively in seawater, which means it exists mainly as Cs^+ in the water masses, without undergoing reactions. ^{137}Cs can therefore travel great distances with the currents, before potentially depositing in sediments (Skjerdal et al., 2015).

2.1.2. Radium-226 and Radium-228

Radium is an alkaline earth metal with atomic number 88. It is expected to have similar chemical characteristics as the other elements in the same group in the periodic table, with all the alkaline earth metals only present in nature in +2 oxidation state (IAEA, 2014).

The half-lives of the natural radionuclides ^{226}Ra and ^{228}Ra, are 1600 years and 5.75 years, respectively. ^{226}Ra decays to ^{222}Rn by alpha decay, and ^{228}Ra decays to ^{228}Ac by beta decay (Figure 2.1), and both Ra-isotopes also emits gamma rays when they decay (Dreher et al., 2015). ^{226}Ra and ^{228}Ra are daughters of ^{238}U and ^{232}Th, respectively, which are primordial

radionuclides (IAEA, 2014). ^{238}U and ^{232}Th are found naturally in varying concentrations in bedrock, and through radioactive decay, constantly give rise to ^{226}Ra and ^{228}Ra. The bedrock-composition is affecting the concentration, and levels of radionuclides like ^{226}Ra and ^{228}Ra are usually higher in igneous rocks compared to sedimentary ones, except in shale, deep-sea sediments and phosphate rocks. The high levels in shale is likely due to clay rich material of organic origin, while phosphate rocks of sedimentary origin are known as minerals high in uranium (IAEA, 2014).

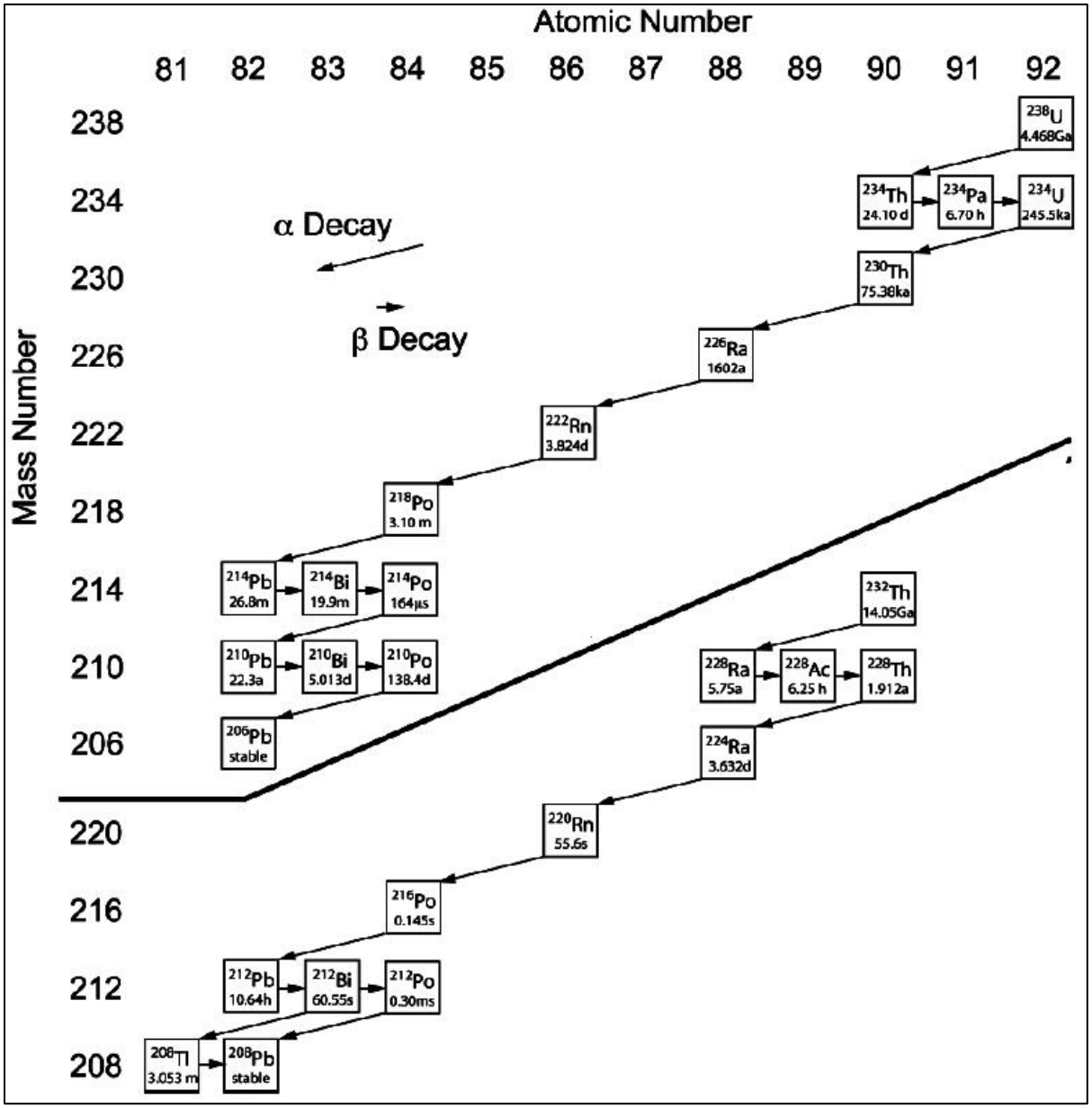

Figure 2.1: The ^{238}U decay series and ^{232}Th decay series. The figure is edited after a figure found in: (IAEA, 2014).

The mobility of radium in waters and sediments can be described by the distribution coefficient (K_d) in equation (1), chapter 2.1.1. Data on K_d values of radium is listed in Table 1. It is important to have in mind there are many factors contributing to K_d. However, earlier studies reviewed in IAEA (2014) do indicate that radium is readily adsorbed to clay, organic material and mineral oxides in soil, especially at near neutral and alkaline pH conditions. For pH values of most natural waters, it will be present primarily as dissolved Ra^{2+}. At very acidic pH values the adsorption were negligible, but increasing with increasing pH (IAEA, 2014).

2.1.3. Lead-210

Lead is found in group IV in the periodic table. ^{210}Pb is a naturally occurring radionuclide, and one of many radioactive isotopes of lead. The nuclide is part of the decay-chain of ^{238}U, has a half-life of 22,3 years, and decays to ^{210}Bi by beta-radiation (Figure 2.1). The nuclide also emits gamma radiation when it decays (Dreher et al, 2015). Lead is a highly toxic element, and it accumulates in organisms. Lead can cause damage to the nervous system, give immunological effects and damage the brain (Strålberg et al., 2003).

In the marine environment, lead is primarily present as dissolved (90%). However, when interacting with particles in the water, it is removed from the water column by adsorption onto these (Strålberg et al., 2003). ^{210}Pb is present in sediments due to continuous decay from ^{226}Ra (Appleby & Oldfield, 1978), and also introduced to the marine environment by atmospheric deposition following decay of ^{222}Rn via short-lived metallic daughters, by input from rivers and additional run-off from terrestrial areas (chapter 2.3.1). When ^{210}Pb enters a lake or an ocean it tends to end up in the sediments over the next few months and becomes permanently fixed on the sediment particles (www.flettresearch.ca). This is also substantiated by the K_d values of lead (Table 1) which indicates that it is highly retained in the seabed.

2.1.4. Potassium-40

Potassium is an alkali metal with atomic number 19. ^{40}K is a radioactive isotope of potassium and is included amongst the primordial radionuclides. It is a constant component of all natural potassium, and makes up approximately 0.0117% of the total amount of potassium (Drether et al., 2015., Strålberg et al., 2003). It is found naturally in the environment, and is responsible for most of the radioactivity in the world's oceans. The average activity of both natural and anthropogenic radionuclides for the world's oceans is 13.6 Bq/kg water, and ^{40}K is

responsible for over 88% of that. However, uptake of potassium is homeostatically regulated in higher organisms, and ^{40}K are therefore relatively independent of occurrence and exposure (Strålberg et al., 2003).

^{40}K has a half-life of $1.248*10^9$ years, and decays by beta minus decay to stable ^{40}Ca, and by electron capture to ^{40}Ar, also emitting gamma radiation (see chapter 2.5.5.) (Dreher et al., 2015).

2.2. Sources of Cs-137 and other anthropogenic radionuclides to the marine environment

2.2.1. Nuclear weapons testing

The first atmospheric nuclear weapons testing took place in 1945, and the tests went on until 1980, with periods of intensive testing (UNCEAR, 2000a). In 1963 USA, Soviet-Union and United Kingdom signed a treaty banning nuclear weapon tests in the atmosphere, in space and in the ocean (Choppin et al., 2003., UNCEAR, 2000). After this, most tests were performed below ground, but France and China continued testing above ground until 1980 (Harbitz & Skuterud, 1999). The nuclear weapons tests introduced ^{137}Cs and other radionuclides to the environment, and they are now present in various amounts all over the globe, both in marine and terrestrial areas. United Nations Scientific Committee on the Effects of Atomic Radiation (UNSCEAR) have reported that the total discharges from the 543 atmospheric nuclear tests were about 948 PBq ^{137}Cs, 622 PBq ^{90}Sr and 186 000 PBq ^{3}H, as well as discharges from several other radionuclides (UNSCEAR, 2000a). At the Novaya Zemlya test site in the Russian Artic, 130 nuclear weapons tests were carried out between 1955-1990, most of them high in the atmosphere. The nuclear weapons testing caused radioactive contamination to spread, and precipitate both locally and far away from the source. The deposition was mostly wet, and followed precipitation, resulting in the west-coast of Norway and mid-Norway being most affected (Harbitz & Skuterud, 1999).

2.2.2. The Chernobyl accident

The accident that occurred 26 April 1986 at the Chernobyl nuclear power plant in Ukraine was the most severe in the history of nuclear industry. The emissions from the accident contained many different radionuclides. The radiation exposure was initially due to ^{131}I and

short-lived radionuclides, and subsequently to ^{134}Cs and ^{137}Cs, both from external exposure and from consumption of contaminated foods and milk. The estimated release was about 1760 PBq ^{131}I, 85 PBq ^{137}Cs and 54 PBq ^{134}Cs (OECD, 2002., UNSCEAR, 2000b).

The release of radionuclides from the reactor were in form of gases, aerosols and particles. While heavier particles deposited locally, lighter ones spread over great distances. Weather conditions like wind and rainfall carried and deposited radionuclides across Europe (Figure 2.2) (Harbitz & Skuterud, 1999). Norway was one of the countries outside the former Soviet Union that received the highest levels of nuclear fallout. Especially mountainous areas in southern Norway and the central Norwegian counties were affected (Figure 2.2) (NRPA, 2006).

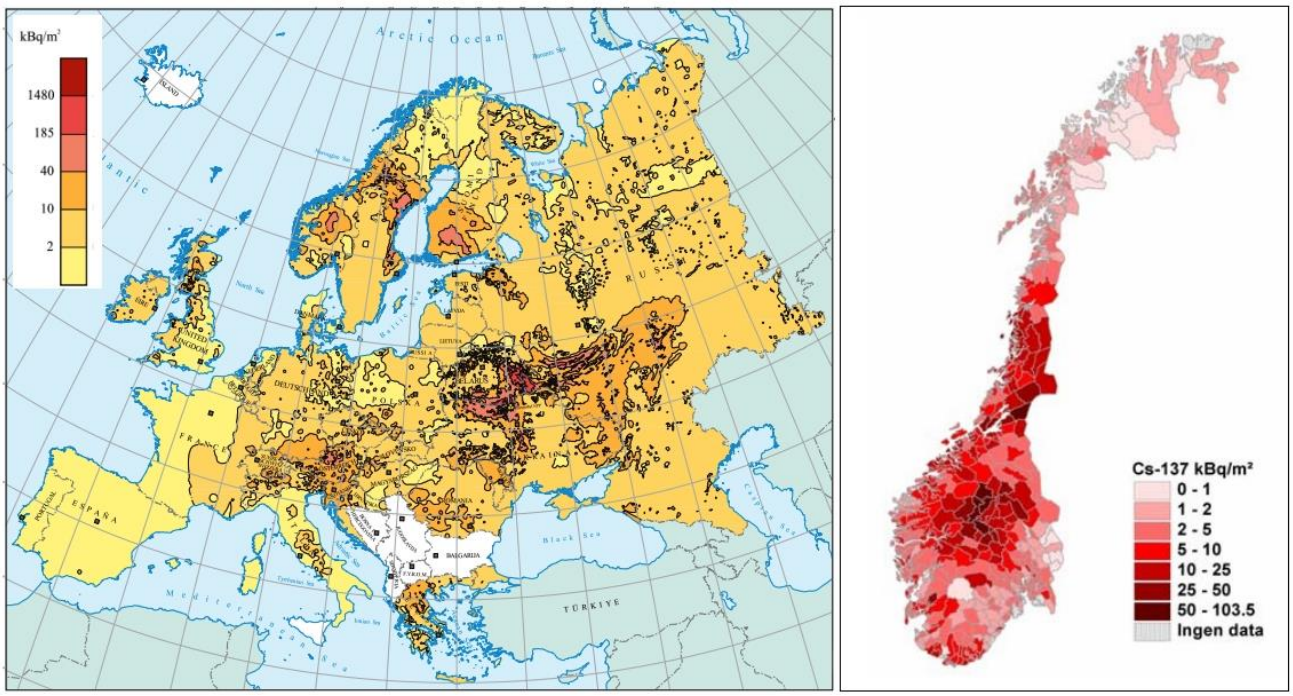

Figure 2.2: Left: the activity concentration of ^{137}Cs (kBq/m^3) in surface ground after the Chernobyl accident (originating from the Chernobyl accident and from nuclear weapons testing) (OECD, 2002). Right: the activity concentrations of ^{137}Cs (kBq/m^3) in soil in Norway after the Chernobyl accident is presented (NRPA, 2006).

Among the main radionuclides deposited in Norway after the accident were ^{134}Cs and ^{137}Cs (Kinn & Gjelsvik, 2017). While ^{134}Cs accounted for about 36 % of the total fallout of caesium at the time of the accident, this number had fallen below 1 % after 1999 due to radioactive decay. It is now an insignificant contribution to the dose compared to ^{137}Cs (Thørring et al., 2014). Because of ^{137}Cs having a much longer half-life, it is still present in the environment today (e.g. Kinn & Gjelsvik, 2017., Skjerdal et al., 2017). ^{137}Cs originally

deposited in the terrestrial environment is introduced to the marine environment by run-off (chapter 2.2.4) (Skjerdal et al., 2017).

2.2.3. Discharges from reprocessing plants

Sellafield

Sellafield is a reprocessing plant for spent nuclear fuel located at the northwest coast of England, and it has been responsible for discharges of various radionuclides (e.g. ^{137}Cs, ^{134}Cs, ^{99}Tc, ^{90}Sr and Pu isotopes) since it started operating in the 1950s (Liland et al., 2012., UNSCEAR, 2000a., Vintró et al., 2000). The discharges of ^{137}Cs from Sellafield were greatest in the time period 1974-1983, when the annual discharges in liquid effluents were in the range of 1000-5000 TBq (with a maximum discharge of 5230 TBq in 1975) (UNSCEAR, 2000a). The discharges have been significantly reduced since 1985 (UNSCEAR, 2000a). Discharges of ^{134}Cs were lower, with a maximum discharge of about 1100 TBq in 1974-1975 (Figure 2.3) (Vintró et al., 2000).

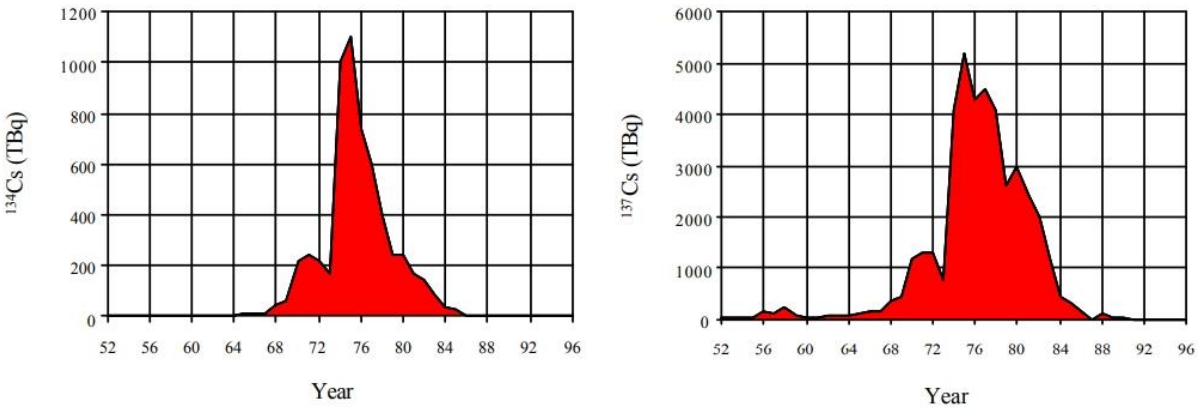

Figure 2.3: Discharges of ^{134}Cs and ^{137}Cs from Sellafield reprocessing plant in the time period 1952-1994 (Grey et al., 1995., found in: Vintró et al., 2000).

La Hague

The reprocessing plant at Cap de la Hague in France has since the start in 1966 reprocessed spent nuclear fuel from nuclear powerplants in France, Germany and other countries (Schneider & Marignac, 2008). The reprocessing plant has discharged radionuclides like ^{129}I, ^{90}Sr, ^{109}Ru and ^{137}Cs (UNSCEAR,2000a). The discharge of ^{137}Cs to the marine environment from Cap de la Hague plant peaked in 1971 with a release of 243 TBq and have decreased by

an order or two of magnitude since (UNSCEAR, 2000a). The radionuclides are discharged into the English Channel, and can from there be carried further away to the North Sea and Norwegian Sea by ocean currents (chapter 2.4.1 (sea currents)).

Other reprocessing plants

In Scotland, the Dounreay recycling plant has contributed to discharges to the marine environment. It ended its activities in 1996 (Liland et al., 2012). In Russia reprocessing plants like Mayak, Tomsk and Krasnoyarsk (Figure 2.4) are responsible for discharges to the rivers Ob and Yenisei. (Harbitz & Skuterud, 1999). These rivers end up in the Kara Sea, and the reprocessing plants can therefore also be a potentially source to contamination of the Kara Sea.

2.2.4. Secondary sources

In addition to direct discharges, run-off and remobilization of radionuclides from contaminated areas, both terrestrial and marine, contributes as secondary sources to radioactive pollution (Skjerdal et al., 2017). An example is remobilization of ^{137}Cs from highly contaminated sediment in the Irish Sea (from Sellafield discharges), which is now the dominant source of water contamination of the North Sea (IAEA, 2005). The Baltic Sea is an example where run-off from the terrestrial environment is significant. With regards to ^{137}Cs, the Baltic Sea is one of the most contaminated of the world oceans, mainly due to the Chernobyl accident (chapter 2.2.2). The Baltic Sea received ^{137}Cs both as direct input to the sea, and from continuous run-off from contaminated land areas. Since the Chernobyl accident, the Baltic Sea has been a main source of fresh inflow of ^{137}Cs to the NE Atlantic Ocean (Herrmann et al., 2009., IAEA, 2005).

2.2.5 Potential sources to radioactive contamination

The risk of an accident affecting Norway is considered to be low. But still, many potential sources of radioactive contamination are present, among them accidents at nuclear power plants; accidents concerning nuclear weapons and storing; transport and disposal of radioactive waste (Figure 2.4). An accident involving nuclear material can have serious consequences (DSB, 2014).

There are currently 452 nuclear reactors in operation worldwide, and there are more reactors under construction. They are spread over 31 countries, many of these located in Europe (IAEA PRIS, 2019). Even though accidents can occur, the safety standards for new reactors improve. Many of the reactors running today were built in the 1970-1980, and are often licenced for use up to 25-40 years. Many of these reactors have been approved for further use after safety upgrades and technical evaluations (Selnæs et al., 2018).

The Kola peninsula (Figure 2.4) is a storage place for large volumes of spent nuclear fuel, and the radioactive material is often poorly stored (Selnæs et al., 2018). Discharges to the marine environment from these sites is therefore possible by run-off. The former marine base in Andrejeva Bay, sixty kilometres from the Norwegian border, is of most concern to Norwegian authorities. The Norwegian authorities have been working together with Russia since 1997 to improve the conditions at the base, and have since June 2017 been working on transporting radioactive waste to a reprocessing plant in Mayak. The work is estimated to take years, and includes the risk of accidents while it is carried out (Selnæs et al., 2018).

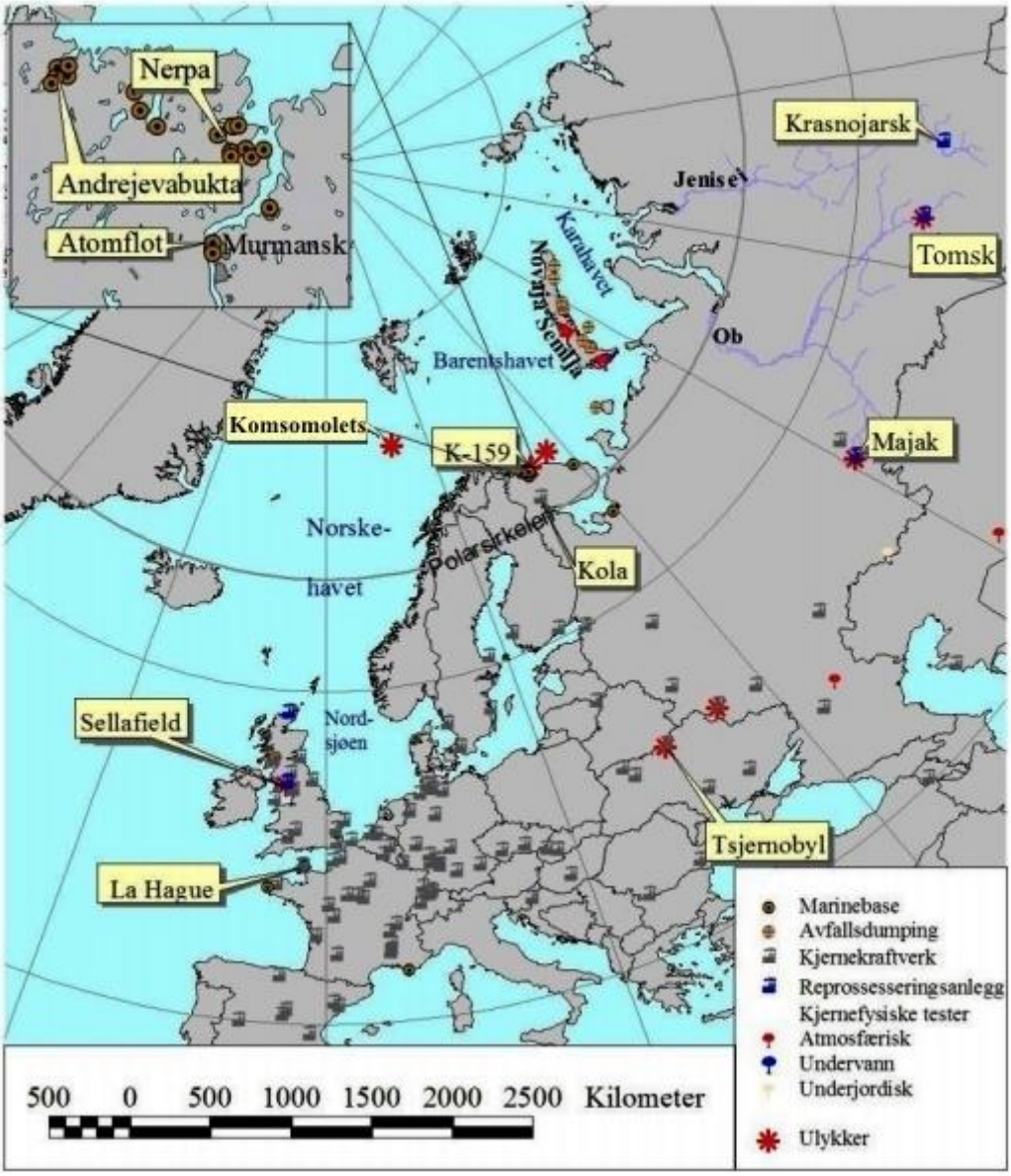

Figure 2.4: Sources and potential sources to radioactive discharges to Norwegian sea areas (NRPA).

Spent nuclear fuel from the former Soviet Union is being transported from Eastern Europe to Murmansk by ships along the Norwegian coast. The Norwegian authorities assume that waste management of radioactive material in Russia will expand, and that transport of the waste along the Norwegian coast will continue (Selnæs et al., 2018). An increase in transport may increase the risk of accidents, and the consequences of such an accident may be severe for the marine environment.

Two sunken submarines containing radioactive materials are resting on the seabed in areas close to Norway; Komsomolets in the Norwegian Sea, and K-159 in the Murmansk Fjord (Figure 2.4). Both wrecks can potentially discharge radioactive materials to the marine

environment. Komsomolets sank in 1989, and lies at a depth of 1680 meters. Earlier investigations from expeditions have detected releases of radionuclides (^{137}Cs, ^{134}Cs, ^{60}Co) from the wreck of Komsomolets. In 2019, it is estimated that remaining activity from the wreck is about 3 PBq, mainly due to ^{137}Cs and ^{90}Sr (DSA, 2019, Heldal et al., 2013). However, modelling studies have shown that any releases from Komsomolets would have little impact on the marine environment, and not contribute to any increase in concentration in fish in the Barents Sea (DSA, 2019). The nuclear submarine K-159 sank in 2003, and rests at 246 meters depth at the entrance of Murmansk Fjord. At a joint Norwegian-Russian expedition to the wreck in 2014 it was not detected any leakage of radioactive material, based on analyses done close to, and in the area of the submarine. However, it was revealed that the submarine had several damages (NRPA, 2018). At the time of the expedition, the total radioactive inventory was estimated at 2.6 PBq, mainly due to ^{137}Cs and ^{90}Sr (NRPA, 2018). Because K-159 lays at only 246 meters depth, the consequences of a radioactive release would be more severe than with Komsomolets. Studies have shown that a potential release from K-159 would increase the levels of ^{137}Cs in cod of above 100 times the present levels in the eastern Barents Sea. However, the levels would still be beneath the safety regulation levels of ^{137}Cs in fish of 600 Bq/kg (Heldal et al, 2013).

A large volume of radioactive waste is dumped in Artic sea areas. Dumping nuclear waste has earlier been an internationally accepted method of disposing radioactive waste. Most countries stopped this practice in 1985, but the former Soviet Union, and later Russia, continued the dumping in the Kara and Barents Seas until 1992. Dumped items includes 19 ships loaded with solid radioactive waste, and over 17.000 containers filled with radioactive waste (NRPA, 2012). The dumped waste is a potential source to radioactive contamination in the northern areas. Three Norwegian-Russian missions to the dumping sites in the Kara Sea took place in the early 1990s, concluding that the contamination in the area at the time was low, but that there was risk of future contamination (NRPA, 2012). Baxter et al. (1998) have modelled dose-estimates to humans from sea-food consumption from seafood harvested in the Artic Sea areas after a hypothetical release. The study reveals that doses from a hypothetical instantaneous release of 1 PBq ^{137}Cs from four dump sites in the Kara Sea, including Stepovogo Fjord (in Novaya Zemlya), would be negligible on global and regional scales. However, the study also concluded that potential individual doses could exceed the annual limit recommended for the public (1 mSv/year) on a local scale, but concluded that the scale impacts were unrealistic, as the fjords in question were uninhabited (Baxter et al., 1998).

Another potential threat considering radioactive contamination is terror. Since the millennium there has been an increasing concerning international terror. Terror organizations with great resources have arisen. The risk of terror has also changed. There has in the last years been increased focus on the risk of nuclear material getting lost and end up in the "wrong hands" and used in terror actions (Selnæs et al., 2018).

2.3. Important sources to naturally occurring radionuclides in the marine environment

Naturally occurring radionuclides are often present in greater amounts in the environment compared to the anthropogenic, and is generally accountable for most of the radiation exposure. When assessing naturally occurring radionuclides, the terms NORM and TENORM are frequently used in literature, being short for "Naturally Occurring Radioactive Material" and "Technologically Enhanced Naturally Occurring Radioactive Material" (US EPA, 2018). The first one includes, as the name imply, the radioactive material that occurs naturally in the environment, being the primordial radionuclides and its decay products. The latter one, is defined as NORM that is being exposed or concentrated in the environment as a result of human activities. The activities include different types of industry (US EPA, 2018). In chapter 2.3.2 and 2.3.3 oil and gas industry, as well as some other industries, are discussed.

2.3.1. The seafloor and run-off from terrestrial areas

^{226}Ra and ^{210}Pb, and ^{228}Ra, are decay products of ^{238}U and ^{232}Th, respectively (Figure 2.1). ^{238}U and ^{232}Th originates in the earth's crust, and thus, give continuously rise to the decay-products (chapter 2.1.2) (IAEA, 2014). In Table 2, an overview of total amount of radium, uranium and thorium in the ocean and the earth crust is presented.

Table 2: The total inventory of radium, uranium and thorium in the ocean and in the earth crust (from IAEA,1990., found in Strålberg et al., 2003).

	Ocean	Earth crust (land)	Earth crust (under the ocean)
Uranium	6×10^{19}Bq	5.7×10^{23}Bq	4.4×10^{22}Bq
^{226}Ra	5×10^{18}Bq	5.7×10^{23}Bq	4.4×10^{22}Bq
Thorium	5×10^{15}Bq	6.1×10^{23}Bq	5.1×10^{22}Bq
^{228}Ra	5×10^{15}Bq	6.1×10^{23}Bq	5.1×10^{22}Bq

As the table shows, there is less radium than uranium in the ocean. A reason for this is that ^{230}Th, the parent of ^{226}Ra, is removed from the water column via adsorption to sedimenting particles. Radium is more soluble in water than thorium, and will in turn leak out from the sediments (Strålberg et al., 2003). ^{210}Pb in the ocean comes from atmospheric deposition (chapter 2.6), in addition to decay of ^{226}Ra in the water. On the ocean surface, atmospheric ^{210}Pb is the most important source, while decay of ^{226}Ra is the most important source in the deeper water masses (Strålberg et al., 2003).

An additional source to radium and lead in the marine environment is run-off from terrestrial environment. Radionuclides deposited in the terrestrial environment may be transported to groundwater, lakes and rivers, and from there be transported further, ending up in the sea (IAEA, 2014).

2.3.2. Oil and gas industry

Radium is naturally present in various amounts in bedrock (chapter 2.1.2), but levels can be enhanced due to extraction of oil and gas, and discharged to the marine environment. Radium is more soluble in formation water (which is produced in large volumes in the oil and gas industry) than both uranium and thorium, and will be dissolved into the formation water and transported upwards in the production equipment. Radium has similar chemical properties as barium and strontium, and will therefore precipitate together with these as carbonates and sulphates when pressure and temperature changes in the production equipment. This precipitate is often referred to as scale (Strålberg et al., 2003). The scales tend to be relatively insoluble, thus only releasing the radionuclides slowly into the environment. Studies of scales and sludges in production equipment have shown to contain radionuclide activity concentrations as high as millions of Bq/kg, while in the range of 1000 to 100.000 is more

common (IAEA, 2003). To avoid scale, scale inhibitors may be added. These inhibitors prevent the formation of $BaSO_4$ and other salts, and keeps radium in solution rather than concentrated in solid form. The problem then is that radium and other radioactive elements such as ^{210}Pb and ^{210}Po is pumped directly into the sea. The activity concentration of radium isotopes in produced water is variable, and so are the volumes of produced water discharged from the different installations. Typically, older wells have a higher water to oil ratio (IAEA, 2003). The concentration of radium in produced water is usually low, but because of the large volumes of produced water, discharges can still be an environmental problem. It is also hard to store or treat the waste, because of the large volumes (Gwynn, 2018., IAEA, 2003., Lind, 2018). Annual discharges of radium and produced water from the Norwegian oil and gas industry in the period 2005-2017 is shown in Figure 2.5. In 2017 the reported discharge from the Norwegian oil and gas industry were 389 GBq ^{226}Ra and 360 GBq ^{228}Ra (DSA, in prep).

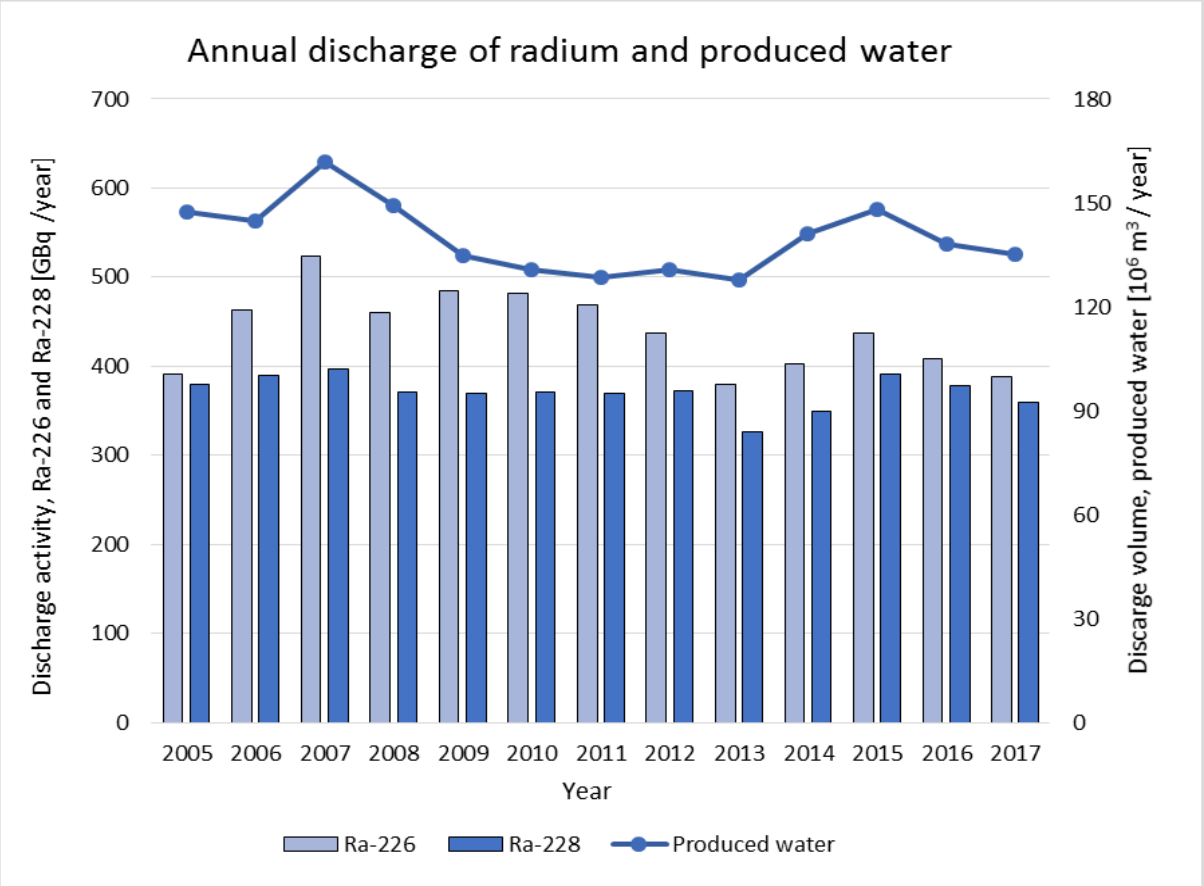

Figure 2.5: Annual discharge of ^{226}Ra and ^{228}Ra to the marine environment via produced water, and the discharged volume of produced water by the Norwegian oil and gas industry from 2005 to 2017 (DSA, in prep).

2.3.3. Other industries/activities

Other industries and activities that contribute to discharges of naturally occurring radionuclides to the marine environment includes the phosphate industry, the mineral sand industry, production of thorium products, ceramic industry, combustion of fossil fuels and mining activities (IAEA, 2003., Strålberg et al., 2003). The phosphate industry is considered to contribute the most. In this industry, phosphorous gypsum (phosphogypsym), a by-product, and containing natural radionuclides, is often discharged into seawater and waters. The activity concentrations of radium in the gypsum range from background to 1700 Bq/kg (IAEA, 2003). The discharges to the North Sea, however, is significantly reduced due to improved treatment of discharged water and changes in storage of the phosphorous gypsum, among other things (Strålberg et al., 2003). In Western Europe, all production facilities are now shut down, so this is no longer a source of radionuclides in most European marine environments (IAEA, 2014).

2.4. The study areas

2.4.1. The Norwegian Trench

The Norwegian Trench is the deepest depression in the North Sea. It is located along the Norwegian coast, from the inner part of Skagerrak and continues for about 900 kilometres until terminating at the shelf edge west of Nordfjord (Figure 3.2). The trench is at its deepest in the easternmost part of Skagerrak, where maximum water depths are about 700 metres. Westwards, the Norwegian Trench gets gradually shallower to about 280 meters water depths west of Stavanger. The northern slope of the trench is generally steeper and more irregular then the southern, and the seafloor is especially irregular along the coast (Ottesen et al., 2000). Grain size analyses of sediments in the Skagerrak showed that they consist of silt and clay in large areas of the Norwegian Trench and along its northern slope. Some of the sediments also contain high amounts of organic material (Bøe, 1993, Ottesen et al., 2000). The Norwegian Trench may serve as a sink for pollution in the North Sea. This is because it is one of the main sedimentation areas of the North Sea, and because of the nature of the different ocean currents (Figure 2.6) (Dowdall & Lepland, 2012., NSTF, 1993).

Sea currents and transport

The north-eastern part of the North Sea is supplied with warm, salty Atlantic water. North of Shetland the water currents follow along the Norwegian Trench. The Atlantic water gives the water a maximum salinity in the western part of the slope, typically above 35.3 ‰. The southern part of the North Sea is shallower, mostly around 50 meters deep, and the salinity is mostly below 35.0‰. The currents in this area are dependent on wind directions and freshwater supplies from rivers like the Rhine and the Elbe, but is mostly following a counter clock wise direction along the Norwegian coast (Albretsen, 2014).

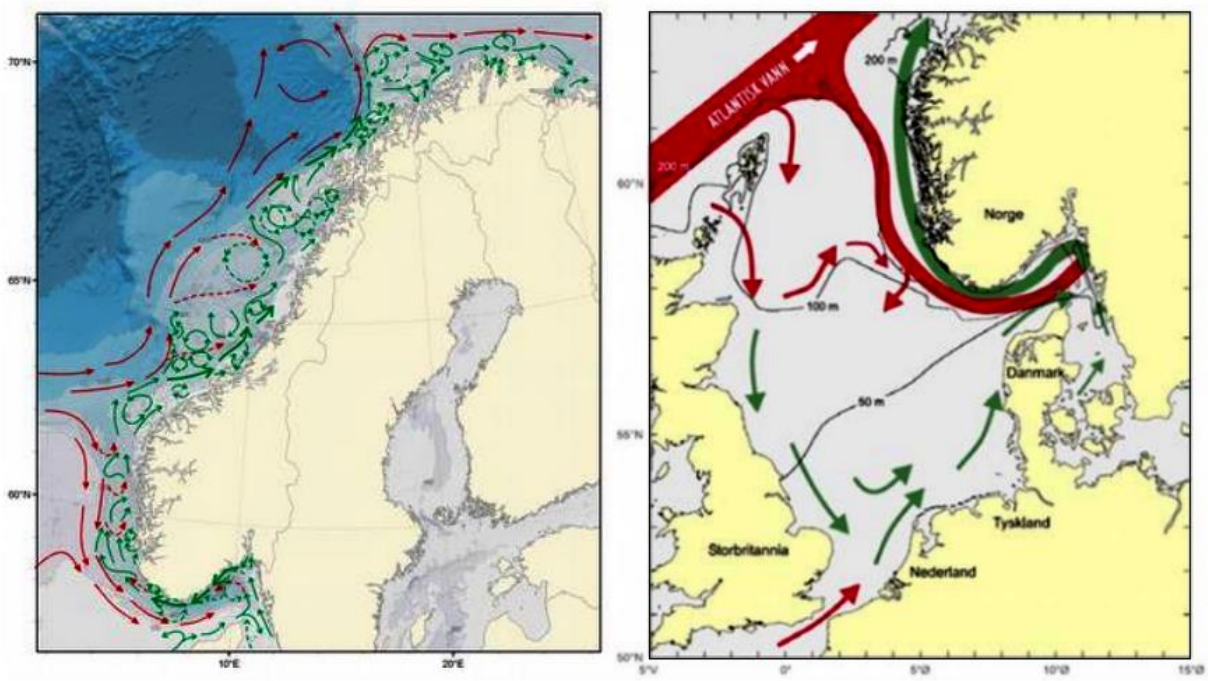

Figure 2.6: Main sea currents along the Norwegian coast. Green arrows denote coastal water and red arrows denote Atlantic water (left: Asplin, 2014, right: Albretsen, 2014).

The Norwegian coastal current originates in the eastern Skagerrak and follows the Norwegian coastline all the way north to the Barents Sea (Figure 2.6). It is supplied with brackish water from the Baltic Sea, and freshwater from all the rivers along the Norwegian coastline, resulting in low salinity. Northwards the salinity increases due to mixing with the Atlantic Sea current. The properties of the coastal current are affected by this, as well as tides and winds (Asplin, 2014).

Sea currents transport radionuclides disposed far away from Norway. Examples are radionuclides originating from atmospheric nuclear weapons testing, and discharges from reprocessing plants, e.g. Sellafield and La Hauge (chapter 2.2.3) (Harbitz & Skuterud, 1999).

Depending on the properties of radionuclides and the sediments, the radionuclides in the sea can be removed from the water column by sedimentation. Radionuclides can be transported from water to sediments by physical (e.g. sedimentation), chemical (e.g. ion exchange or colloid aggregation) and biological processes. Physical remobilization of radionuclides from sediments to water may occur due to flooding, erosion and estuary dredging, and chemical remobilisation from ion-exchange, leaching and dissolution. Biological processes like bioturbation may affect both physical and chemical remobilization of sediments (Rudjord et al., 1999).

Caesium-137 in sediments in the Norwegian Trench

Figure 2.7 shows activity concentration of ^{137}Cs in sediments in the area in 2013 and 2010 (Gäfvert et al., 2012., Skjerdal et al., 2017). It shows that activity concentrations in samples closer to the coastline is generally higher. One reason for this can be run-off from terrestrial environment. Further from the coast, the activity concentrations drop. A reason for this can be that large parts of the North Sea seabed, especially the shallower parts, consists of sand, shell sand and gravel, which do not bind caesium like clay does (Ottersen et al., 2010). In the Skagerrak area, the activity concentrations are generally higher, because the area receives contaminated water from the Baltic Sea.

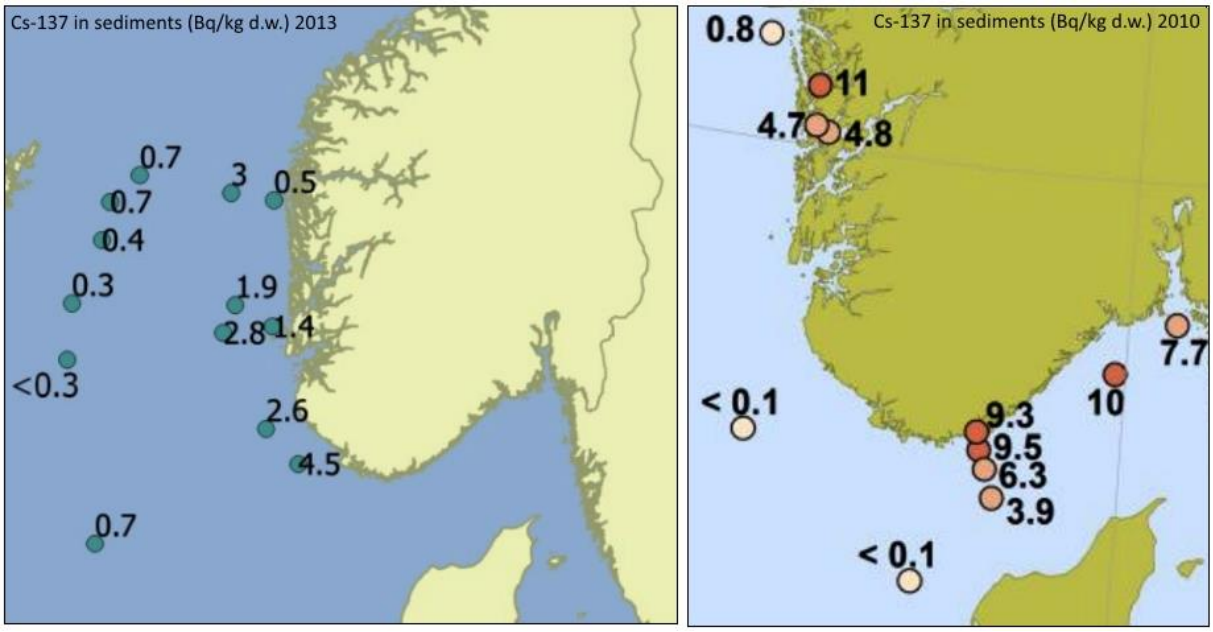

Figure 2.7: Activity concentration of ^{137}Cs (Bq/kg d.w.) in surface sediments from 2013 (left) (Skjerdal et al., 2017) and 2010 (right) (Gäfvert et al., 2012).

Radium-228 and Radium-226 in sediments in the Norwegian Trench

Data on the content of radium isotopes in marine sediments in the Norwegian Trench is sparse. However, some results by Dowdall and Lepland (2012) from the area (Figure 2.8) are presented in Table 3. The paper indicates elevated levels of radium isotopes in upper layers of the cores, but cannot with certainty conclude whether the source may be oil and gas activities in the North Sea, other anthropogenic activity, run-off, concentration of natural background levels, or other natural processes (Dowdall & Lepland, 2012).

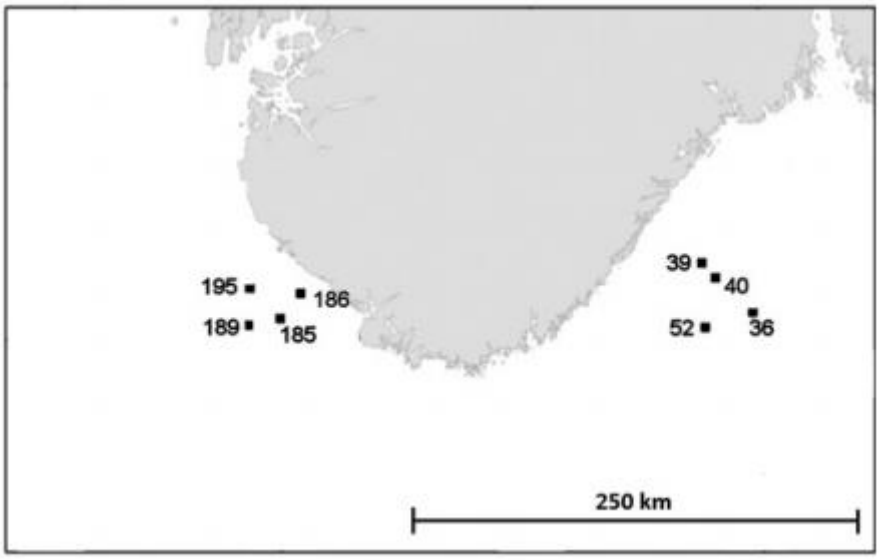

Figure 2.8: Figure obtained from Dowdall and Lepland (2012), showing sampling sites for sediments cores analysed for ^{226}Ra, ^{228}Ra and ^{40}K.

Table 3: Levels of ^{226}Ra, ^{228}Ra and ^{40}K (Bq/kg d.w.) in sediment cores from eight locations in the Norwegian Trench (Figure 2.8) (Dowdall and Lepland, 2012).

	Station 36			**Station 39**		
	^{228}Ra	^{226}Ra	^{40}K	^{228}Ra	^{226}Ra	^{40}K
Mean	38.5	22.1	663.1	40.4	29.3	682.2
Min-max	26.0-67.0	11.9-34.0	593.0-721.0	29.4-109.0	17.9-107.0	518.0-765.0
	Station 40			**Station 52**		
	^{228}Ra	^{226}Ra	^{40}K	^{228}Ra	^{226}Ra	^{40}K
Mean	38.1	35.2	683.5	37.9	27.8	687.8
Min-max	28.9-110.0	17.9-252.0	579.0-756.0	29.0-43.1	16.9-42.0	614.0-754.0
	Station 185			**Station 186**		
	^{228}Ra	^{226}Ra	^{40}K	^{228}Ra	^{226}Ra	^{40}K
Mean	40.5	25.7	730.7	33.4	19.9	654.5
Min-max	23.6-66.0	17.3-32.2	600.0-834.0	24.3-41.2	16.8-22.2	583.0-732.0

	Station 189			Station 195		
	^{228}Ra	^{226}Ra	^{40}K	^{228}Ra	^{226}Ra	^{40}K
Mean	37.1	23.8	641.0	36.2	21.1	644.9
Min-max	31.1-55.6	17.8-35.4	610.0-706.0	29.9-68.9	17.8-36.3	576.0-711.0

2.4.2. The Vefsnfjord

The Vefsnfjord is located in Helgeland in Nordland. It is about 52 kilometres long, and stretches from Tjøtta to Mosjøen (Figure 2.9).

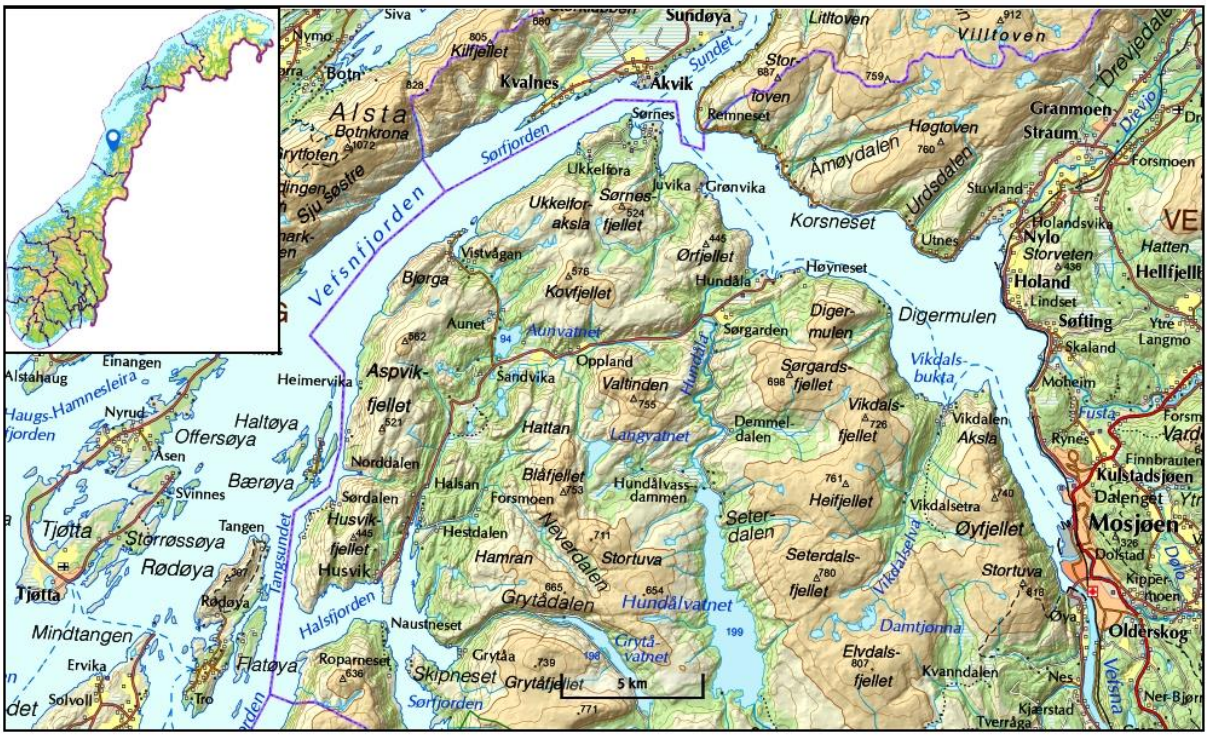

Figure 2.9: The Vefsnfjord is stretching from Tjøtta (lower left corner) to Mosjøen (lower right corner). Screenshot from a map from the Norwegian Mapping Authority (www.norgeskart.no).

The Vefsnfjord reaches a maximum depth of about 450 meters (Haugen et al., 1981). It is considered a "threshold fjord", and the threshold is about 100 meters at the west and east of Mindland (Island in lower left corner in Figure 2.9), and about 50 meters between Dagsvik and Sundhammeren in Sundet (seen in the middle of the Vefsnfjord, Figur 2.9) (Haugen et al., 1981). A threshold affects and limits the water exchange, especially in the deeper parts of the fjord. Freshwater supply to the fjord is dominated by the two rivers Vefsna and Fusta, as well as some smaller rivers; Drevja, Skjerva and Hundåla (Figure 2.9 and 3.3). These rivers have a total catchment area of about 4.900 km^2 (Haugen et al., 1981). Vefsna is responsible for most

of the freshwater supply, with a catchment area of 4119 km^2 (Figure 2.10) (Stenius, 2017). The freshwater supply gives the surface water in the Vedfsnfjord lower and varying salinity (Haugen et al., 1981).

Figure 2.10: The red line indicates the catchment area of Vefsna (blue line to the left), which ends in the Vefsnfjord (in the upper left corner) (Stenius, 2017).

The Vefsnfjord is one of the fjords in Norway with the highest ^{137}Cs levels in sediments (e.g. Skjerdal et al., 2017). Results from the monitoring program RAME show that the activity concentrations vary between in the outer and inner part of the fjord, and the levels are typically higher in the inner part of the fjord (Figure 2.11). The highest level (348 Bq/kg d.w.) was found in 2010 in the inner part of the fjord.

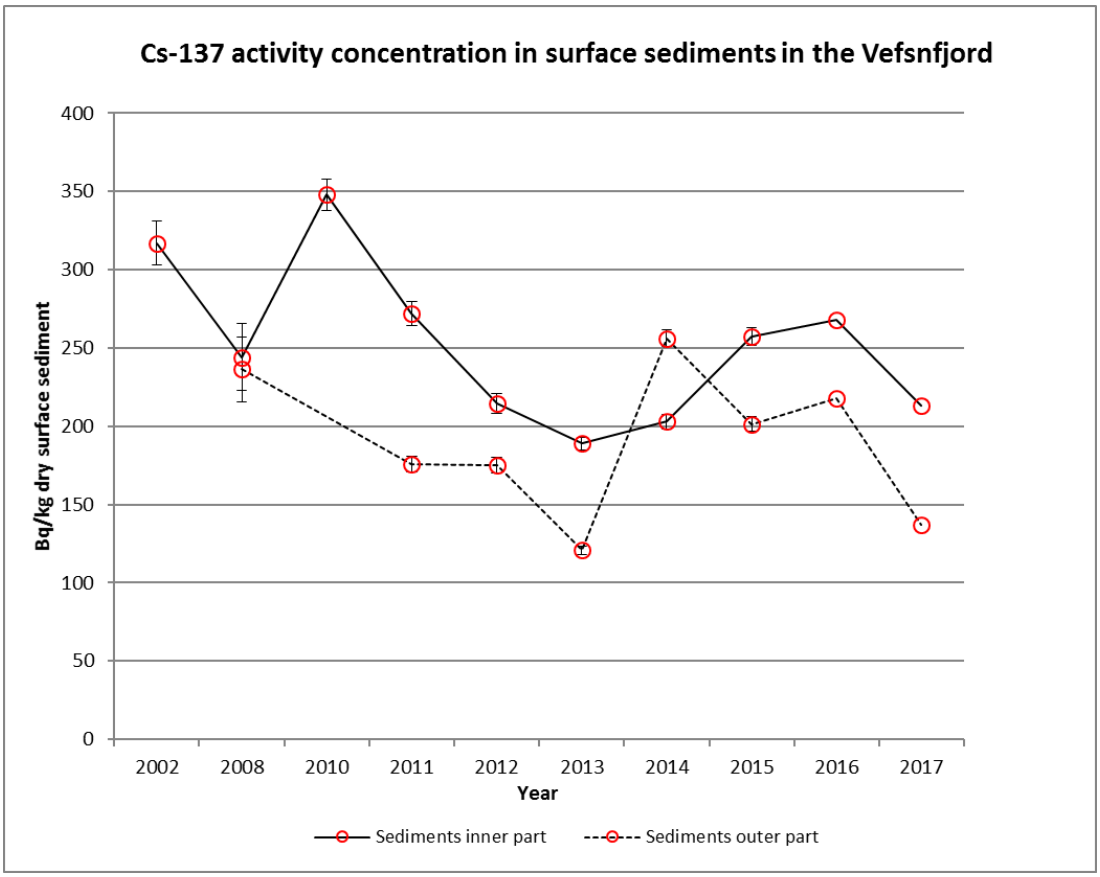

Figure 2.11: Activity concentration of ^{137}Cs (Bq/kg d.w.) in surface sediment (0-2 cm) in the inner and outer part of the Vefsnfjord from 2002-2017 (data compiled from RAME (IMR/DSA)).

The high levels of ^{137}Cs in sediments in the area is due to run-off from land, which is contaminated by the Chernobyl accident (chapter 2.2.2). From Figure 2.12 (Gjelsvik & Steinnes, 2013), one can see that the coastal areas have had a bigger reduction in ^{137}Cs in surface soil than in the inland areas. From a conventional radiological view, one might expect these differences to be caused by differences in precipitation. The paper does, however, point at the chemical composition of the precipitation as a potential important role. Precipitation in coastal zones contains higher concentration of Na^+ and Mg^{2+}, which are likely to compete with Cs^+ in cation exchange in soils (Gjelsvik & Steinnes, 2013). This may contribute to increased runoff of ^{137}Cs to waters and marine areas.

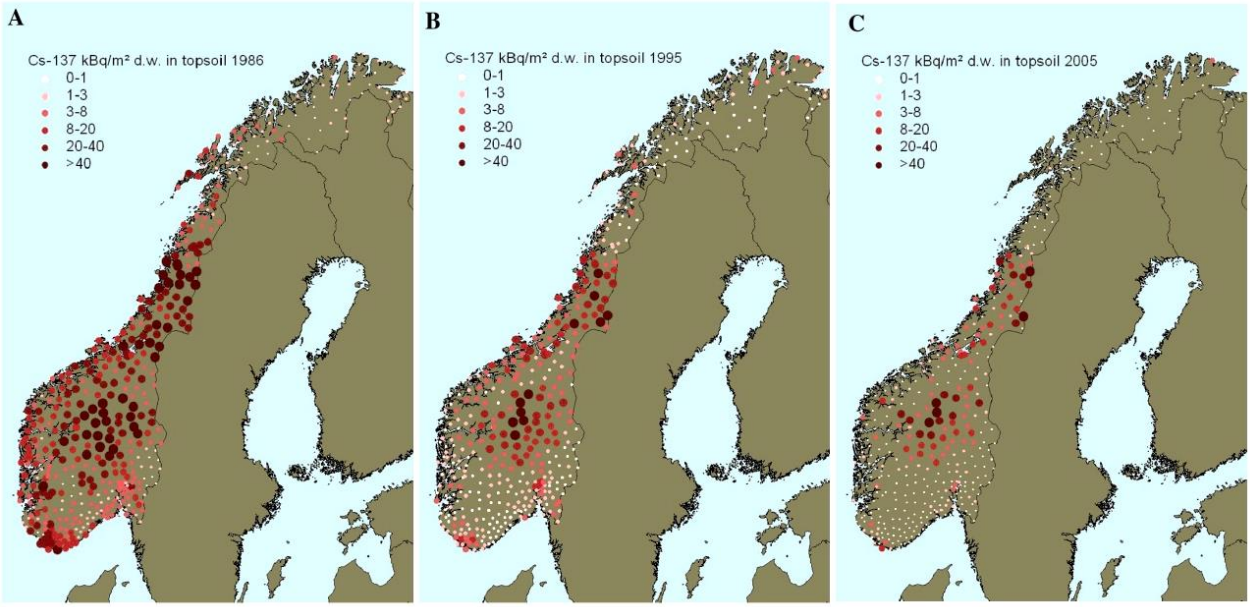

Figure 2.12: Geographical distribution of ^{137}Cs (Bq/m^2) in surface soil (0-3 cm) in Norway measured in 1986 (A), 1995 (B) and 2005 (C) (Gjelsvik & Steinnes, 2013).

In Figure 2.13 ^{137}Cs (Bq/m^2) in surface soil from four municipalities in Nordland bordering to Vefsn, (where the Vefsnfjord is located), measured in 1986, 1995, 2005 (and 2015), is presented. As mentioned earlier, the area received substantially fallout from the Chernobyl accident. The levels of ^{137}Cs in soils in the area have, however, decreased significantly since. Leirfjord municipality is located north of Vefsn municipality, while Grane, Hattfjelldal and Vevelstad municipalities are located south of Vefsn.

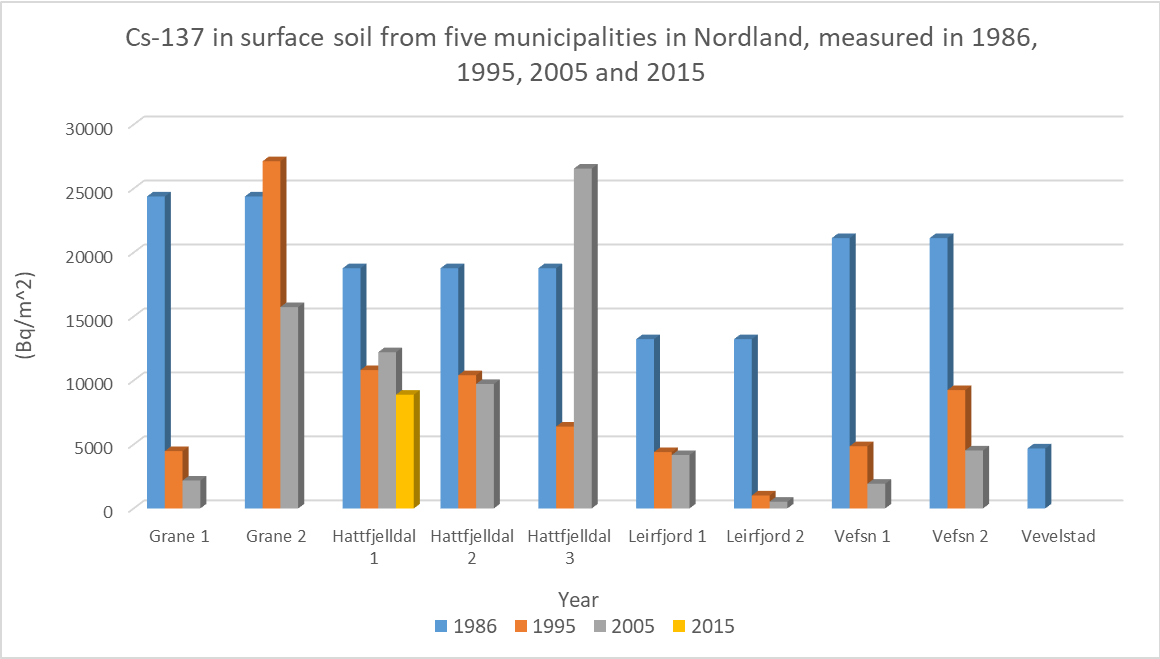

Figure 2.13: ^{137}Cs in surface soil from five municipalities in Nordland measured in 1986, 1995, 2005 and 2015. The location within the municipalities for samples from 1986 is unknown, while samples from 1995 and 2005 (and 2015) are taken at the same location (Bache et al., 1986., Gjelsvik & Steinnes, 2013., Gjelsvik/ DSA, unpublished data).

Data on the levels of natural radionuclides in sediments from the Vefsnfjord is not available. However, Haugen et al (1981) analysed two sediment cores for ^{210}Pb in a study of the fjord in 1978-1981. The two cores (10 cm deep) were taken in the inner part of the fjord and did contain ^{210}Pb-levels ranging from approximately 8.5 to 1 pCi/g (from ~315 to 37 Bq/kg) down the core.

2.5. Gamma spectroscopy

2.5.1. Principle

Alpha- and beta-decay may leave the nucleus in an exited state. One way this excess energy is removed is by gamma-ray emission. When the exited nuclide emits gamma-radiation, the composition of the nucleus does not change (equation 2) (Choppin et al., 2013).

$$ {}^{A}_{Z}X^{*}_{N} \rightarrow {}^{A}_{Z}X_{N} + \gamma \qquad (2) $$

The gamma rays have no charge, and cannot produce an electrical signal in the instrument directly. The detection of gamma rays depends upon production of charged secondary particles (electrons) from interaction with the detector material. This can happen

through the different interactions “photoelectric effect”, “compton scattering” and “pair production”, given in Figure 2.14. The exited electrons, lose their energy by ionization and excitation of nearby atoms, giving rise to an electric current which can be measured (Gilmore, 2008).

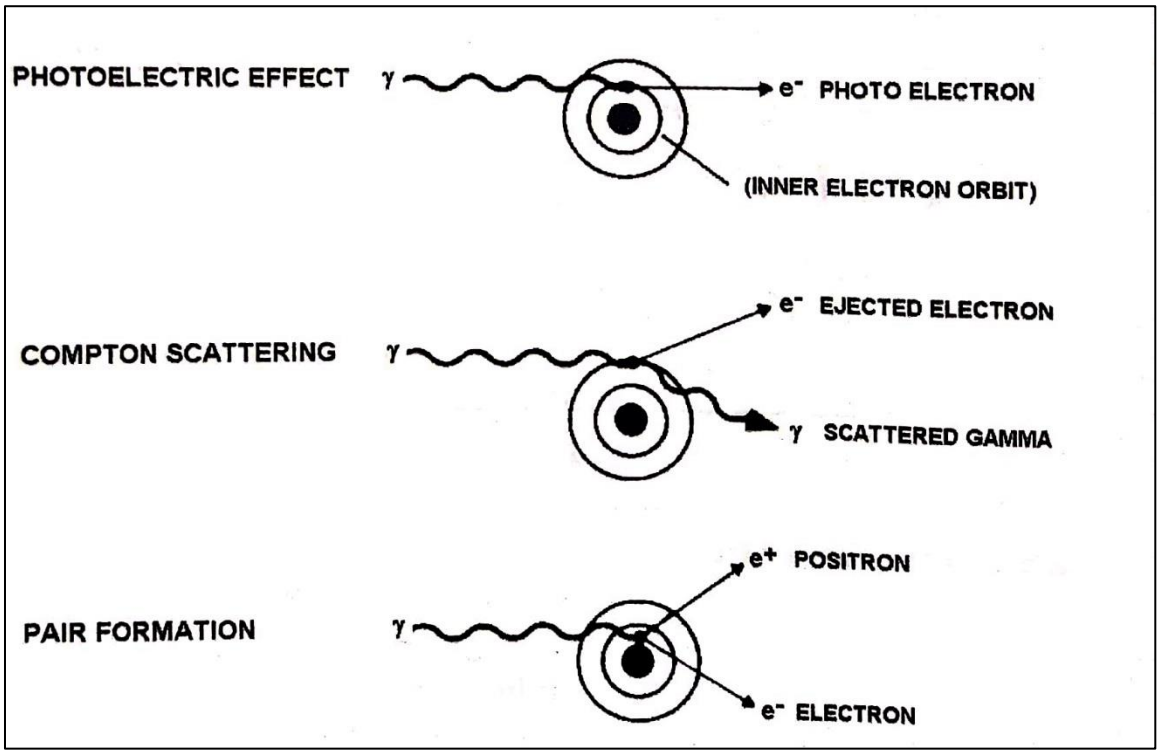

Figure 2.14: Schematic description of the three processes “photoelectric effect”, “Compton scattering” and “pair production”, accounting for gamma ray interactions with the detector when measuring gamma radiation (Choppin et al., 2013).

2.5.2. Measuring Cs-137 with HPGe-detector

^{137}Cs decays by beta minus to the ground state of barium-137 (5.6%), and to the meta-stable barium-137m (94.4%). ^{137m}Ba (t ½: 2.55 min) decays to stable ^{137}Ba by emission of gamma rays with energy of 661.6 keV (0.662 MeV) (Figure 2.15). (LnHB, 2008a., Dreher et al., 2015).

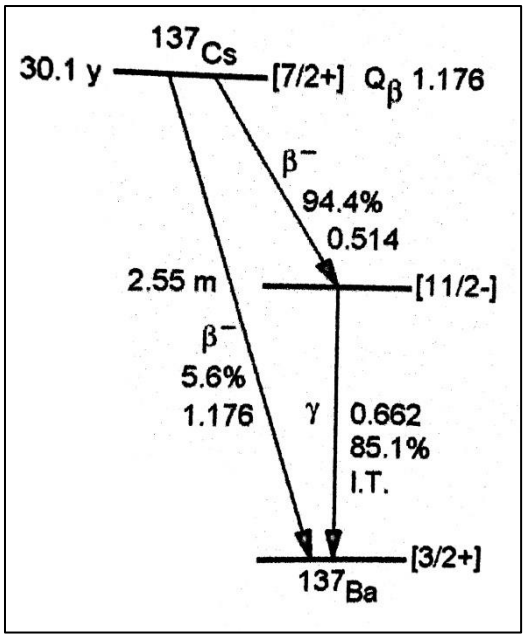

Figure 2.15: Decay scheme of ^{137}Cs (Choppin et al., 2013).

Because the half-life of the mother nuclide (^{137}Cs) is much larger than the daughter nuclide (^{137m}Ba), a secular equilibrium is established. Thus, it does not matter which of the nuclides that is measured (Choppin et al., 2013). Due to easier sample preparations (beta analyses require radiochemical separation), it is more convenient to measure the gamma-emitting ^{137m}Ba than the beta emitting ^{137}Cs.

2.5.3. Measuring 226-Ra and 228-Ra with HPGe-detector

Both ^{226}Ra and ^{228}Ra emits gamma rays when they decay, and can therefore be measured by gamma spectroscopy. However, the gamma lines for ^{226}Ra and ^{228}Ra have low energy, the main gamma lines being 186.2 keV and 13.5 keV, respectively (lnHB, 2008b, lnHB, 2012b), and can be difficult to measure. Also, interfering photo-peaks are a challenge (Gäfvert and Mauring, 2013., IAEA, 214). A solution to the problem is sealing the samples in aluminium bags to prevent radon, which is in gaseous state, to leak out (Gäfvert and Mauring, 2013). After about four weeks a secular equilibrium is established, and ^{226}Ra can be measured from the gamma lines of ^{214}Pb (295 keV and 352 keV) and ^{214}Bi (609 keV) (Sværen, 2010., Zaborska et al., 2008). ^{228}Ra can be measured from the gamma lines of the daughter ^{228}Ac (338 keV and 911 keV) (Dulaiova & Burnett, 2004). Other gamma lines of ^{214}Pb, ^{214}Bi and ^{228}Ac can be used as well.

2.5.4. Measuring Pb-210 with HPGe-detector and correction for self-absorption

It is possible to do direct analysis of ^{210}Pb by measuring the 46.54 keV gamma-ray, which is emitted in approximately 4% of the decays of the nuclide (Cutshall et al., 1983, LnHB, 2012a). A challenge with the method is self-absorption of the radiation by the sample. A gamma photon that passes through material, including the sample in which it is made, will with a certain probability undergo specific interactions. The photon is either absorbed or scattered, it loses energy, and will not contribute to the peak count-rate (Robu & Giovani, 2009). One can correct for self-absorption by computing a self-attenuation coefficient. It can, however, be relatively difficult because the attenuation coefficient is highly dependent on the sample composition. As a result, the relative gamma-ray emission will depend on the composition of the sediment samples. This obstacle can be solved either by accurately knowing the sample composition or by using a method to correct for self-absorption (Cutshall et al., 1983). The last option was used in this thesis. The procedure followed, and equations used, is after Cutshall et al (1983) "Direct analysis of ^{210}Pb in sediment samples: self-absorption corrections":

For a transmitted gamma-ray the attenuation follows:

$$\boldsymbol{T = Ie^{-\mu\rho x}} \tag{3}$$

Where T and I are the attenuated and unattenuated beam intensities. μ is the total attenuation coefficient (cm^2/g), ρ is the material density (g/cm^3) and x is the path length (cm).

One also has the equation for self-absorption:

$$\boldsymbol{O = A\frac{1-e^{-\mu\rho x}}{\mu\rho x}} \tag{4}$$

Where O is the attenuated sample output and A is the sample photon emission rate. By combining equation (3) and (4), one can compute a correction factor for self-attenuation:

$$\boldsymbol{\frac{A}{O} = -\frac{ln(\frac{T}{I})}{1-\left(\frac{T}{I-1}\right)}} \tag{5}$$

The result is then multiplied by the measured sample output, to estimate the unattenuated output.

2.5.5. Measuring K-40 with HPGe-detector

^{40}K decays to stable ^{40}Ca by beta minus decay 80.25% of the time (Figure 2.16). 0.2% and 0.001% of the time it decays to stable ^{40}Ar by electron capture and beta plus radiation, respectively. The remaining 10.55% of the time it decays to ^{40}Ar by electron capture, also emitting gamma radiation at 1460.85 keV as it decays to stable ^{40}Ar (LnHB, 2012c). The gamma line at 1460.85 keV can be measured using a HPGe-detector.

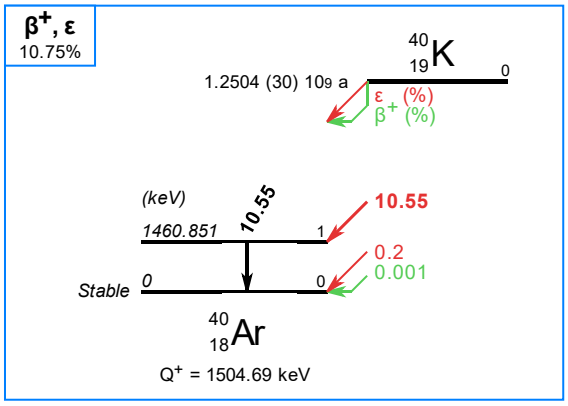

Figure 2.16: Decay scheme of ^{40}K (LnHB, 2012c).

2.6. Lead-210 (^{210}Pb) dating

Using the radioactive nuclide ^{210}Pb to determine the age of sediments has become a very important and well used method to date samples deposited in the past 100 years (Cutshall et al., 1983). The method is dependent on the naturally existing radionuclide ^{238}U and its daughters which are produced in the uranium decay chain (Figure 2.1). Among the daughters is ^{222}Rn, an inert gas with a half-life of 3.8 days, and it is the decay-product of ^{226}Ra. The ^{222}Rn-gas escapes from the earth's crust into the atmosphere. When it decays to its daughters, which all are in solid state, it is removed from the atmosphere and deposited on the surface of the earth. ^{210}Pb is the daughter with the longest half-life, 22 years. In aquatic systems, ^{210}Pb is removed from the water column by settling particles and deposited in sedimentation zones (Figure 2.17) (e.g. Cutshall et al., 1983). The total ^{210}Pb content in sediments has its origin from ^{226}Ra in the sediments (^{210}Pb-supported), and from deposit of Rn-daughters (^{210}Pb-excess or ^{210}Pb-unsupported) (Appleby & Oldfield, 1978). This results in the highest levels of ^{210}Pb being found in the uppermost layers, and decreasing exponentially down the core, until being equal to the ^{226}Ra levels, due to radioactive decay. By measuring ^{210}Pb and ^{226}Ra in sediments from marine areas, one can estimate the excess or unsupported ^{210}Pb content (equation 6). The excess ^{210}Pb activity concentration in each sediment layer declines with age

in accordance with radioactive decay, and from this information one can obtain information about the age of the sediment layers (Cutshall et al., 1983., Lubis, 2006). Since the development by Goldberg (1963), using ^{210}Pb in age dating of sediments is well known, and there have been made several methods based on the radionuclide. In this thesis the most widely used one, the CRS method, will be used (chapter 2.7.1.).

Additional analyses of anthropogenic radionuclides, like ^{137}Cs can often provide a valuable check of the accuracy of the ^{210}Pb-results, and is often used in addition to ^{210}Pb when dating sediment samples (chapter 2.7.3.) (Tadjiki & Erten).

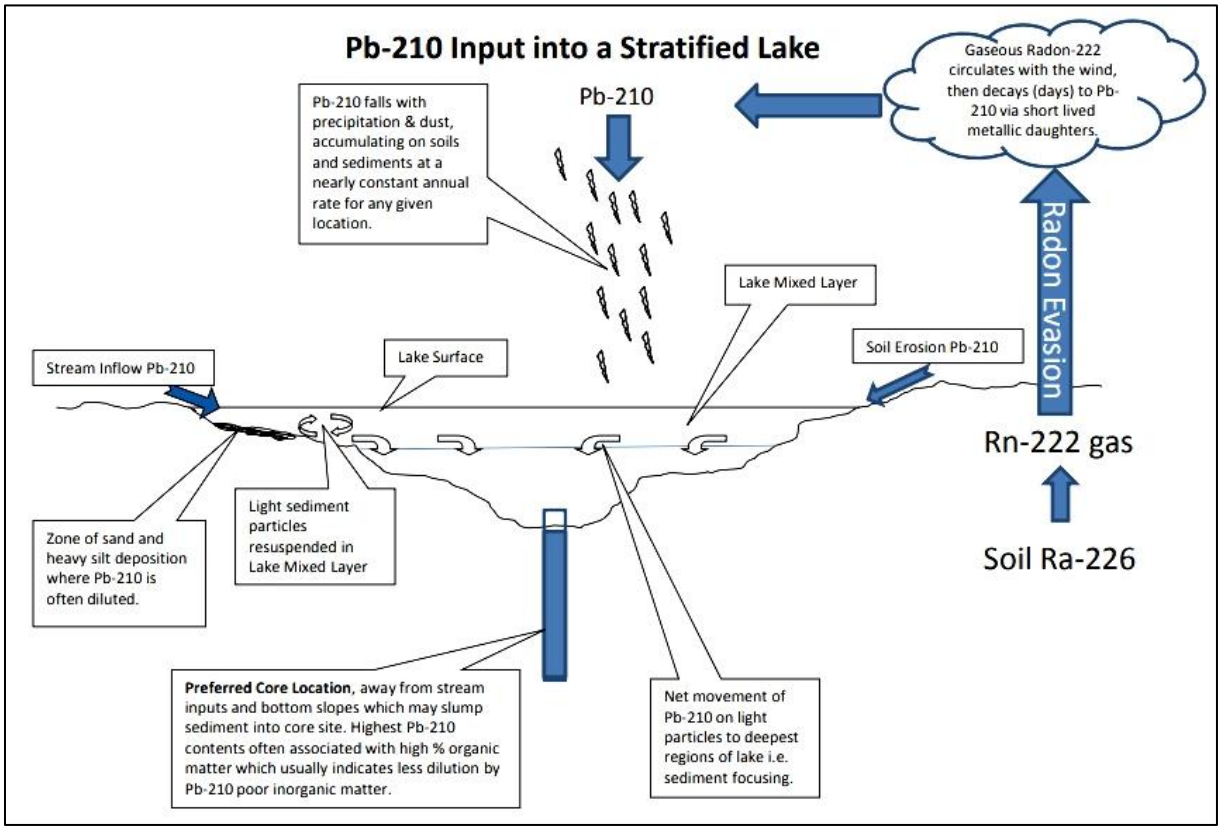

Figure 2.17: The circulation of Pb-210 in the environment (www.flettresearch.ca).

2.6.1. Dating sediments using the CRS method

The age of the sediment layers can be determined using the CRS method (Constant Rate of Supply method). The procedures and equations below are found in Appleby and Oldfield (1978).

The content of excess ^{210}Pb in a layer, *X*, can be calculated as followed:

$$C_{210_{Pbex}} = C_{210_{Pb}total} - C_{226_{Ra}} \quad (6)$$

Where *C* is activity concentration (Bq/kg).

The Constant Rate of Supply (CRS) model (Appleby and Oldfield, 1978) is the most commonly used ^{210}Pb-dating model for dating sediments (Olid, et al., 2016, MacKenzie et al., 2011). The model assumes a constant fallout of ^{210}Pb from the atmosphere to marine waters (^{210}Pb-excess), resulting in a constant rate of supply of ^{210}Pb in marine sediments, irrespective of any variation in sediment accumulation rate (Lubis, 2006).

The content of excess ^{210}Pb in each layer is calculated as:

$$C_{210_{Pb\,ex}} = C_{210_{Pb\,ex}} * LW\ , Bq \quad (7)$$

LW = Layer Weight, kg

The amount of excess ^{210}Pb, A_0 in the entire core can then be calculated:

$$A_0 = \int_0^L C\ , Bq \quad (8)$$

Where *L* is the core length.

The amount of excess ^{210}Pb in layers beneath the layer of depth *X*, A_X, can then be found:

$$A_X = \int_X^L C\ , Bq \quad (9)$$

The age of the layer *X* can then be calculated by:

$$Age\ of\ layer\ X = \frac{1}{\lambda} * ln\frac{A_0}{A_X}\ , years \quad (10)$$

Where λ is the decay constant for ^{210}Pb:

$$\lambda = \frac{ln2}{t_{\frac{1}{2}}} = \frac{ln2}{22.23\ years} = 0.0312\ years^{-1} \quad (11)$$

$t_{1/2}$ is 22.23 years for ^{210}Pb (Dreher et al., 2015).

Uncertainty for ^{210}Pb-dating results:

The uncertainty for the dating results is assessed according to Binford (1990), as also done in the internal method at IMR. Binford estimates with 95% confidence interval range from about 1 to 2 (10-20%) years at ten years of age, 10 to 20 (10-20%) years at 100 years of age, and 8 to 90 (5-60%) years at 150 years age when using the CRS method.

2.6.2. Calculating sedimentation rates:

A way to determine the age of the sediment layers is to determine the sedimentation rate in an area. The following method is described in Tadjiki & Erten (1994):

Assuming that the flux Þ (dpm*cm^{-2}*y^{-1}) of the sediment-water interface has remained constant during the dating interval, and no migration of Pb^{210} has occurred post-deposition, the activity of Pb^{210} in the sediment at any depth (z) is given by the equation:

$$A(z) = A_0 * e^{-\lambda} * \frac{z}{s} \quad (12)$$

Where $A(z)$ is activity of Pb^{210} in dpm/g at depth z, A_0 is activity of Pb^{210} in dpm/g at z=0, z is depth of sediment in cm, s is the sedimentation rate in y^{-1}, and λ is the decay constant.

If initial activity (A_0) is assumed to be constant, which implies that both the flux of the radionuclide, and the sedimentation rate, is constant, a semilogarithmic plot of $A(z)$ versus z should give a straight line with an intercept of log A_0 and a slope of $-\lambda/s$. From the slope, the sedimentation rate can be determined.

2.6.3. Using ^{137}Cs to date/ verify age of sediment layers

In many cases it can be valuable to compare the ^{210}Pb dating results with other radionuclides to help verify the results. A commonly used radionuclide is ^{137}Cs (e.g. Appleby, 1998., Appleby & Oldfield,1978., Tadjiki & Erten, 1994., Zaborska et al., 2008). ^{137}Cs can be used in several ways to determine the age of sediments deposited approximately the last 70 years. Peaks in ^{137}Cs levels in a sediment core may arise from events like the Chernobyl accident in 1986, or from the fallout maximum from the atmospheric testing of nuclear weapons in 1963, and may help verify dating results found from ^{210}Pb (Appleby, 2008). Another method, used in e.g. Zaborska et al (2008), is to assign the sediment layer at the deepest depth were ^{137}Cs is

found, the age of when nuclear tests started (1950 is used in the paper). This method requires that the sediment core is long enough to obtain sediments from ages before ^{137}Cs was introduced to the environment. The method also assumes no migration of ^{137}Cs to deeper depths.

2.7. Density correction of sediment layers

With increasing depth, sediments can get compressed. It is possible to correct for this compression by using data on porosity of the sediment layers (equation 13). With the data, a corrected thickness of each sediment layer can be found (equation 14), and thereafter the density corrected depth of the sediment core can be found (equation 15) (Tadjiki and Erten, 1994).

$$\boldsymbol{Porosity}\ (\%) = \frac{\boldsymbol{Sample,wet\ weight\ (g) - Sample,dry\ weight\ (g)}}{\boldsymbol{Sample,wet\ weight\ (g)}} * \mathbf{100}\% \qquad (13)$$

$$\boldsymbol{CT_i = NT_i + NT_i * \frac{P_1 - P_i}{100 - P_1}} \qquad (14)$$

Where CT_i is Corrected thickness of layer i, NT_i is the normal thickness of layer i and P_1 and P_i are the porosity of layer 1 (the upper layer) and the porosity of layer i, respectively.

$$\boldsymbol{CD_i = CD_{i-1} + \frac{CT_{i-1}}{2} + \frac{CT_i}{2}} \qquad (15)$$

where CD_i is corrected depth of layer i (in the middle of the sediment layer).

3. MATERIALS AND METHODS

3.1. Sample collection

Sediment cores were collected at five different sites; one in the Norwegian Trench and four in the Vefsnfjord (Figure 3.1). The sampling locations were chosen by two main factors; the seafloor at the sampling site had to be suitable for sediment core sampling (not consist of stones and gravel etc.), and it had to be on the route of the research expedition. IMR have taken samples of sediment and seawater earlier at the sampling site in the Norwegian Trench (CTD906), as well as the inner and outer sites in the Vefsnfjord (CTD1121 and CTD1124). To be able to come back to the same sampling sites over a time period can give important information on time trends in the marine environment. The two remaining sampling sites in the Vefsnfjord (CTD1122 and CTD1123) were chosen to cover a wide range of the fjord, and to investigate any gradient trend within the fjord.

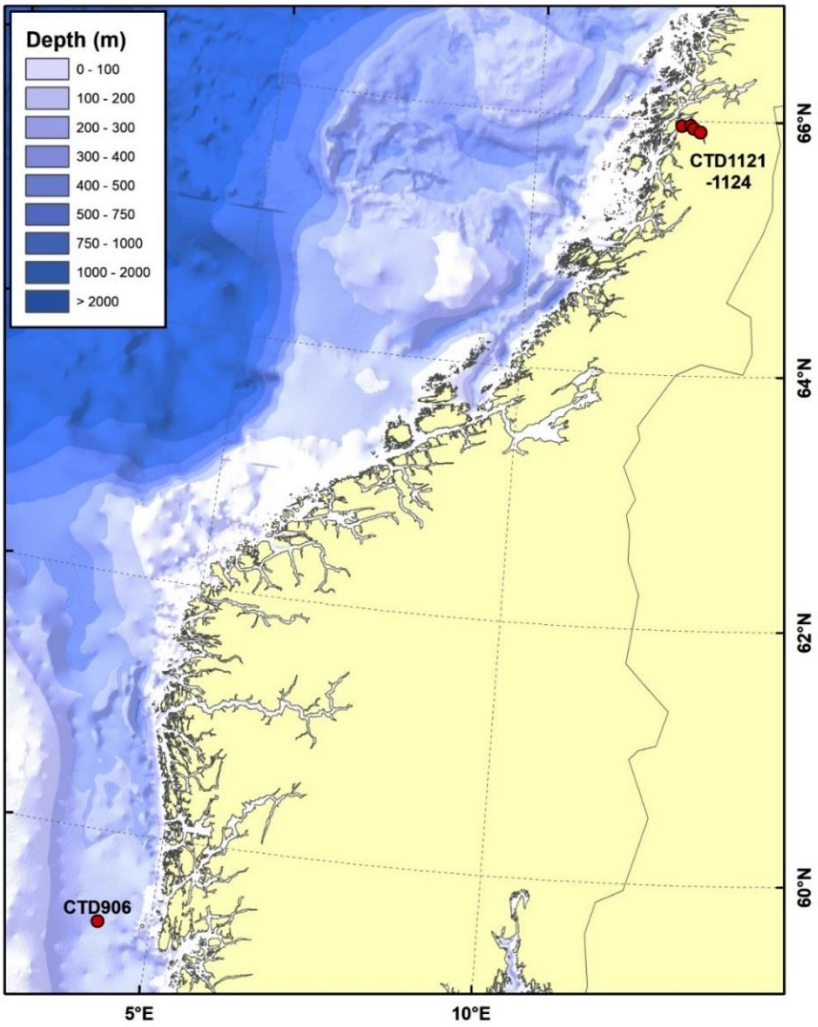

Figure 3.1: The sampling sites; CTD906 in the Norwegian Trench and CTD 1121-1124 in the Vefsnfjord (Figure: K. Bakkeplass, IMR).

All the samples were collected using a Smøgen box corer. The device includes a box (30*30*40 cm) in stainless steel which can take sediment samples and bring them to the surface undisturbed. From the "cube" of sediment brought on board the research vessel, the cores were collected using PVC tubes (10 cm diameter). The tubes were manually pressed carefully into the sediment. The tubes were slightly sharpened in the end to minimize compression of the sediments. After the tube was pressed all the way to the bottom, excess material from outside the core was removed, and lids put on each end of the tube.

3.1.1. Samples from the Norwegian Trench

The samples from the Norwegian Trench were collected aboard R/V Kristine Bonnevie in November 2017. Four cores and one surface sample were collected from the same box corer. The samples were stored in standing position in a freezer until further preparation took place at the laboratory at IMR (chapter 3.2). Data on the sampling site and more is presented in Table 4, and Figure 3.2.

Table 4: Data from the samples collected in the Norwegian Trench.

Sampling site	Latitude/ Longitude	Ecodepth (m)	Number of cores/ samples	Sampling date
CTD906	59.29N 4.20E	276	4 cores with 15, 11, 12 and 14 slices, respectively (52 samples total) and 1 surface sample. All cores appeared fine-grained, without any large fragments.	13.11.2017

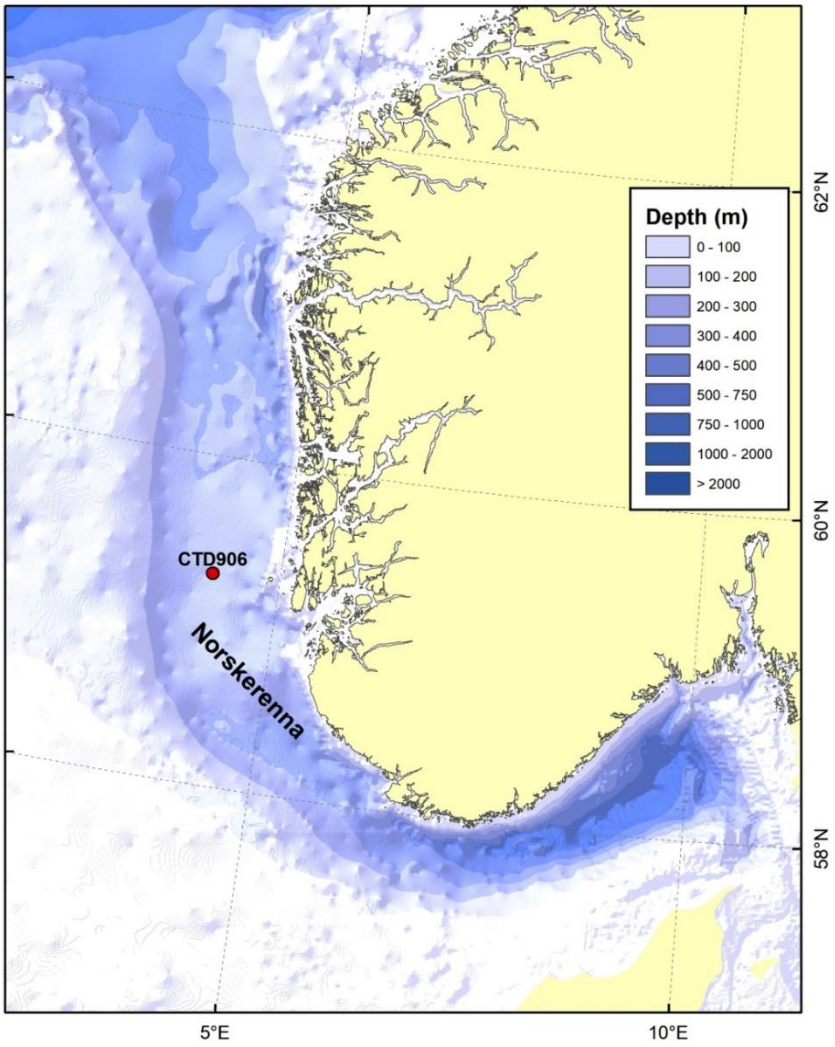

Figure 3.2: The position of the sampling site in the Norwegian Trench (Figure: K. Bakkeplass, IMR).

3.1.2. Samples from the Vefsnfjord

The samples from the Vefsnfjord were collected aboard R/V Kristine Bonnevie in October 2018. Three cores were collected from the same box corer, at four different sites (CTD 1121-1124) in the fjord (Figure 3.3). The inner and outer sampling site (CTD1121 and CTD1124) were at approximately the same location where IMR have taken surface samples for the RAME project. The samples were cut in slices and transferred to aluminium containers on board the research vessel, and stored in a freezer until further preparation took place at IMR (chapter 3.2). One core from each site were sent to the Norwegian Geological Surveys (NGU) (after they were freeze-dried at IMR) for grain size analyses and analyses of organic content, and not analysed for radionuclides. Data on the sampling sites and more is presented in Table 5, and Figure 3.3.

Table 5: Data from the samples collected in the Vefsnfjord.

Sampling site	Latitude/ Longitude	Ecodepth (m)	Number of cores/ samples	Sampling date
CTD1121	65.96N 12.75E	226	3 cores with 15 slices per core (45 samples total). All cores appeared fine-grained, without any large fragments.	28.10.2018
CTD1122	65.96N 12.91E	487	3 cores with 12, 12 and 13 slices, respectively (37 samples total). All cores appeared fine-grained, without any large fragments.	28.10.2018
CTD1123	65.94N 12.97E	486	3 cores with 14, 13 and 14 slices, respectively (41samples total). All cores appeared fine-grained, without any large fragments.	28.10.2018
CTD1124	65.91N 13.10E	448	3 cores with 11, 12 and 11 slices, respectively (34 samples total). All cores appeared fine-grained, without any large fragments.	28.10.2018

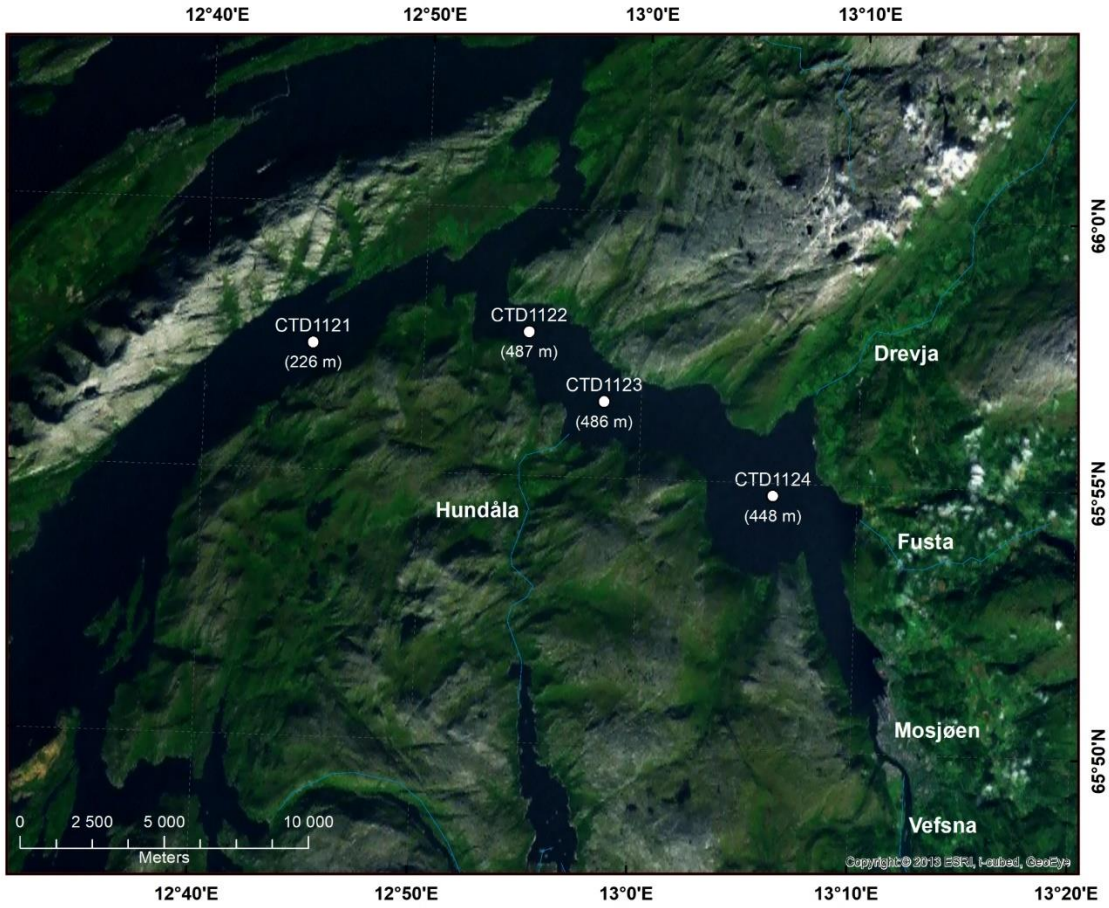

Figure 3.3: The position and depths of the four sampling sites in the Vefsnfjord (Figure: K. Bakkeplass, IMR).

3.2. Sample preparation

3.2.1. Slicing the cores

The PVC tubes with the frozen sediment samples from the Norwegian Trench were put in a refrigerator the day before slicing, to thaw up and be easier to cut. They were stored in standing position, to prevent the sediment to mix inside the tubes (Figure 3.4). Before slicing, excess water from the top of the tube was carefully removed using a pipette. When slicing the sediment cores, the tubes were placed in standing position, and a piston was used to carefully press the sediment core upwards (Figure 3.4, right). The first 10 cm of the cores were cut in 1 cm slices, and from 10 cm and deeper, they were cut in 2 cm slices. A ruler was used to measure the thickness of the slices. The slices were transferred to pre-weighed aluminium containers. The containers had information about research vessel name, sample collection date, station number/ sampling site, core number and depth of sediment slice. The wet weights were determined after slicing, using a Mettler Toledo PG 5001-S weight. The containers were then stored in a freezer until further preparation.

The samples from the Vefsnfjord were cut aboard R/V Kristine Bonnevie, following the same procedure as above, and wet weight were determined aboard. The samples were then stored in a freezer until further preparation at IMR.

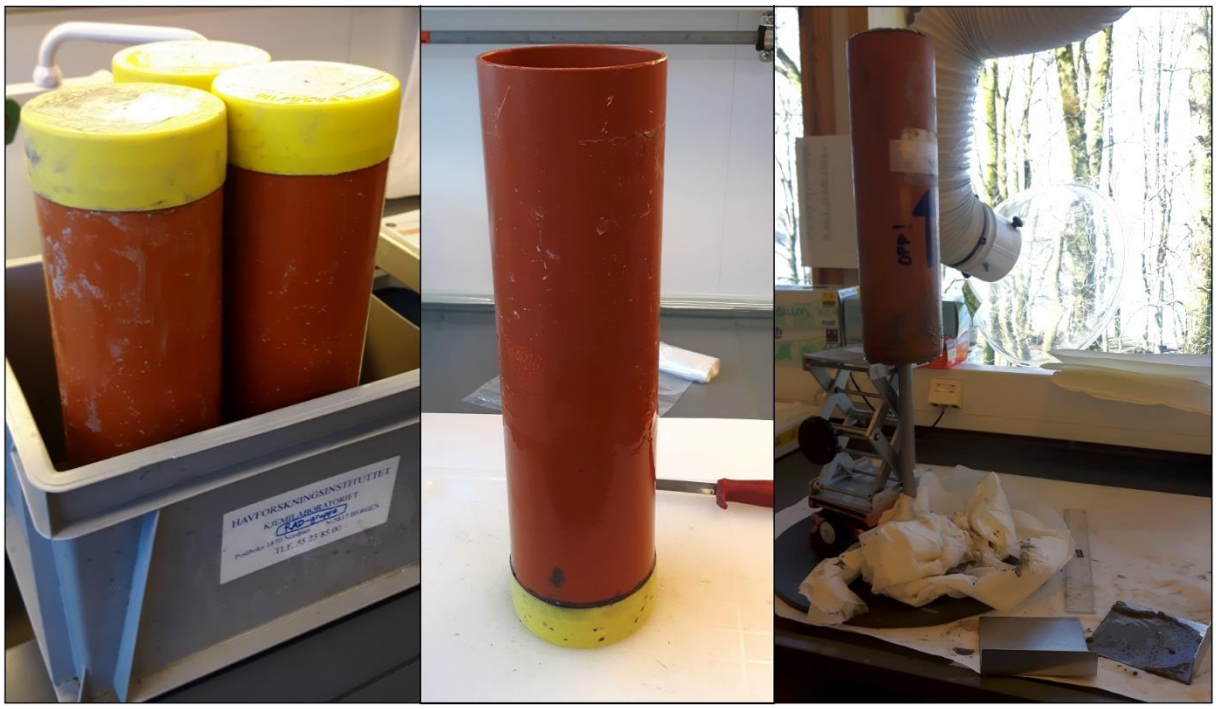

Figure 3.4: Left and middle: sediment cores in the pwc-tubes. Right: setup for slicing the cores.

3.2.2. Freeze-drying and homogenizing the samples

The frozen sediment samples in aluminium containers were freeze-dried using CHRIST ALPHA 1-4 freeze dryer connected with an Edwards RW3 vacuum pump. When the samples were completely dried (approximately 2-3 days), they were weighed to determine dry weight. The weighing was done shortly after freeze-drying to prevent the sediment samples from contracting moist. The samples were homogenized using a Retsch Planetary Ball Mill PM 100 (Figure 3.5). After being homogenized, the sediment samples were put back in the aluminium containers and stored in small plastic bags, to prevent moisture and contamination in the samples until further preparation. The equipment for homogenizing was cleaned between every sample, to prevent cross contamination. Between sediment samples the from the same core, the equipment was cleaned with damp paper and dried off. Between samples from different cores, the equipment was proper washed with water and soap, and dried overnight or in a drying oven.

Figure 3.5: Left: A sediment sample ready to be homogenized using a ball mill. Right top: A freeze-dried sample before homogenizing. Right bottom: sediment sample after being homogenized.

3.2.3. Transferring samples to a measurement-container and vacuum sealing it

The homogenized samples were transferred to a 60 ml polyethylene box: Nolato AB, art.no 110170 (box) and 112040 (lid). The box was pre-weighed with lid on, to be able to determine sample mass of finished sample. The box containing sample was put on an "JT-51B Powerful dental vibrator" which shook the sample gently, allowing air bubbles to be released and the sample to be properly packed (Figure 3.6). The box was filled up to ~3 mm from the top (an empty sample box with marked height was used to ensure equal sample heights in all samples). This was done to ensure all the samples had the same geometry as the calibrated standard samples (chapter 3.3.2). The lid was then put on, and the sample weighed. The lid was marked with research vessel name, journal number, sample collection date, station number, core number, depth of sediment slice and sample weight.

Figure 3.6: Packing sediment sample in polyethylene box. The instrument shook the sample gently, releasing air from the sediment.

Also, to ensure all samples were properly packed and equally filled, a polycarbonate disc was put between the sample and the lid. The disc made sure there were no empty space between the sample and the lid. In the thesis one of the objectives was to measure ^{226}Ra, and to do so, it is important to ensure equal distribution of the uranium-daughter ^{222}Rn in the sample, which is in gaseous state. The disc also prevented the box from imploding during

vacuum sealing, due to the lid being made from soft plastic. The disc was packed in aluminium foil to be easier to re-use. The lid was glued with silicone glue. A small cut in the lid was made to prevent air pressure inside the box. The glue was left to dry for one day before vacuum sealing the samples.

Samples were vacuum sealed using a Turbovac T20 Table Top Vacuum Packing Machine, and aluminium bags (Figure 3.7). Sealing the samples prevent ^{222}Rn gas to escape. After vacuum sealing, the samples were stored for four weeks or more before analysis, to establish a secular equilibrium between the ^{238}U daughters.

Figure 3.7: Left: a sample ready to be vacuum sealed using a Turbovac T20 Table Top Vacuum Packing Machine. A lead weight was put on top of the sample to prevent the sample from moving during the vacuum procedure, and to secure a result without air inside. Right: sediment samples after being sealed.

3.3. Gamma Spectroscopy

3.3.1. Facilities and high purity germanium detectors (HPGe) at IMR

Two different detectors were used, both high purity germanium detectors (HPGe-detectors). RAD12 is an ORTEC GMX-series N-type coaxial HPGe detector with X-Cooler cooling machine, Cryosecure compressor Power Controller and DSPEC analysis system. It has a crystal diameter of 59.0 mm and length 78.3 mm. Resolution (FWHM) at 1.33 MeV (^{60}Co) is 1.78 keV, and the relative efficiency at 1.33 MeV is 47%. The detector and associated equipment are manufactured by ORTEC and supplied by Gammadata. The detector is shielded by an approximately 10 cm thick lead tower made of low-activity lead and a cadmium and copper lining inside. The lead tower is manufactured by Apparatusbau Goslar (Quality assurance data sheet, 2005., Sværen and Volynkin, 2019).

RAD14 is an ORTEC GEM-series P-type coaxial HPGe detector with X-Cooler III cooling machine, Cryosecure Compressor Power Controller and DSPEC-50 analysis system. It has a crystal diameter of 84.7 mm and length 33.1 mm. Resolution (FWHM) at 1.33 MeV (^{60}Co) is 1.83 keV, and the relative efficiency at 1.33 MeV is 52%. The detector and associated equipment are manufactured by ORTEC and supplied by Gammadata. The lead tower surrounding the detector is containing low-activity lead and has a copper lining inside. The lead tower is produced by Gammadata (Quality assurance data sheet, 2015., Sværen and Volynkin, 2019).

The counting room at IMR has 195 mm concrete walls containing high content of olivine, giving the room low background radiation levels and therefore low quantification limits (Sværen, 2010).

Counting times for the sediment samples ranged from approximately 65000 to 270000 seconds.

3.3.2. Analysis in GammaVision

The computer program ORTEC GammaVision (Version 8) was used to collect gammaspectra and analyse the results. The sediment samples were all analysed according to Volynkin (2019); “464 - Determination of radionuclides in sediments and biota, measured by gamma spectroscopy on the HPGe detector”. The method is intended used for analyses of environmental samples with low activity concentrations, below 1000 Bq/kg for sediment

samples. The method is accredited in accordance with the standard ISO 17025 for one of the detectors (RAD15) at IMR, but not for the detectors used in this thesis. However, the same procedures are followed for all three detectors, and there is an ongoing work on getting the method accredited for RAD12 and RAD14 as well.

In the ORTEC GammaVision program an efficiency calibration file and an energy calibration file are added, both created by a certified analyst. The efficiency calibration of the detector is done by measuring a sample of same geometry as the samples, and with a known activity concentration. The area of the lines in the gamma spectra, or counts, can then be used to calculate the activity concentration of certain nuclides. The type of efficiency calibration file used in analysis in this thesis was a "PTP – point to point" calibration, or interpolative calibration. This file let you analyse the same radionuclides in samples of same geometry as the standard material used in the calibration. The energy calibration file is used to identify the energy of the lines in the gamma spectra. This is necessary to be able to identify radionuclide that emits the radiation (Volynkin, 2019).

Also added in the GammaVision program is a "pbc-file" (peak background correction file). This file is based on a background measurement to obtain information on the background activity concentration in the detector without any sample. The file subtracts any background radiation from the sample results (Volynkin, 2019).

A library file is uploaded in the GammaVision program. This file contains information on the radionuclides of interest. The information includes half-life of the nuclides, the energies/lines that will be used in the analysis and emission efficiency (Volynkin, 2019). In Table 6 data on nuclides and energies, retrieved from the library file used in the analysis of the sediment samples in this thesis, is listed.

Table 6: Table of the radionuclides and energies of interest in this thesis.

Nuclide	Half-life	2-sigma nuclide uncertainty (%)	Rank	Energy (keV)	Percent (%)	Nuclide	Half-life	2-sigma nuclide uncertainty (%)	Rank	Energy (keV)	Percent (%)
Caesium-137	30,05 Yrs	0,4706	1	661,66	84,99	Actinium-228	1,4*10^10 Yrs	7,018	1	911,2	26,2
			2	32,19	3,59				2	968,96	15,9
			3	31,82	1,95				3	338,32	11,4
			4	36,45	1,06				4	964,79	4,99
Potassium-40	1,25*10^9 Yrs	2,085	1	1460,82	10,6				5	463	4,45
Bismut-214	1600 Yrs	0,8353	1	609,31	45,49				6	794,94	4,31
			2	1764,49	15,31				7	93,35	4,1
			3	1120,29	14,91				8	209,25	3,97
			4	1238,11	5,83				9	270,25	3,55
			5	2204,21	4,91				10	1588,2	3,06
			6	768,36	4,89				11	328	3,04
			7	1377,67	3,97				12	89,95	2,5
			8	934,06	3,1				13	129,07	2,5
			9	1729,60	2,84				14	409,46	2,02
			10	1407,98	2,39				15	835,7	1,7
			11	1509,23	2,13				16	772,29	1,52
			12	1847,42	2,03				17	1630,62	1,52
			13	1155,19	1,64				18	105,55	1,5
			14	665,45	1,53				19	99,51	1,26
			15	1280,96	1,435				20	755,31	1,03
			16	1401,50	1,33				21	840,37	0,97
			17	806,17	1,26				22	1495,9	0,92
			18	2118,55	1,16				23	562,5	0,89
			19	1661,28	1,05				24	1459,13	0,87
			20	1385,31	0,795				25	478,4	0,224
			21	1583,22	0,707	Lead-210	22,23 Yrs	1,881	1	46,54	4,25
			22	703,11	0,479						
			23	1207,68	0,454						
			24	1538,50	0,401						

When measuring ^{226}Ra and ^{228}Ra it is assumed secular equilibrium with Bi-214 and Ac-228, and the radionuclides are measured using the gamma lines in Table 6 (chapter 2.5.3.).

All activity concentrations are decay corrected back to sampling date, and are given with 2σ uncertainty bars.

3.3.3. Uncertainties in method and measurement of sediment samples

The detection limit and uncertainty for the analysis results is individual for each sample, and is dependent on many factors, such as counting time, background levels, the properties of the nuclide, sample amount, geometry, self-absorption, and the efficiency of the detector for certain energies of the gamma radiation. The detection limit is calculated as "MDA – minimum detected activity" in the GammaVision software. (Volynkin, 2019). The total uncertainty estimate is also calculated in GammaVision, as described in the GammaVision user manual (GammaVision, 2017). All the variables have a standard deviation (σ), and the

total uncertainty is given in equation (16), with all standard deviations as K=1 (Table 7). The final result is converted, and given as ±2σ (Gammavision, 2017., Volynkin, 2019).

$$\sigma_{tot} = \sqrt{\sigma_{count}^2 + \sigma_{nor}^2 + \sigma_{rsum}^2 + \sigma_{abs}^2 + \sigma_{nuc}^2 + \sigma_{eff}^2 + \sigma_{geo}^2 + \frac{\sigma_{sys}^2}{3} + \sigma_{adl}^2 + \sigma_s^2} \quad (16)$$

Table 7: Sources to uncertainty accounted for in the total uncertainty budget (Gammavision, 2017., Volynkin, 2019).

Uncertainty source	**Amount, K=1**	**Taken into account in:**
σ_{count}: counting uncertainty. Uncertainty in number of measurements. Includes uncertainty in background measurements.	Varies.	Automatically in GV.
σ_{nor}: additional normally distributed uncertainty estimate. - Uncertainty in sample weight due to water content.	2.5% for sediment samples*.	Sample type settings file in GV (additional random).
σ_{rsum}: random summing uncertainty estimate.	Negligible if deadtime for detector <15%.	Not used because deadtime is low because of low. activity concentration in samples.
σ_{abs}: absorption uncertainty estimate. Possible differences in absorption between sample and standard, due to differences in density and chemical composition.	2.5%.	Sample type settings file in GV (additional random).
σ_{nuc}: nuclide uncertainty estimate. Uncertainty in possibility of emission. Data obtained from Laboratorie National Henri Becquerel (www.lnhb.fr/en) or from certificate from certified standards to minimize the uncertainties.	Varies.	Library file in GV.
σ_{eff}: efficiency uncertainty for the detector. For a PTP-calibration the uncertainty is equal to the uncertainty for the sources used in the calibration.	Varies.	Efficiency calibration file in GV.
σ_{geo}: geometry uncertainty estimate. Random errors in sample preparation. Includes uncertainty in sample volume.	2.5%**.	Sample type settings file in GV (additional random).
σ_{sys}: systematic uncertainty estimate.	≈ 0.0%.	Not used.
σ_{adl}: additional user-defined uncertainty factor. - Uncertainty in placement of sample on detector. - Uncertainty in half-life of radionuclides.	≈ 0.0%**.	Not used.
σ_{s}: sample size uncertainty. Uncertainty in sample size or weight uncertainty.	0.125%***.	Sample type settings file in GV (additional random).

* Based on measurements of water content in varies samples done at IMR.
** Based on sample measurements done at IMR.
*** Based on minimum sample weight being 40.0g and the weight used gives the result with one decimal. Maximum uncertainty is therefore 0.25%, and therefore 0.125% at K=1.

3.3.4. Quality assurance

Quality assurance of the detectors includes measurements of a point source once a week, measurements of samples with known activity concentration, and background measurements, see Table 8, and appendix B for results.

Table 8: Samples/ sources used to control the detectors at IMR (Volynkin, 2019).

Sample/ source	Description	Counting time (sec. live time)	measurement frequency (minimum)
Cs-Eu point source	A high activity concentration source containing both ^{137}Cs and ^{152}Eu	100	Once a week, or if any major changes is done to the detector.
Control sample "Murmansk"	Dried sediment sample (85,3g in a 60 ml p.e. box) from the Murmansk-area. Contains about 54 Bq/kg d.w. ^{137}Cs and 375 Bq/kg d.w. ^{40}K per reference date.	20000-30000	Every other month.
Control sample "Kara"	Dried sediment sample (62,9g in a 60 ml p.e. box) from the Kara Sea. Contains about 8.6±0,5 Bq/kg d.w. ^{137}Cs and 700-720 Bq/kg d.w. ^{40}K per reference date.	65000-90000	Every other month.
Background measurements	A measurement is done without any sample on the detector.	>200000	Every other month.

In addition, the laboratory at IMR regularly participates in intercomparison exercises on sediment and aqueous samples. The intercomparison exercises have been organized by NKS, IAEA, IMR and NRPA, and NPL.

3.4. Pb-210 measurements and self-absorption corrections

The samples were already analyzed for ^{210}Pb when measured overnight (minimum 65 000 seconds). Also, a ^{210}Pb standard was measured overnight. The results did not get calculated using GammaVision (chapter 3.3.2) as the other radionuclides, but by following a method at IMR, described in (Sværen, 2010) (Table 9). To correct for self-absorption (chapter 3.4), all samples were measured once more, for 600 seconds, with a point source on top (Figure 3.8). The point source used was a QSA Global GmbH with 255 kBq Pb-210 at reference date 1 of

July 2008, and calibrated at Deutscher Kalibrierdienst, DKD. In addition, an empty container (with a disc under the lid, like the samples) and a ^{210}Pb standard (chapter below) were measured with the same point source on top.

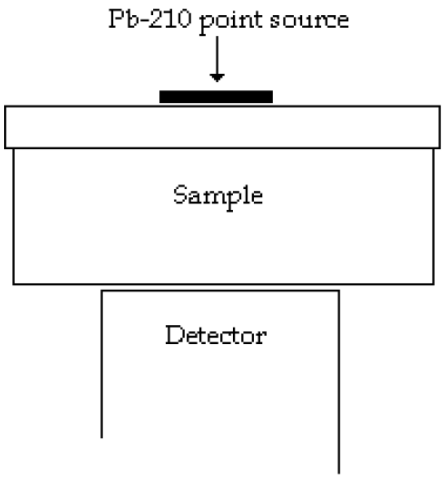

Figure 3.8: Simplified representation of point source measurement for self-attenuaton correction. In reality, the sample is sealed in an aluminum bag (Figure: Sværen, 2010).

From the data obtained, the corrected values of ^{210}Pb in the samples were computed using the equations in Table 9 found in (Sværen, 2010). The corrected ^{210}Pb results were then used, along with the ^{226}Ra results, to date the sediment cores (see chapter 2.6)

Table 9: Variables and equations used in ^{210}Pb measurements and calculations (Sværen, 2010).

Variable	Symbol	Pb-210 peak at 46.5 keV Equation	Uncertainty
Background measurement	BK	BK = net area/ counting time, cps	sBK = s(net area) / counting time, cps
Calibration:			
Counting rate standard	R_{cal}	R_{cal} = net area/ counting time, cps	sR_{cal} = s(net area) / counting time, cps
Activity in standard on reference date	$A_{0Pb-210}$	A_0 = 7,46 kBq	4,4 %
Half life	t½	t½ = 8145 days	8 days
Days decayed	t	t = days from reference date to measuring date	
Activity in standard on calibration date	A_{Pb-210}	$A_{Pb-210} = A_0 \cdot e^{-\ln\frac{2}{t\frac{1}{2}}t}$, Bq	sA_{Pb-210} = +/- 5 %
geometry factor	g	= A_{Pb-210} / R_{cal} , Bq/cps	sg = sA / R_{cal}, Bq/cps
Counting rate standard point source on top	R_{cal+}	R_{cal+}= net area/ counting time, cps	sR_{cal+} = s(net area) / counting time, cps
Counting rate empty container point source on top	R_s	R_s= net area/ counting time, cps	sR_s = s(net area) / counting time, cps
Density correction factor standard	KF	KF= ln [(R_{cal+} - R) / R_s] / [((R_{cal+} - R) / R_s) –1]	sKF is set to 0,01.
Geometry factor	G	G_k = g / KF, Bq/cps	$sG = \sqrt{[\frac{sg}{KF}]^2+[\frac{-g\cdot sKF}{KF^2}]^2}$, Bq/cps
Sample Measurement:			
Count rate sample	R	R=(net area/counting time)–BK, cps	sR = s(net area) / counting time, cps
Count rate sample point source on top	R_+	R_+ = net area/ counting time, cps	sR_+ = s(net area) / counting time, cps
Density correction factor for the sample	KF	KF = ln (R_+ - R) / R_s / (R_+ - R) / R_s - 1	sKF is set to 0,01.
Activity in sample on measuring date	A	A = $G_k \cdot R \cdot KF / V$, Bq/kg	$sA = \sqrt{\left(\frac{sG\cdot R\cdot KF}{V}\right)^2+\left(\frac{sR\cdot G\cdot KF}{V}\right)^2+\left(\frac{sKF\cdot G\cdot R}{V}\right)^2+\left(\frac{-G\cdot R\cdot KF}{V^2}\right)^2}$, Bq/kg
Sample weight	V	kg	$1 \cdot 10^{-4}$ kg
Activity in sample on sampling date	A_0	$A_0 = \frac{A_{Pb-210}}{e^{-\ln\frac{2}{t\frac{1}{2}}t}}$, Bq/kg	

Quality assurance for Pb-210 measurements:

The standard used for calibrating the detector is delivered from QSA Global GmbH. The reference date is 1 of July 2008, with associated activity concentration of 7.46 kBq Pb-210, and a total uncertainty of 4.4%. It is calibrated at Deutscher Kalibrierdienst, DKD. Density is approximately 1.0 g/cm3 (Sværen, 2010). The standard is made in a 60 ml container, to have similar geometry as the samples. As well as measuring the standard, another reference sample (NKS-2017) with known activity were measured with satisfactory results (Table 10). The NKS-2017 sample is a sediment sample used in an intercomparison exercise, and is prepared by the Radiation and Nuclear Safety Authority of Finland (STUK).

Table 10: Measurements of ^{210}Pb standard and reference material at IMR.

Reference material	Reference value (Bq/kg d.w. ^{210}Pb)	Reference date	Detector used	Measured value (Bq/kg d.w. ^{210}Pb). Decay corrected to reference date	Measure date
Pb-210 STD	7460	01.07.2008	RAD12	7500 ± 765*	13.09.2018
Pb-210 STD	7460	01.07.2008	RAD12	7513 ± 766*	15.01.2019
Pb-210 STD	7460	01.07.2008	RAD14	7403 ± 754*	27.03.2019
NKS-2017	~256	24.02.2017	RAD12	241.4 ± 13.7	18.10.2018
NKS-2017	~256	24.02.2017	RAD12	248.6 ± 13.8	01.02.2019
NKS-2017	~256	24.02.2017	RAD12	265.0 ± 14.4	15.01.2019
NKS-2017	~256	24.02.2017	RAD14	251.9 ± 13.2	28.03.2019

* Sample not corrected for self-attenuation. analyzed using GammaVision, not according to Sværen, 2010.

3.5. LECO analyses

LECO analyses (for measuring the content of total organic carbon (TOC), total carbon (TC), and total sulphur (TS)) was performed by NGU on one core from each station in the Vefsnfjord. For the determination of TOC, TC and TS the instrument LECO SC-632 was used. For the determination of TC and TS the sediment sample is held in an oven with high temperatures (normally 1350 °C) with continually access to pure oxygen. The sample will then be completely combusted while producing CO_2 and SO_2. The gas can then be detected. When detecting TOC the sample is first treated with hydrochloric acid (HCl) to remove inorganic carbon. The methods are accredited and done at NGU laboratories (NGU, 2018).

4. RESULTS

All results are presented in appendix A, C and D.

4.1. Activity concentration in sediment samples from the Norwegian Trench

4.1.1. Cs-137

The activity concentrations in the four cores range from below detection limit (<0.4) to 2.8 ± 0.8 Bq/kg d.w. (Figure 4.1 and 4.2). Figure 4.1a-d shows the results for each of the four cores separately, while Figure 4.2 has all the cores in one figure, for easier comparison. Markers given with uncertainty bars are measurements above the detection limit. The detection limit is individual for all samples (chapter 3.3.3). The cores show similar vertical patterns, with activity concentrations typically higher in the upper most layers, and declining down the core. The activity concentrations are somewhat lower in the upper part of core 2. But taken the uncertainties into account, there is not much difference in the four cores. Because the activity concentrations are so low, almost at the limit of what the detector can measure, the uncertainties are high (ranging from 15 to 65%).

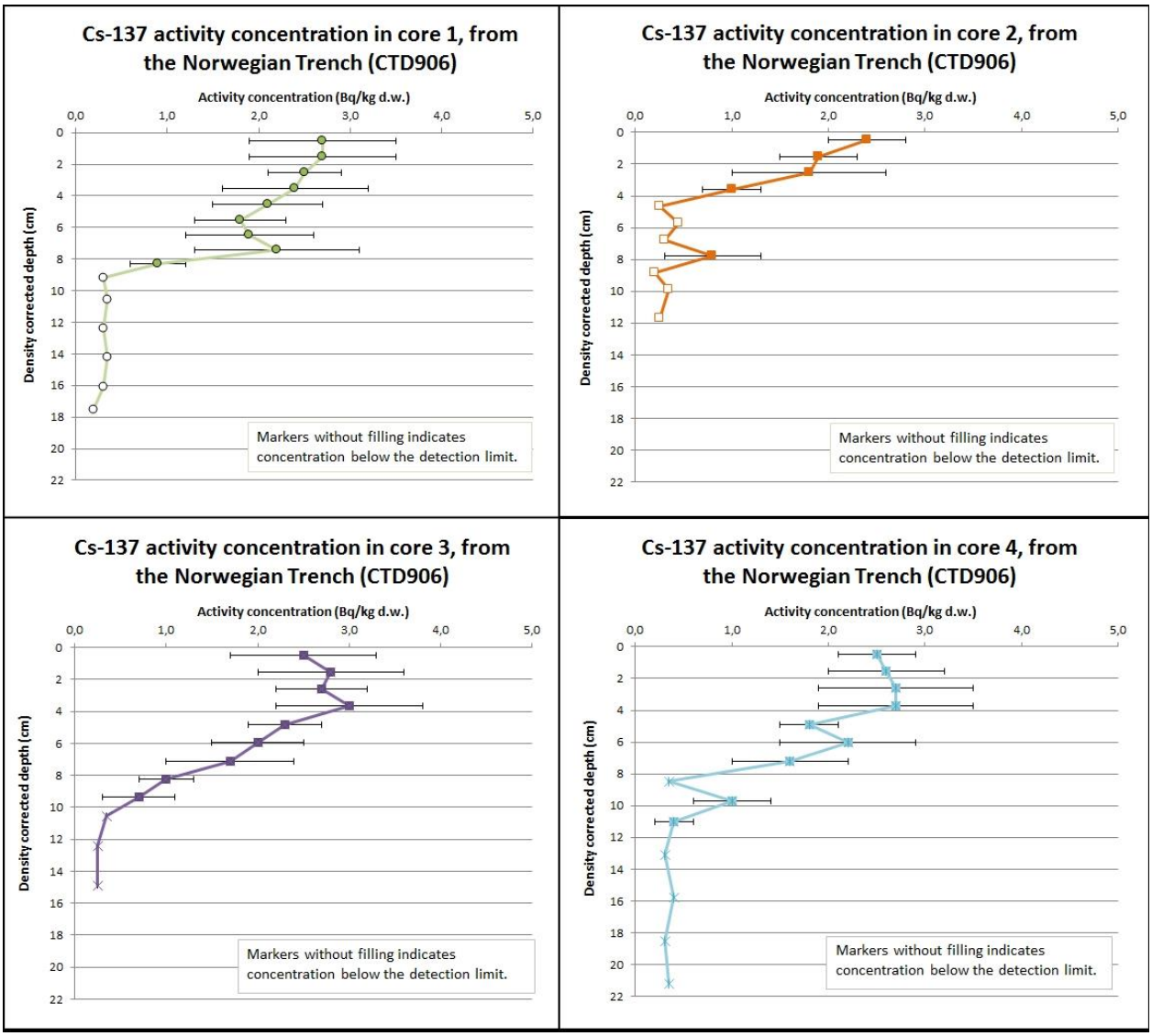

Figure 4.1 a-d: ^{137}Cs activity concentration (Bq/kg d.w.) in core 1-4 from the Norwegian Trench. All cores are taken from the same box corer (30*30*40 cm). Activity concentrations are given with 2σ uncertainties. Markers without filling and uncertainty bars indicates concentrations below the detection limit, and the results are given as half the detection limit. The depths (cm) are density corrected (chapter 2.7).

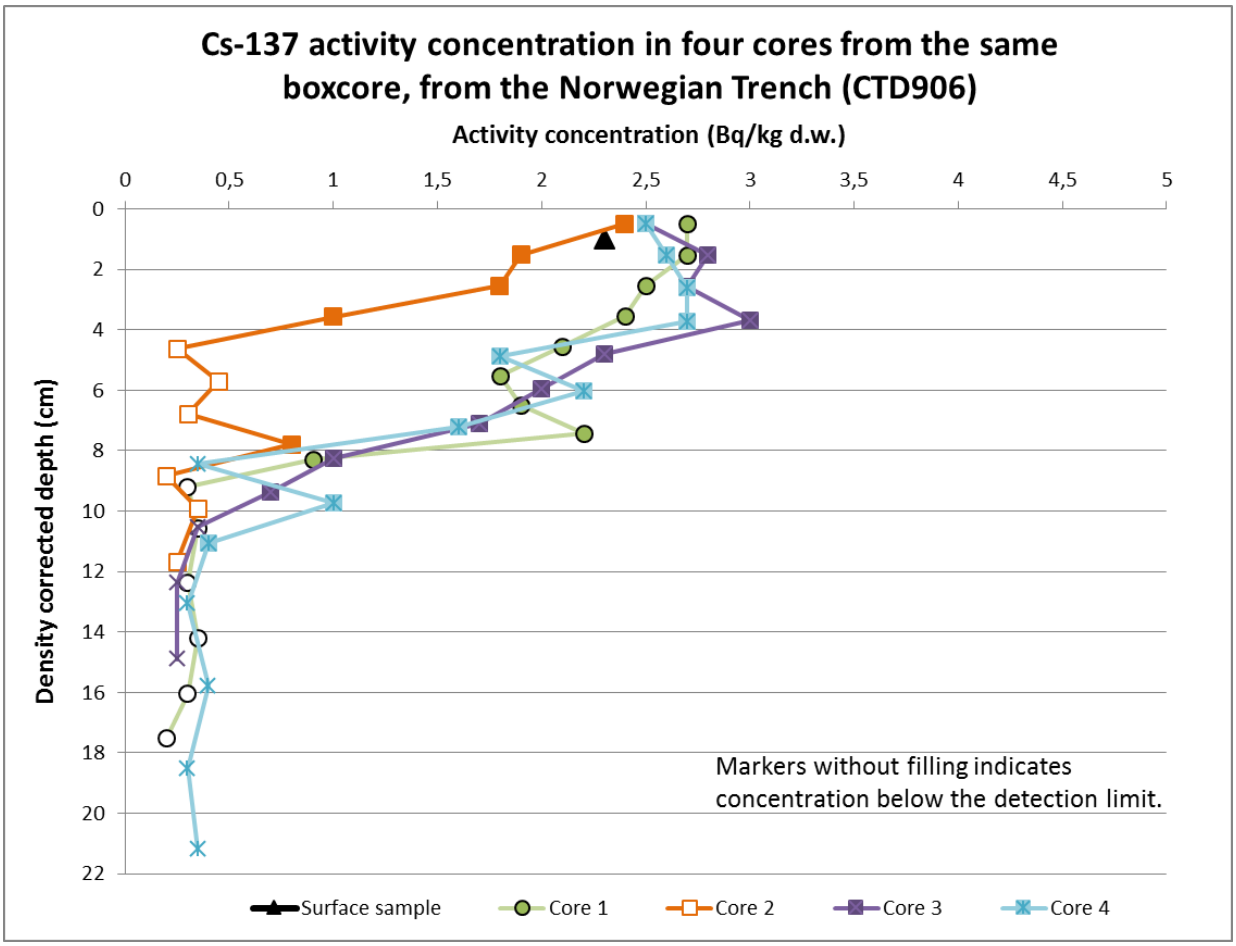

Figure 4.2: ^{137}Cs activity concentration in core 1-4 (from Figure 4.1) from the Norwegian Trench. All cores are taken from the same box corer (30*30*40 cm). Markers without filling indicates that the concentration is below the detection limit, and the results are given as half the detection limit. The depths (cm) are density corrected (chapter 2.7).

4.1.2. Ra-226 and Pb-210

The ^{226}Ra values range from approximately 27 to 39 Bq/kg d.w. within the core, for all four cores. The ^{210}Pb range from 179 to 207 Bq/kg d.w. in the uppermost layer, and from 29 to 42 Bq/kg d.w. at the bottom of the core, for all four cores (Figure 4.3 and 4.4). The ^{210}Pb and ^{226}Ra results are presented together because of the lead-dating method (see chapter 2.6). Figure 4.3a-d shows the results for each of the four cores separately, while Figure 4.4 has all the cores in one figure, for easier comparison. From the figures one can see that all the cores show the same trends, with relatively stable ^{226}Ra activity concentrations, and ^{210}Pb values decreasing rapidly downwards the core until stabilizing at the same activity concentrations as ^{226}Ra, at about 6 to 8 cm.

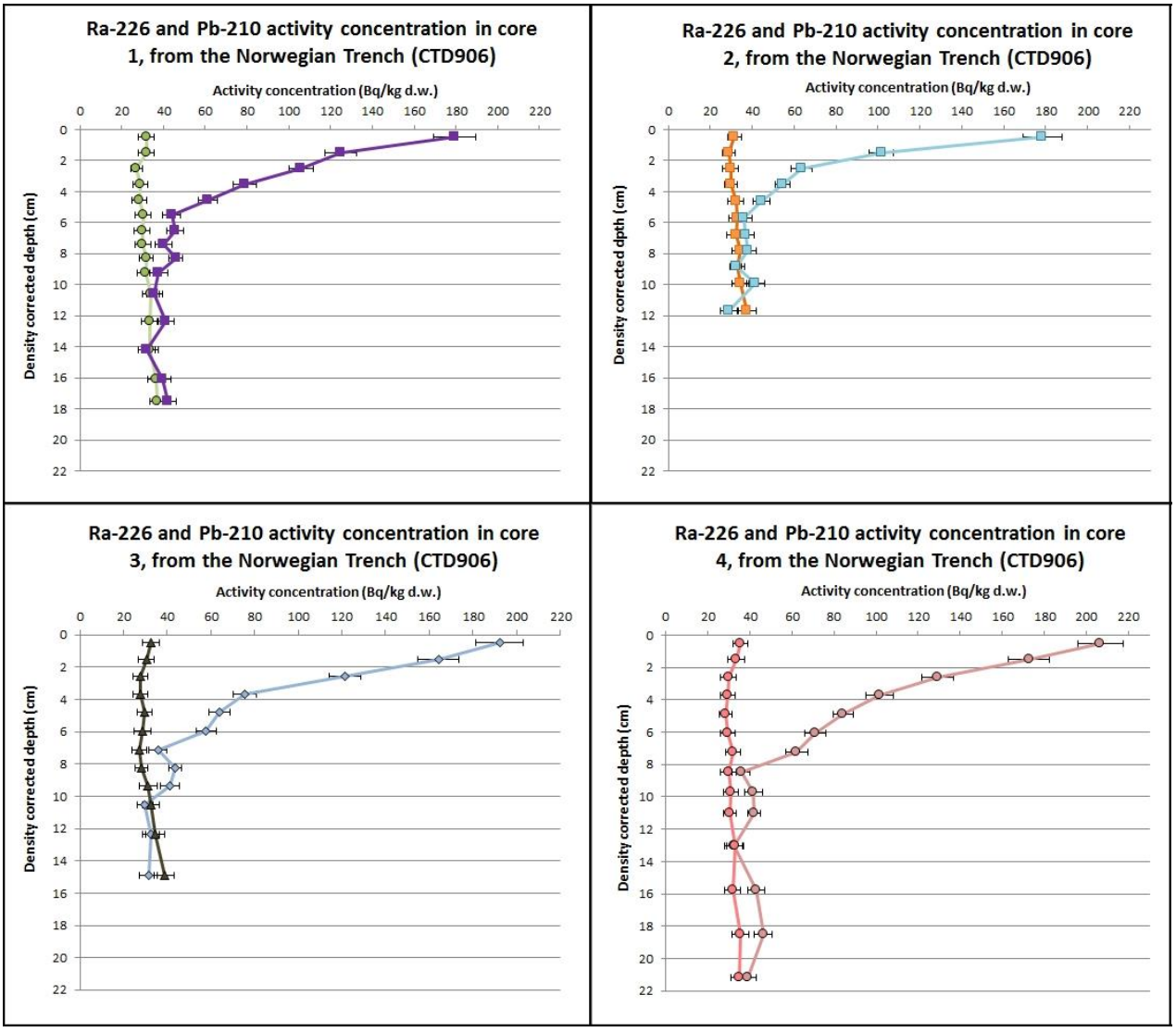

Figure 4.3 a-d: ^{226}Ra (straight lines) and ^{210}Pb (decreasing lines) activity concentration (Bq/kg d.w.) in core 1-4 from the Norwegian Trench. All cores are taken from the same box corer (30*30*40 cm). The horizontal bars show uncertainty (2σ) in activity concentration. The depths (cm) are density corrected (chapter 2.7).

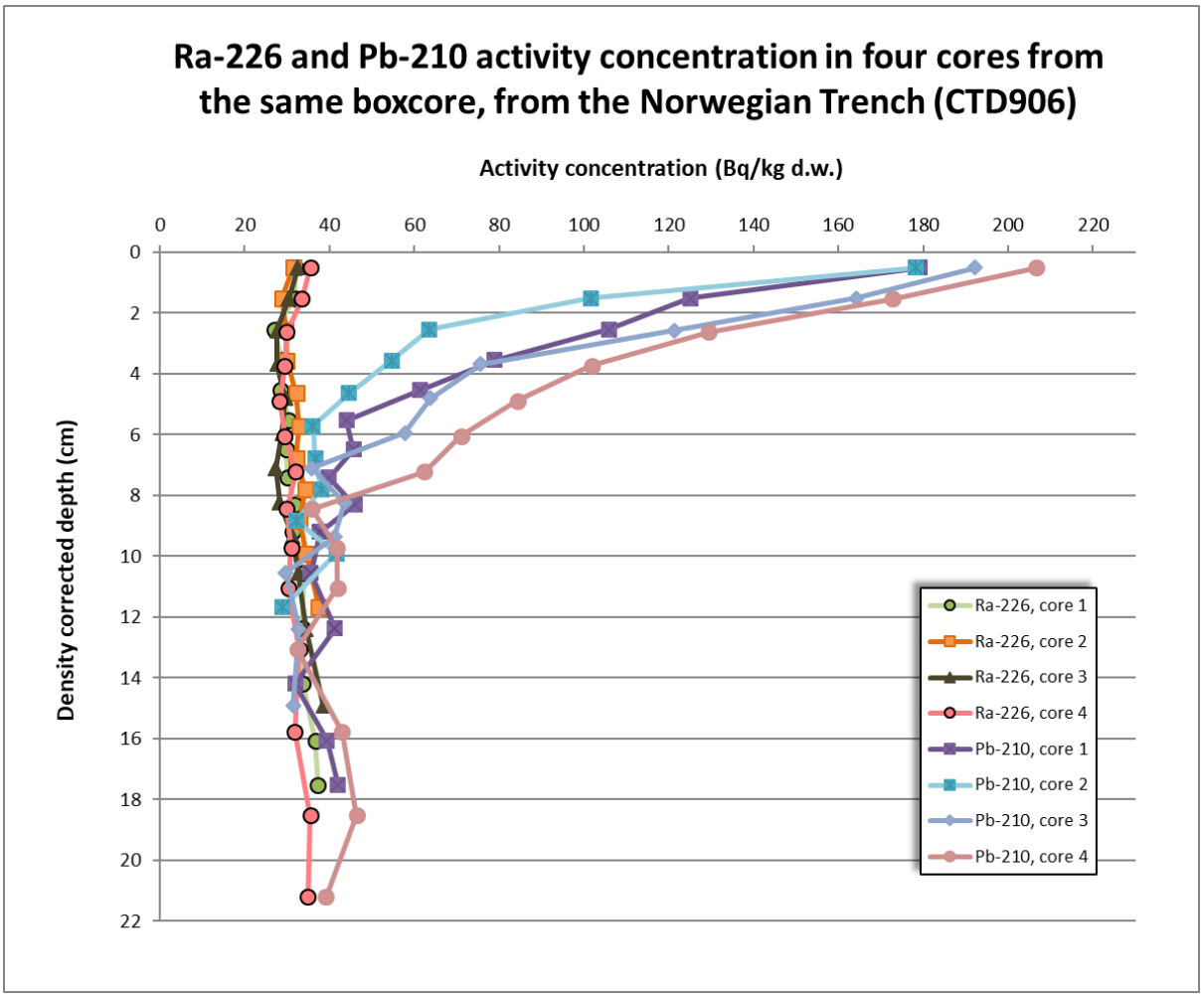

Figure 4.4: ^{226}Ra and ^{210}Pb activity concentration (Bq/kg d.w.) in core 1-4 from the Norwegian Trench. All cores are taken from the same box corer (30*30*40 cm). The depths (cm) are density corrected (chapter 2.7).

4.1.3. Ra-228

The ^{228}Ra activity concentrations range from about 38 to 55 Bq/kg d.w. In Figure 4.5a-d each of the cores is presented. The uncertainties were in the range of 12 to 14 %. In Figure 4.6 all the four cores are presented together, for easier comparison. Small variations between the cores are observed, but taken the uncertainty into account, none of the cores seems to stand out. All the cores show the same tendency; the activity concentration decreases with depth at first, increasing again further down the core. By looking at core four, which is the longest core, it may seem like the activity concentration is stabilising further down, but that is hard to confirm since all the other cores are shorter, and still increasing at the end.

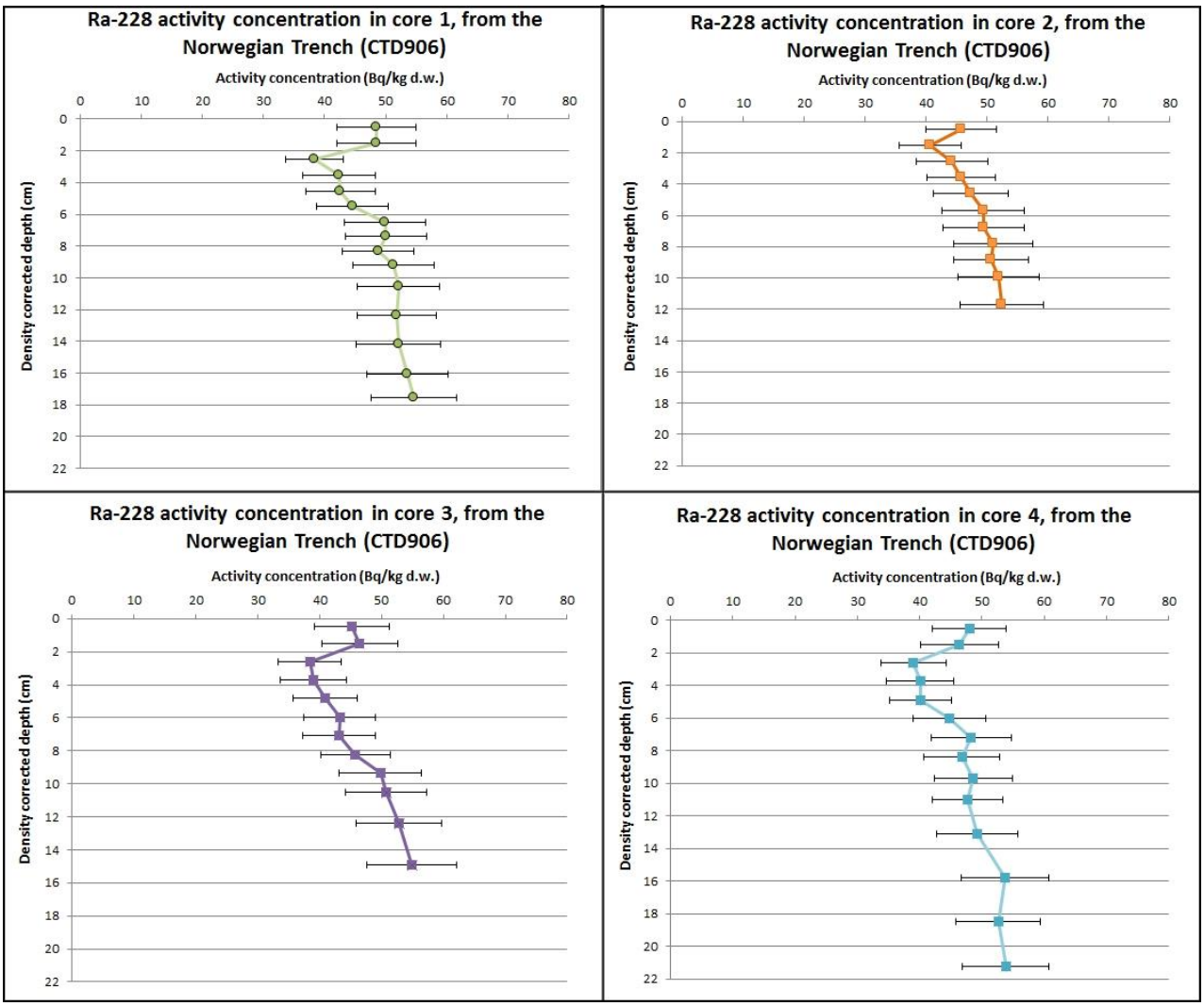

Figure 4.5 a-d: ^{228}Ra activity concentration (Bq/kg d.w.) in core 1-4 from the Norwegian Trench. All cores are taken from the same box corer (30*30*40 cm). The horizontal bars show uncertainty (2σ) in activity concentration. The depths (cm) are density corrected (chapter 2.7).

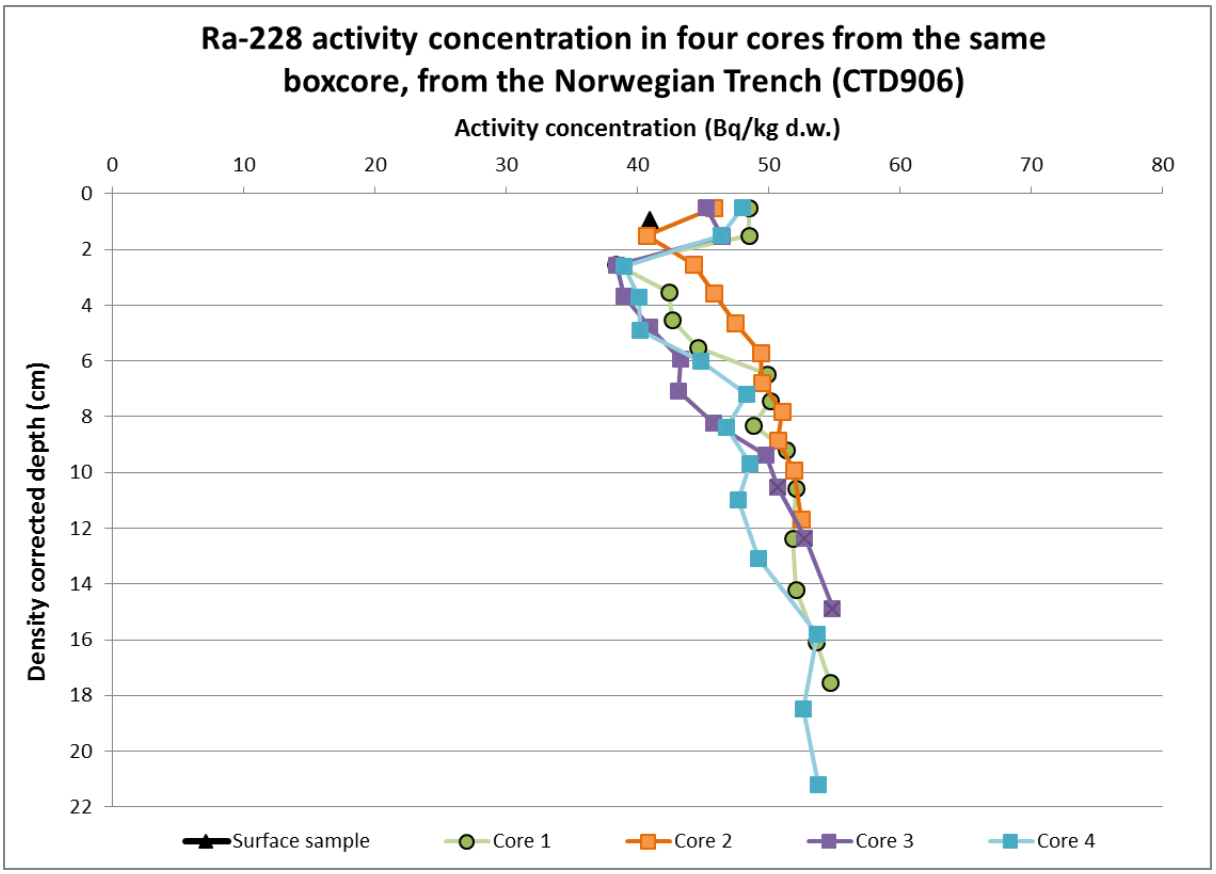

Figure 4.6: ^{228}Ra activity concentration (Bq/kg d.w.) in core 1-4 from the Norwegian Trench. All cores are taken from the same box corer (30*30*40 cm). The depths (cm) are density corrected (chapter 2.7).

4.1.4. K-40

The activity concentration in the samples from each core were in the range of 754 to 949 Bq/kg d.w (Figure 4.7a-d). The uncertainties were 9-10% for all samples. In Figure 4.8 all the four sediment cores are presented for better comparison. All cores show the tendency of increasing activity concentrations down the core, before stabilizing after about 8-10 cm. The activity concentration in the cores do not vary much, except in core 2, were the activity concentration is somewhat higher. Again, taking the uncertainties into account, there is not necessarily any significant variation between the cores.

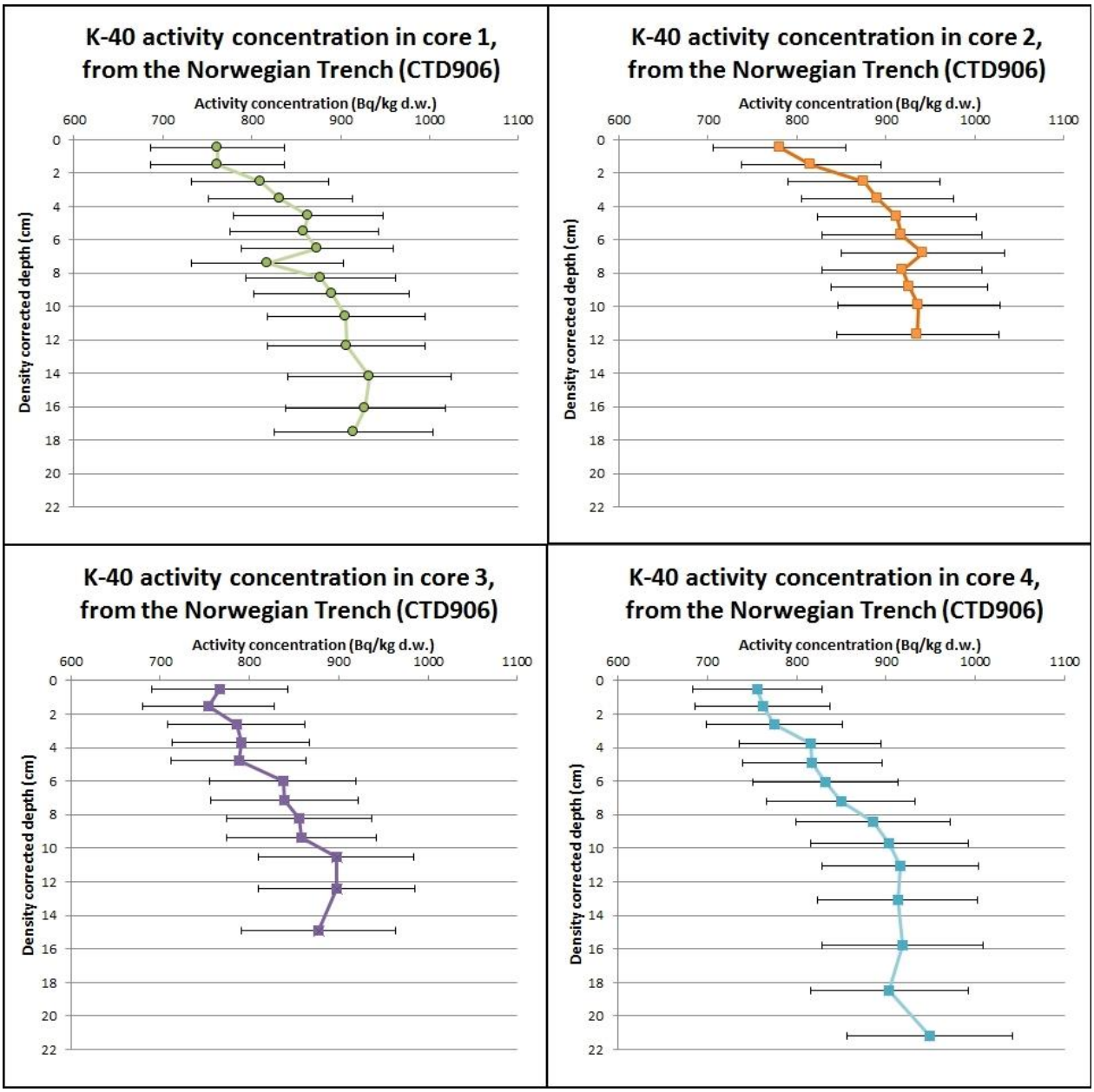

Figure 4.7 a-d: ^{40}K activity concentration (Bq/kg d.w.) in core 1-4 from the Norwegian Trench. All cores are taken from the same box corer (30*30*40 cm). The horizontal bars show uncertainty (2σ) in activity concentration. The depths (cm) are density corrected (chapter 2.7).

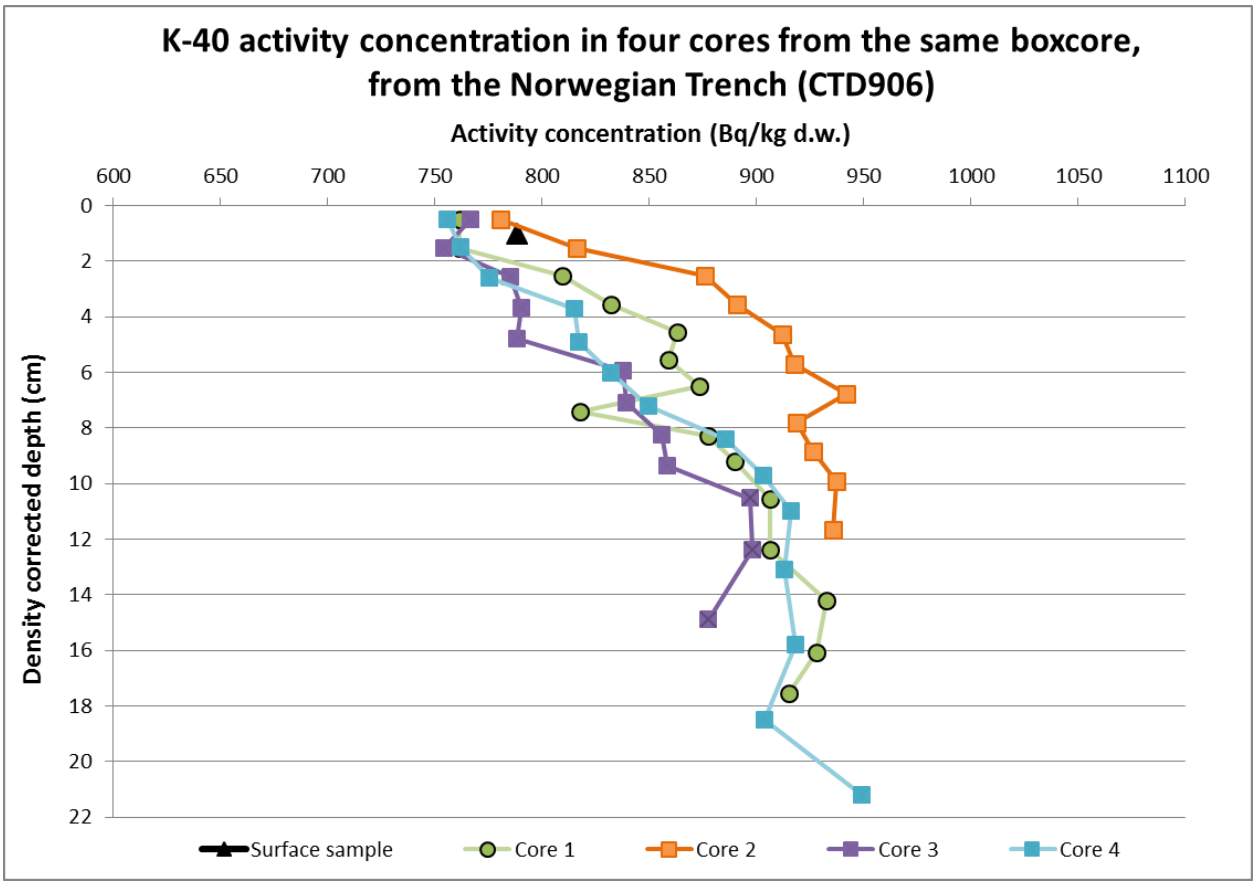

Figure 4.8: ^{40}K activity concentration (Bq/kg d.w.) in core 1-4 from the Norwegian Trench. All cores are taken from the same box corer (30*30*40 cm). The depths (cm) are density corrected (chapter 2.7).

4.2. Activity concentration in sediment samples from the Vefsnfjord

4.2.1. Cs-137

In Figure 4.9 the ^{137}Cs results from two cores from the same box corer is presented for the four sampling sites (CTD 1121-1124) in the fjord. The activity concentration in the surface samples vary from 125 to 185 Bq/kg.d.w., with the highest activity concentration at CTD1124. The cores (with exception of 1124-2) show a similar vertical trend, with a clear maximum-peak in activity concentration in the cores. For both cores in Figure 4.9a, the peak is present further down the core than for the other cores. In these cores, as well as core 1 in Figure 4.9b, the highest activity concentrations are found. The maximum activity concentration ranges from 225 to 432 Bq/kg d.w for the eight cores. Uncertainties ranged from 9 to 12% for all samples. While the two cores at CTD1123 and CTD1124 agrees well, there are larger differences between the two cores taken at CTD1121 and CTD1122. Similar for all cores is that the activity concentration declines rapidly after the maximum peak.

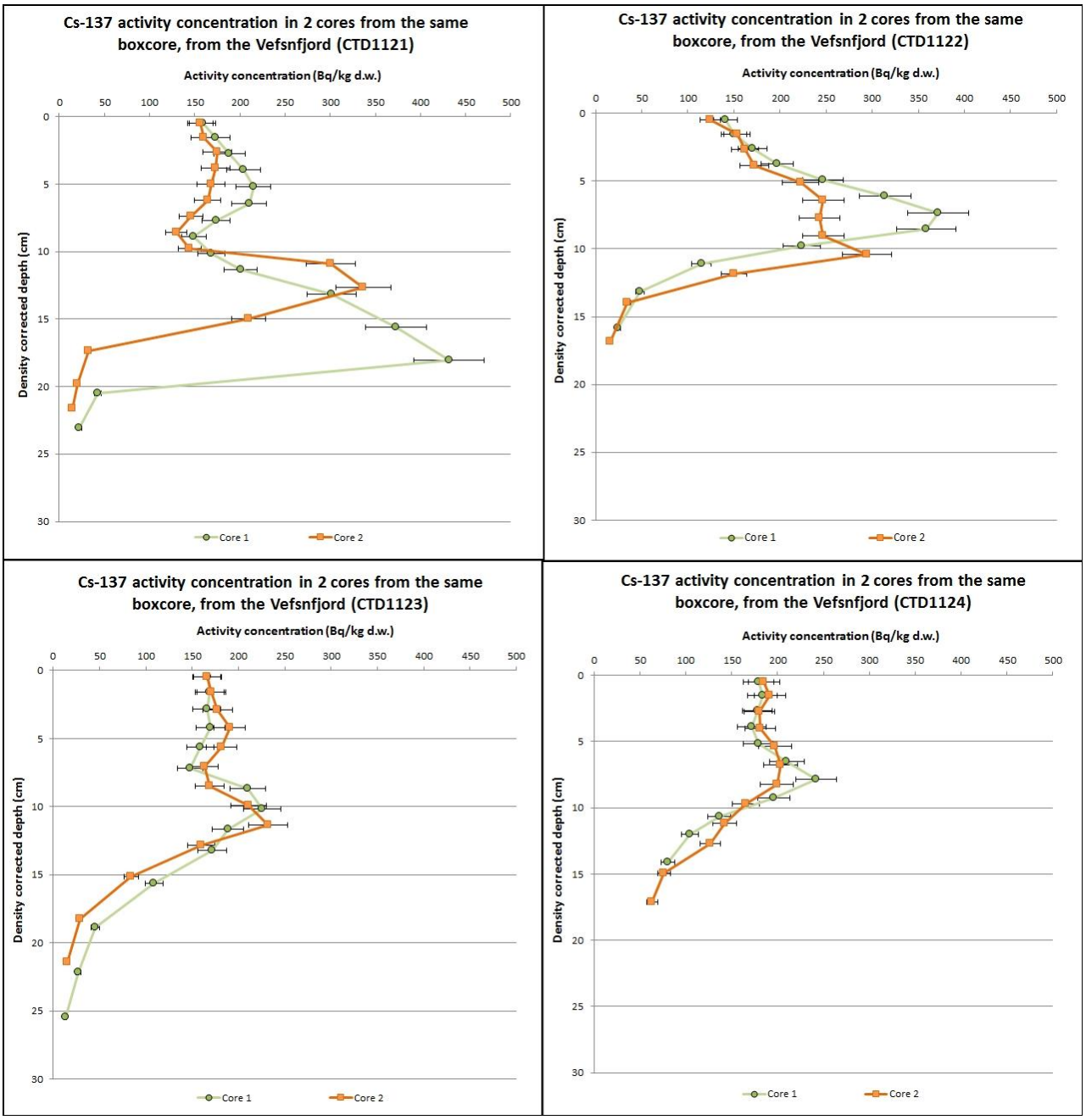

Figure 4.9a-d: ^{137}Cs activity concentration (Bq/kg d.w.) in two cores, at four different sites in the Vefsnfjord (CTD 1121-1124). Both cores are taken from the same box corer (30*30*40 cm). The horizontal bars show uncertainty (2σ) in activity concentration. The depths (cm) are density corrected (chapter 2.7).

4.2.2. Ra-226 and Pb-210

In Figure 4.10 the ^{226}Ra and ^{210}Pb results are presented. As for the results from the Norwegian Trench, these results are also presented together because of the lead-dating method (see chapter 2.6). From the figures one can see that the ^{226}Ra activity concentrations for all the cores are relatively stable downward the cores. In the cores from CTD1122 and CTD1123 and

partly CTD1124 there are somewhat elevated levels in the upper sediment layers. The ^{210}Pb values are decreasing downwards the core for all cores. In CTD1121 however, an increase in activity concentration is measured at the lower half of the core. The ^{226}Ra values range from approximately 23 to 54 Bq/kg d.w., and the ^{210}Pb ranged from approximately 183 to 279 Bq/kg d.w. in the uppermost layer, and from 24 to 68 Bq/kg d.w. at the bottom of the core.

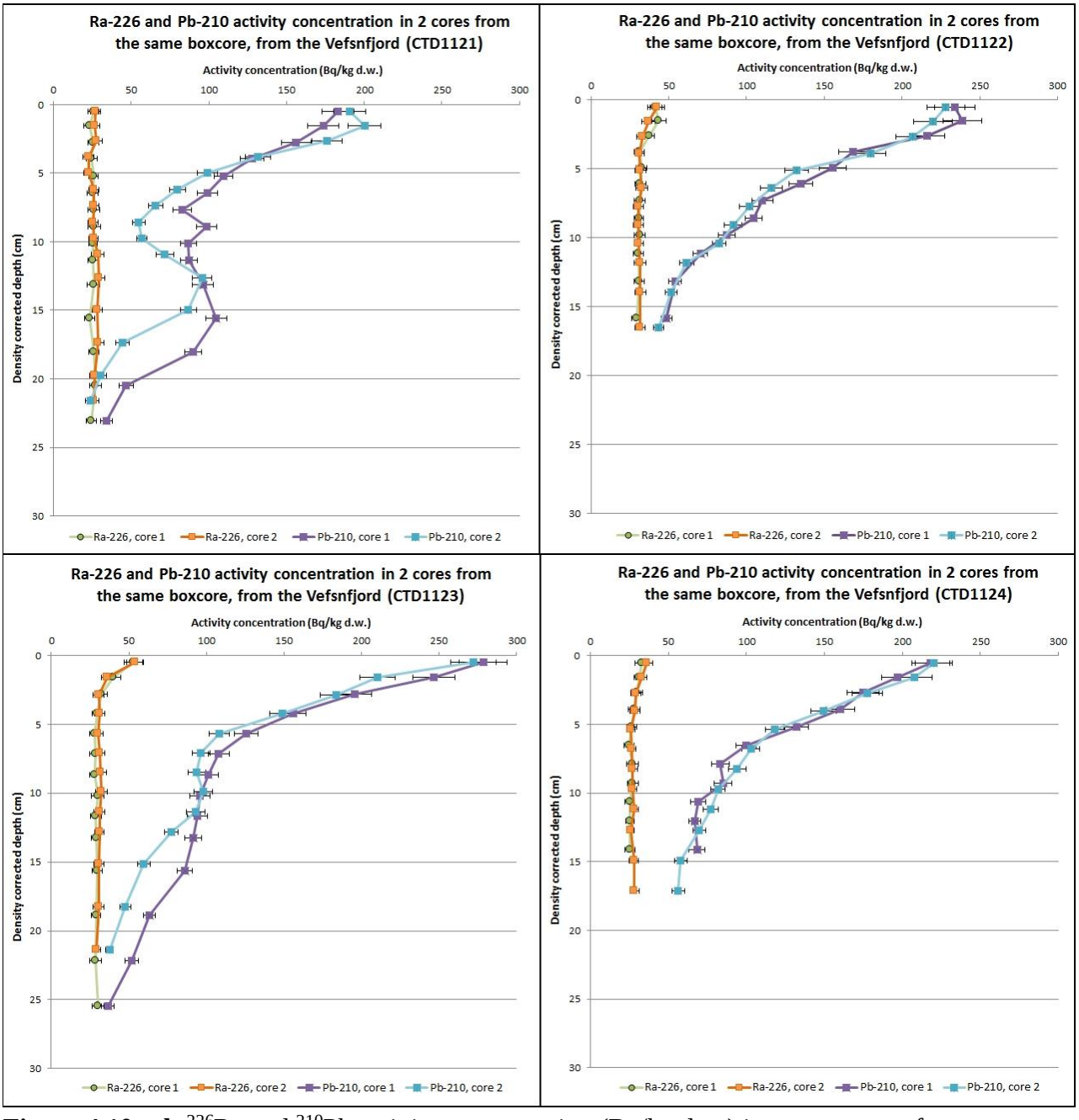

Figure 4.10a-d: ^{226}Ra and ^{210}Pb activity concentration (Bq/kg d.w.) in two cores, at four different sites in the Vefsnfjord (CTD 1121-1124). Both cores are taken from the same box corer (30*30*40 cm). The horizontal bars show uncertainty (2σ) in activity concentration. The depths (cm) are density corrected (chapter 2.7).

4.2.3. Ra-228

The ^{228}Ra activity concentrations range from about 28 to 79 Bq/kg d.w. and uncertainties from 12 to 17% for all samples. Figure 4.11 show that the two cores from the same box corer agrees well, with only small variations. In the cores from CTD1122, CTD1123 and partly CTD1124 there are elevated levels in the upper sediment layers, before decreasing a few cm down the core. Further down, the activity concentration seems to increase slightly in all the cores, except the two cores from CTD1122.

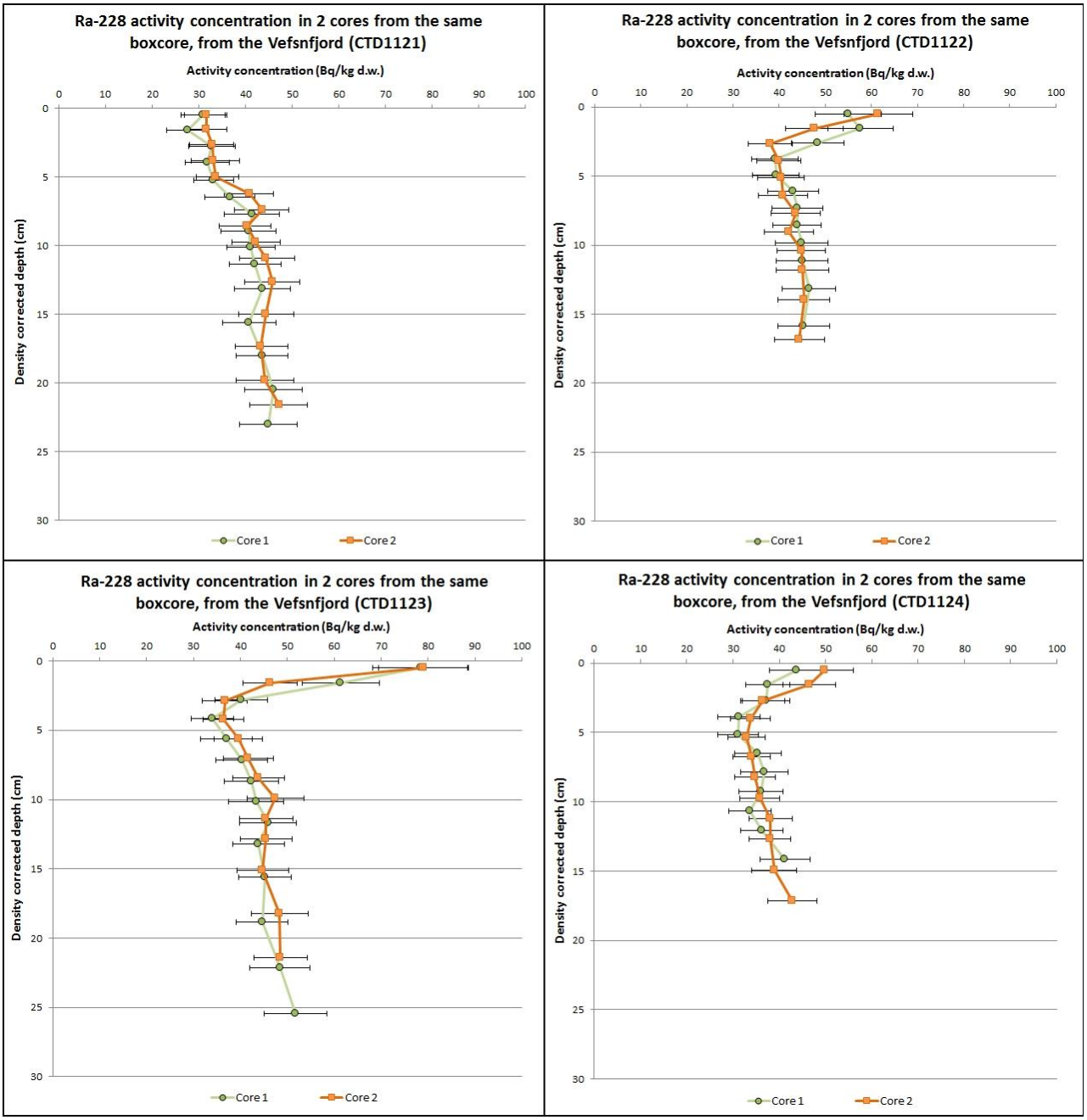

Figure 4.11a-d: ^{228}Ra activity concentration (Bq/kg d.w.) in two cores, at four different sites in the Vefsnfjord (CTD 1121-1124). Both cores are taken from the same box corer (30*30*40

cm). The horizontal bars show uncertainty (2σ) in activity concentration. The depths (cm) are density corrected (chapter 2.7).

4.2.4. K-40

The activity concentrations of ^{40}K range from 581 to 775 Bq/kg d.w. and the uncertainties range from 9-10% (Figure 4.12). The two cores from the same box corer shows good agreement, with all samples within the uncertainty calculations. There is some variation between the different sampling sites. CTD1121 and CTD1123 shows relatively stable activity concentration downward the cores, and so does CTD1122, except for a slight increase in the uppermost sediment layers. The cores at CTD1124 stands out from the rest of the cores, with decreasing activity concentrations downward the cores, before increasing again.

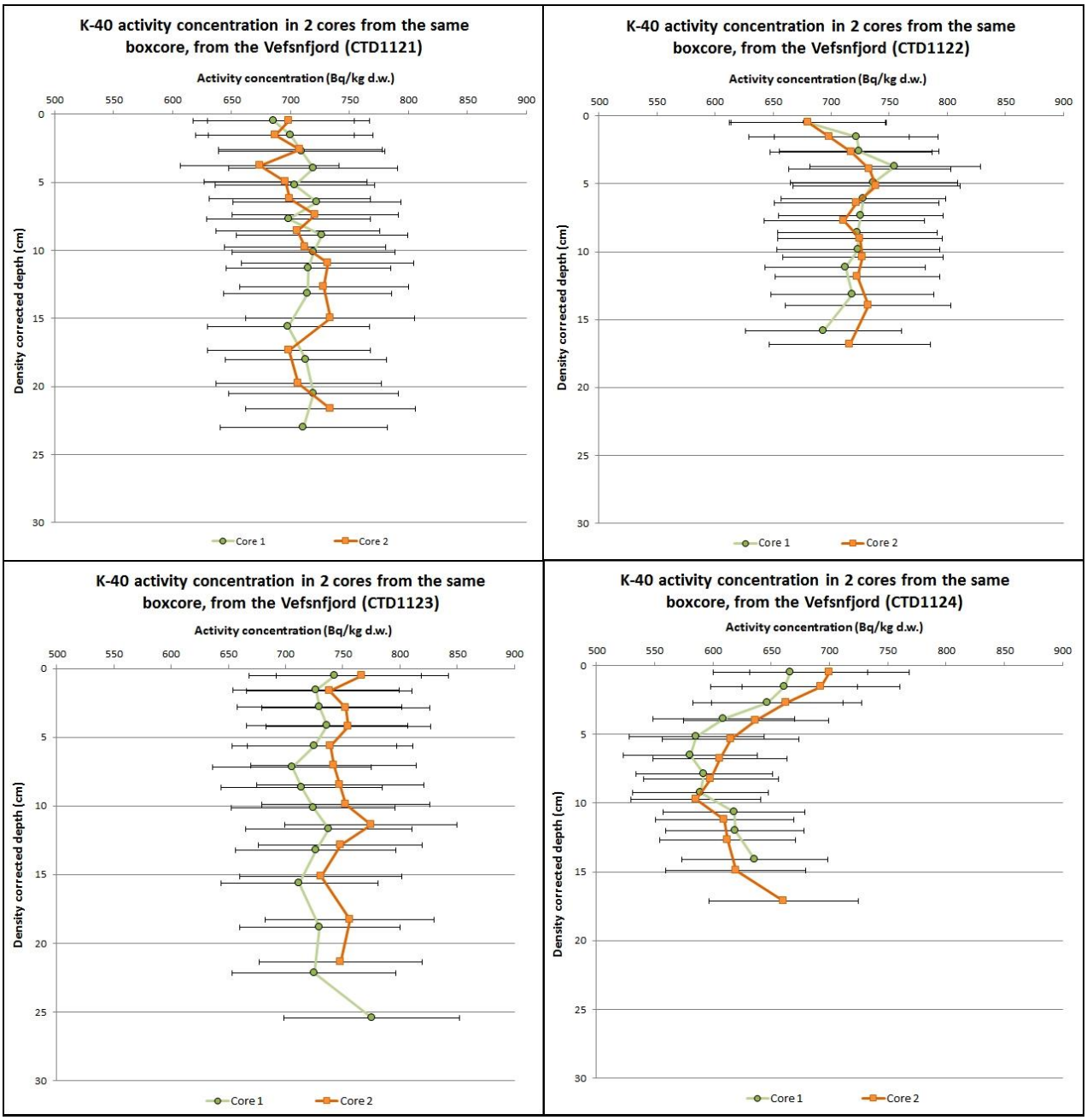

Figure 4.12a-d: ^{40}K activity concentration (Bq/kg d.w.) in two cores, at four different sites in the Vefsnfjord (CTD 1121-1124). Both cores are taken from the same box corer (30*30*40 cm). The horizontal bars show uncertainty (2σ) in activity concentration. The depths (cm) are density corrected (chapter 2.7).

4.3. LECO analyses in sediment samples from the Vefsnfjord

Analyses of content of total sulphur, total carbon and total organic carbon in one core from each location in the Vefsnfjord was performed by NGU (Table 11 and 12). The content of sulphur ranges from 0.10 to 0.49 % for all samples, where the highest levels was found in the lower layers in the cores. The content of total carbon ranges from 1.4 to 2.9 % for all samples. The content of total carbon is found to be stable within the core, but vary slightly between the locations in the fjord. The highest levels were found at CTD1121, and the lowest levels at CTD1124. For total organic carbon (TOC), the content ranges from 1.0 to 2.0 % for all samples. Also, for TOC, the values are mostly stable within the core, but with some variations between the stations. The highest TOC content was found at CTD1121 and the lowest content at CTD1124.

The results given in Table 11 and Table 12 is given with following uncertainties from NGU: 30 % for sulphur (measuring range 0.02-2.0 %) 15 % for total carbon (measuring range 0.4-60 %), and 25 % for TOC (measuring range 0.1-3.0 %).

Table 11: Content of total sulphur (%), total carbon (%) and total organic carbon (TOC) (%) in samples from CTD1121 and 1122.

CTD1121				CTD1122			
Depth	Sulphur (%)	Carbon (%)	TOC (%)	Depth	Sulphur (%)	Carbon (%)	TOC (%)
0-1cm	0,175	2,78	1,98	0-1cm	0,164	2,09	1,41
1-2cm	0,176	2,81	1,95	1-2cm	0,139	2,12	1,52
2-3cm	0,192	2,76	2,02	2-3cm	0,139	2,07	1,45
3-4cm	0,235	2,81	1,92	3-4cm	0,137	1,95	1,31
4-5cm	0,263	2,81	1,87	4-5cm	0,138	1,93	1,30
5-6cm	0,260	2,80	1,92	5-6cm	0,153	1,90	1,23
6-7cm	0,279	2,85	1,85	6-7cm	0,153	1,89	1,20
7-8cm	0,296	2,82	1,89	7-8cm	0,148	1,88	1,24
8-9cm	0,310	2,84	1,91	8-9cm	0,154	1,95	1,22
9-10cm	0,299	2,88	2,02	9-10cm	0,127	1,85	1,19
10-12cm	0,321	2,86	2,01	10-12cm	0,136	1,76	1,14
12-14cm	0,463	2,87	1,90	12-14cm	0,161	1,75	1,20
14-16cm	0,491	2,90	1,91	14-16cm	0,239	1,68	1,18
16-18cm	0,464	2,79	1,82				
18-20cm	0,409	2,71	1,73				

Table 12: Content of total sulphur (%), total carbon (%) and total organic carbon (TOC) (%) in samples from CTD1123 and 1124.

CTD1123				CTD1124			
Depth	Sulphur (%)	Carbon (%)	TOC (%)	Depth	Sulphur (%)	Carbon (%)	TOC (%)
0-1cm	0,155	1,99	1,46	0-1cm	0,140	1,90	1,52
1-2cm	0,145	2,04	1,66	1-2cm	0,111	1,79	1,37
2-3cm	0,127	1,92	1,53	2-3cm	0,106	1,68	1,25
3-4cm	0,104	1,82	1,39	3-4cm	0,103	1,49	1,07
4-5cm	0,119	1,72	1,37	4-5cm	0,110	1,43	1,12
5-6cm	0,151	1,81	1,27	5-6cm	0,107	1,45	1,03
6-7cm	0,138	1,81	1,31	6-7cm	0,101	1,48	1,03
7-8cm	0,141	1,72	1,36	7-8cm	0,122	1,45	1,04
8-9cm	0,149	1,76	1,28	8-9cm	0,124	1,45	1,03
9-10cm	0,157	1,68	1,32	9-10cm	0,115	1,41	1,05
10-12cm	0,166	1,75	1,29	10-12cm	0,127	1,47	1,05
12-14cm	0,184	1,73	1,33				
14-16cm	0,239	1,84	1,43				
16-18cm	0,324	1,88	1,46				

4.4. lead-210 dating

4.4.1. Results from the Norwegian Trench

The sedimentation rates for the four cores in the Norwegian Trench (CTD906) were determined from the slope of an exponential curve fit basted on unsupported ^{210}Pb in the 6-7 uppermost layers in each core, according to Tadjiki & Erten (1994) (chapter 2.6.2) (Figure 4.13). The sedimentation rates for the four cores, without considering effects of potential mixing or doing any corrections, range from 0.07 to 0.12 cm/year (Table 13). None of the cores had any clear ^{137}Cs- peak that could be used to compare the sedimentation rates calculated from the ^{210}Pb results. The age of the sediment layers was also determined by the CRS method (chapter 2.6.1) (Table 14). The ages calculated at the same depth for different sediment cores showed quite different results. From the results obtained from the CRS method, sedimentation rates were calculated to easier compare the CRS method with the sedimentation rates calculated according to Tadjiki & Erten (1994). The sedimentation rates calculated from the CRS method ranged from 0.03 to 0.12 cm/year for the four cores (Table 14).

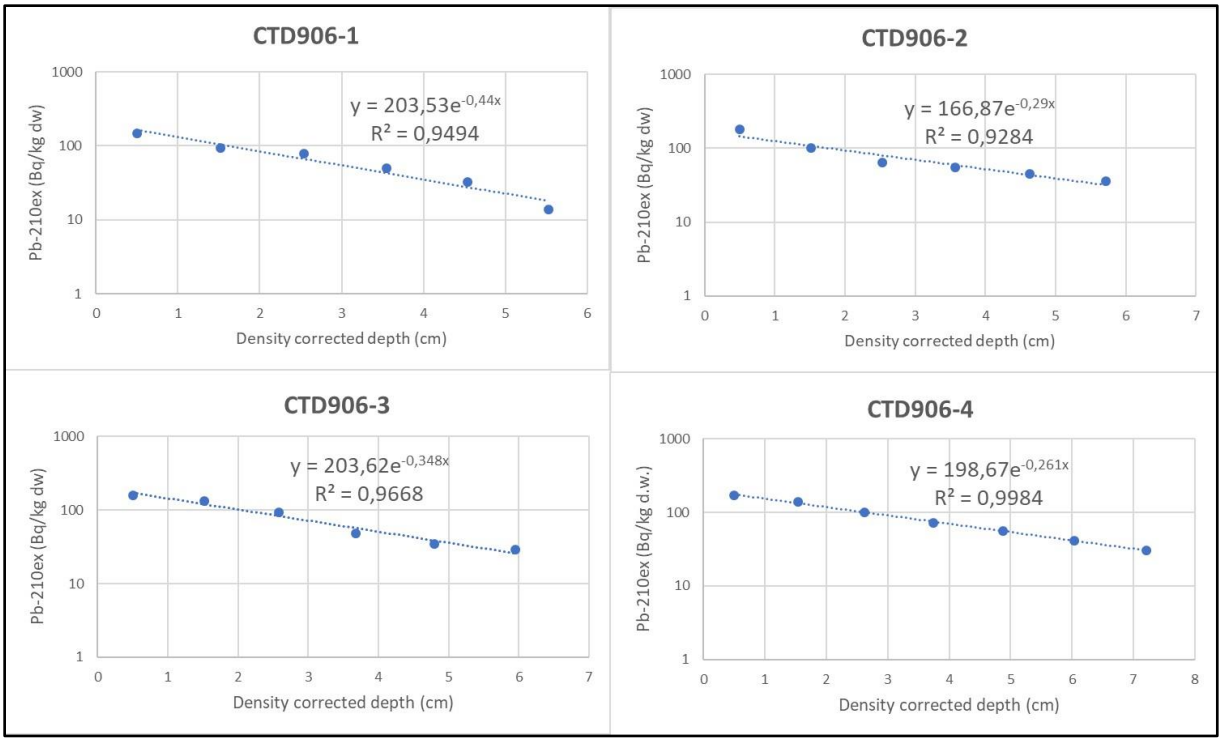

Figure 4.13: Plot of unsupported ^{210}Pb (Bq/kg d.w.) against density corrected depth (cm) in the sediment cores from the Norwegian Trench.

Table 13: Sedimentation rates (cm/year) in sediment cores from the Norwegian Trench.

CTD906	Sedimentation rate (cm/year)	Average sedimentation rate (cm/year) using CRS method
Core 1	0.07	0.09
Core 2	0.11	0.03
Core 3	0.09	0.06
Core 4	0.12	0.12

Table 14: Dating results for sediment cores from the Norwegian Trench, using the CRS model.

	906-1		906-2		906-3		906-4	
Depth	**CRS model (year)**	**Sedimentation rate (cm/year)**	**CRS model (year)**	**Sedimentation rate (cm/year)**	**CRS model (year)**	**Sedimentation rate (cm/year)**	**CRS model (year)**	**Sedimentation rate (cm/year)**
0-1cm	2007	0,046	1997	0,024	2008	0,051	2010	0,063
1-2cm	1996	0,070	1974	0,035	1995	0,066	2001	0,093
2-3cm	1985	0,076	1956	0,041	1978	0,065	1993	0,106
3-4cm	1971	0,076	1919	0,036	1963	0,067	1985	0,113
4-5cm	1961	0,080			1945	0,066	1976	0,115
5-6cm	1956	0,088					1966	0,116
6-7cm	1949	0,093					1956	0,117
7-8cm	1943	0,099					1954	0,132
8-9cm	1934	0,098					1949	0,141
9-10cm	1927	0,101					1942	0,146
10-12cm	1923	0,111					1943	0,174
12-14cm							1922	0,165
Average sedimentation rate (cm/year):		0,09		0,03		0,06		0,12

4.4.2. Results from the Vefsnfjord

The sedimentation rates for the cores in the Vefsnfjord (CTD 1122-1124) were determined from the slope of an exponential curve fit basted on unsupported ^{210}Pb in the entire core, according to Tadjiki & Erten (1994) (chapter 2.6.2) (Figure 4.14). Results from CTD1121 is not included, due to the two cores not being ideal for determination of sedimentation rates because of its uneven decrease in ^{210}Pb (Figure 4.10a). The sedimentation rates for the six remaining cores, without considering effects of potential mixing or doing any corrections, range from 0.18 to 0.27 cm/year (Table 15). Also, the ^{137}Cs-peak in the cores (Figure 4.9) were used to determine sedimentation rates, to compare with the ^{210}Pb method (chapter 2.6.3). The sedimentation rates using ^{137}Cs range from 0.17 to 0.23 cm/year (Table 15). The age of the sediment layers was determined by the CRS method (Table 16) (chapter 2.6.1). From the CRS method, sedimentation rates were determined, to easier compare the CRS method to the sedimentation rates calculated from Tadjiki & Erten (1994). The sedimentation rates determined from the CRS method ranged from 0.14 to 0.21 cm/year.

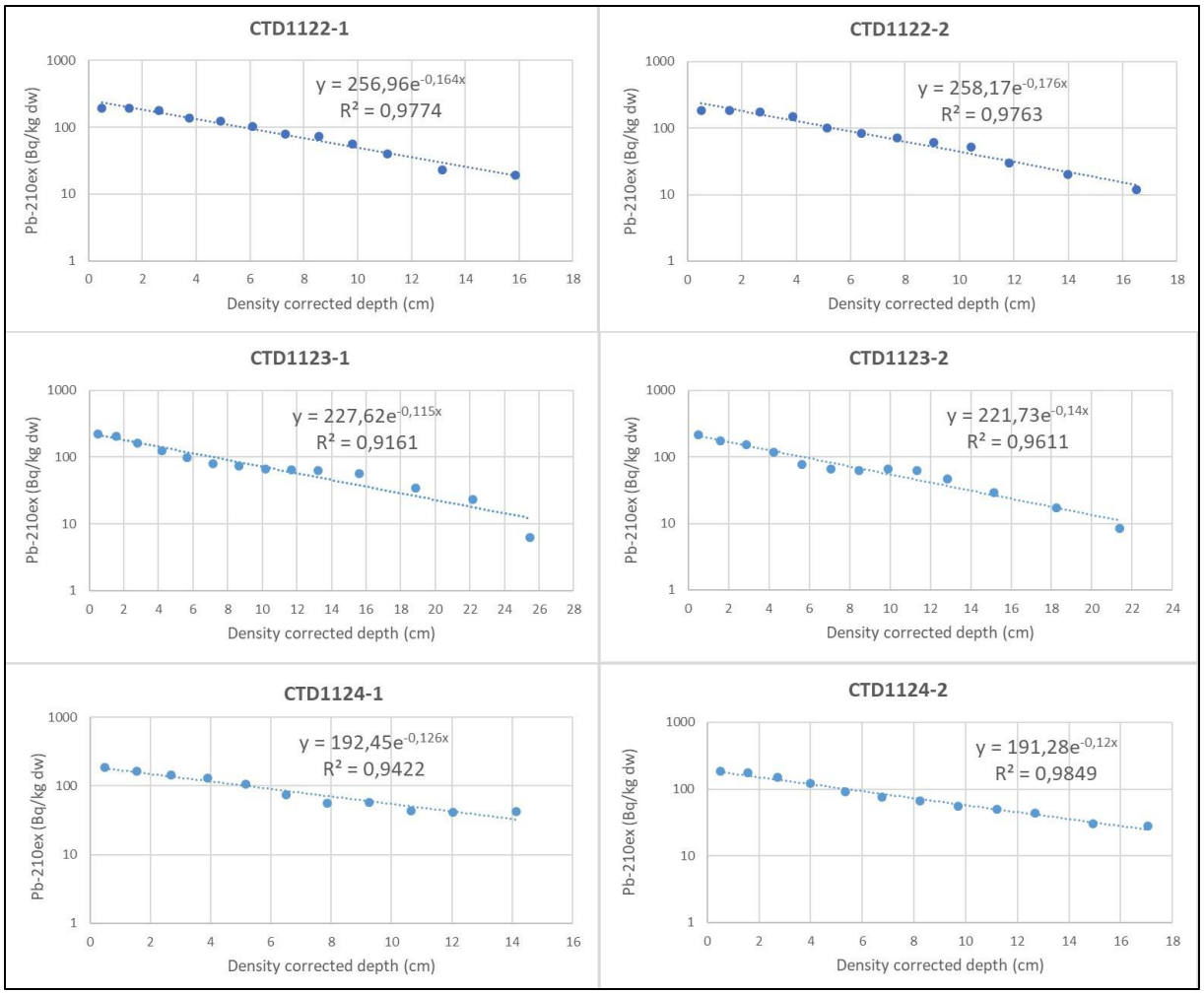

Figure 4.14: Plot of unsupported ^{210}Pb (Bq/kg d.w.) against density corrected depth (cm) in cores from the Vefsnfjord.

Table 15: Sedimentation rates (cm/year) in cores from the Vefsnfjord.

Sampling site		Sedimentation rate (cm/year) using ^{210}Pb	Sedimentation rate (cm/year) using ^{137}Cs	Average sedimentation rate (cm/year) using CRS method
CTD1122	Core 1	0.19	0.20	0.15
	Core 2	0.18	0.27	0.14
CTD1123	Core 1	0.27	0.23	0.21
	Core 2	0.22	0.27	0.17
CTD1124	Core 1	0.25	0.20	0.15
	Core 2	0.26	0.17	0.17

Table 16: Dating results for sediment cores from the Vefsnfjord, using the CRS model.

	CTD1122-1		CTD1122-2	
Depth	**CRS model (year)**	**Sedimentation rate (cm/year)**	**CRS model (year)**	**Sedimentation rate (cm/year)**
0-1cm	2015	0,12	2014	0,09
1-2cm	2009	0,16	2009	0,15
2-3cm	2003	0,16	2002	0,15
3-4cm	1995	0,16	1993	0,15
4-5cm	1988	0,16	1985	0,15
5-6cm	1979	0,15	1977	0,15
6-7cm	1971	0,15	1965	0,14
7-8cm	1961	0,15	1954	0,14
8-9cm	1950	0,14	1938	0,13
9-10cm	1936	0,13	1922	0,12
Average sedimentation rate (cm/year):		0,15		0,14

Table 16 continued: Dating results for sediment cores from the Vefsnfjord, using the CRS model.

	CTD1123-1		CTD1123-2		CTD1124-1		CTD1124-2	
Depth	**CRS model (year)**	**Sedimentation rate (cm/year)**	**CRS model (year)**	**Sedimentation rate (cm/year)**	**CRS model (year)**	**Sedimentation rate (cm/year)**	**CRS model (year)**	**Sedimentation rate (cm/year)**
0-1cm	2015	0,14	2013	0,08	2013	0,09	2014	0,11
1-2cm	2010	0,17	2007	0,14	2008	0,14	2009	0,16
2-3cm	2005	0,20	2001	0,16	2002	0,16	2003	0,17
3-4cm	2000	0,22	1994	0,17	1995	0,17	1997	0,18
4-5cm	1994	0,23	1987	0,18	1988	0,17	1990	0,19
5-6cm	1989	0,24	1982	0,19	1980	0,17	1983	0,19
6-7cm	1983	0,24	1976	0,20	1973	0,17	1975	0,19
7-8cm	1978	0,25	1969	0,20	1963	0,17	1967	0,19
8-9cm	1971	0,25	1959	0,19	1955	0,17	1957	0,18
9-10cm	1964	0,24	1947	0,18	1941	0,15	1943	0,17
10-12cm	1945	0,21	1923	0,16				
12-14cm	1922	0,20						
Average sedimentation rate (cm/year):		0,21		0,17		0,15		0,17

5. DISCUSSION

5.1. Local variation in sediment samples

Most of the time there were good agreement between the cores sampled from the same box corer with regards to radionuclide content (Figure 4.1-4.12). This is the case for both the samples taken in the Norwegian Trench and in the Vefsnfjord. From the results, one can assume local homogeneity in the sediments, resulting in no or little variation in radionuclide content. Minor variation in these cases may be caused when sampling, preparing or measuring the sediment samples. However, at most cases the results were within estimated uncertainties.

In some cases, some variation between the sediment profiles from the same box corer is found. An example is core number two from the Norwegian Trench (CTD906-2), which stands out a bit from the other three cores both when measuring ^{137}Cs and ^{40}K. There can be several causes for these results. For ^{137}Cs the activity concentration is very low, and the results have large uncertainties, so the results may be arbitrary (chapter 5.3.1). For ^{40}K, which is present in varies amounts in different sediments, varying sediment composition within the box corer may explain the results (chapter 5.3.3). Another reason that may cause local variation between the sediment cores is bioturbation. Bioturbation is rework of soils and sediments by organisms, and is considered one of the major processes affecting aquatic eco-system functions, causing incorporation of radionuclides in sediments, and vertical redistribution of sediments and radionuclides (Cournane et al., 2010). Crusius et al. (2004) have found disturbance caused by bioturbation to depths of 25-35 cm in sediment cores, and in a microcosm experiment Cournane et al. (2010) found that as much as 35% of a ^{137}Cs-labelled particulate tracer deposited on the surface was redistributed to depths of up to 11 cm by polychaete over a 40-day experiment. Bioturbation may therefore be why ^{137}Cs is found in deeper sediment layers than expected from dating results in the Vefsnfjord (chapter 5.5.2).

The sediment cores were dated using ^{210}Pb and the CRS method. Sediment layers from the same depth in different cores collected from the same box corer in the Norwegian Trench showed quite different ages. Especially one of the four cores stood out (CTD906-2). Reasons for the varying results may be disturbance of the sediments, e.g. from bioturbation. Also, the method includes large uncertainties, and the results can only be used as estimates. None of the cores from the Norwegian Trench had any clear ^{137}Cs peaks that could be used to verify the results. Age determination of the sediments from the Vefsnfjord using the CRS-

method gave results that were in good agreement with each other, both between cores from the same box corer, and between the different sampling locations.

Another form of variation between cores from the same box corer is found for ^{137}Cs in cores at location CTD1121 and CTD1122 in the Vefsnfjord. The cores have the same profile pattern, but is somewhat offset to each other (Figure 4.9a-b). This may also be a result of bioturbation, but more likely when sampling, due to the same vertical pattern is present. If the box corer has not penetrated the seabed perpendicularly, one will get sediment cores non-parallel to the seabed, and sediment slices could contain sediment from more than one layer (chapter 5.7). Also, errors in calculation of density corrected depths could have caused the two cores from the same box corer to be offset (chapter 2.7). Errors in density corrected depths are most likely due to errors when determining wet and dry weight of the sediment samples.

5.2. Regional variation in sediment samples from the Vefsnfjord

Some variation was found within the Vefsnfjord. In surface sediments, the ^{137}Cs levels are comparable, but with slightly higher levels found in the inner part of the fjord (CTD1124, Figure 4.9). This was expected due to former studies of ^{137}Cs in fjords done by RAME (see chapter 5.4.1). The reason is most likely run-off from river Vefsna. Poorer water exchange in the inner part of the fjord, compared to the outlet, may also contribute to the results. The depth profiles have similar trends, with a maximum peak, and rapid decrease in activity concentration below this. However, the cores from the different locations vary both with regards to maximum activity concentration, and how deep in the sediments this maximum is found. The cores sampled in the outlet of the fjord (CTD1121) stands out with both higher maximum activity concentration, and with the maximum peak present further down the core (chapter 4.2.1). The sediment cores at CTD1121 are taken at 226 meters depth, while the other three stations inward in the fjord lays at deeper depths of 448 to 487 meters depth. The difference in sampling depth may contribute to the observed differences. Also, the inner part of the fjord is supplied with freshwater from several rivers, which may affect the salinity of the waters in the part of the fjord. However, because the fjord is so deep in the inner part, and the lighter freshwater will “float on top” of the heavier salty water, this may not cause different salinity of the bottom waters in the area. Still, the difference in salinity may affect the radionuclide distribution to the fjord.

Also for ^{228}Ra (chapter 4.2.3 and 5.4.2), ^{210}Pb (chapter 4.2.2 and 5.4.2) and ^{40}K (chapter 4.2.4 and 5.4.3) some regional variations was found. This may be due to difference in sediment composition, or from bioturbation, as described in 5.1. Another reason may be difference in water supply and water exchange in different parts of the fjord. The inner part is supplied with freshwater from rivers Vefsna, Fusta, Drevjo and Hundåla, while the outer part of the fjord is thought to have better water supply from the Norwegian Sea. The rivers may also carry particles to the fjord. If the rivers carried large amounts of sand/ sediments to the fjord, one might expect higher sedimentation rates in the inner part of the fjord, even though this would depend on water currents and particle size. There is no clear trend of higher sedimentation rates in the inner part of the fjord by results in this thesis, even though the sedimentation rates may seem to be somewhat higher in the inner part of the fjord (CTD1123 and CTD1124) (Table 15). Because of the uncertainty linked to these results, a certain conclusion is not possible. Also, it may have been easier seeing a trend within the fjord, if the results from the outlet of the fjord (CTD1121) could be included.

5.3. Activity concentrations in sediment samples from the Norwegian Trench

5.3.1. ^{137}Cs

The ^{137}Cs activity concentrations found in the four sediment cores in the present study (Figure 4.1 and 4.2) are in good agreement with findings in surface sediment (0-2 cm) from the same area during the last 10-20 years, with activity concentrations from below detection limit <0.1 to 5.5 Bq/kg d.w. (Gäfvert et al., 2003; 2006; 2007; 2011; 2012., Skjerdal et al., 2017). The activity concentration was below the detection limit in the lower part of all four cores. The cores were in good agreement with each other, except perhaps core 2 (chapter 4.1.1).

The RAME monitoring program has analysed sediment cores taken in the Norwegian Trench area in 2013 and 2016. The sampling sites are presented in Figure 5.1, and the results in Figure 5.2. The results are comparable with the results found in this thesis. Most of the cores show the same vertical trend as the cores analysed in the Norwegian Trench this thesis, with the highest ^{137}Cs levels in the upper part of the cores, and decreasing levels down the core. This pattern suggest that the sediments still are receiving minor amounts of ^{137}Cs, and that it gets buried by sedimentation, and decays by time. Most of the sediment cores reach the detection limit for ^{137}Cs, as is the case for the cores in this thesis. From the profiles found in

this thesis, and the associated dating results (table 14), one can conclude that no severe contamination of the sediments at the location have found place in later times.

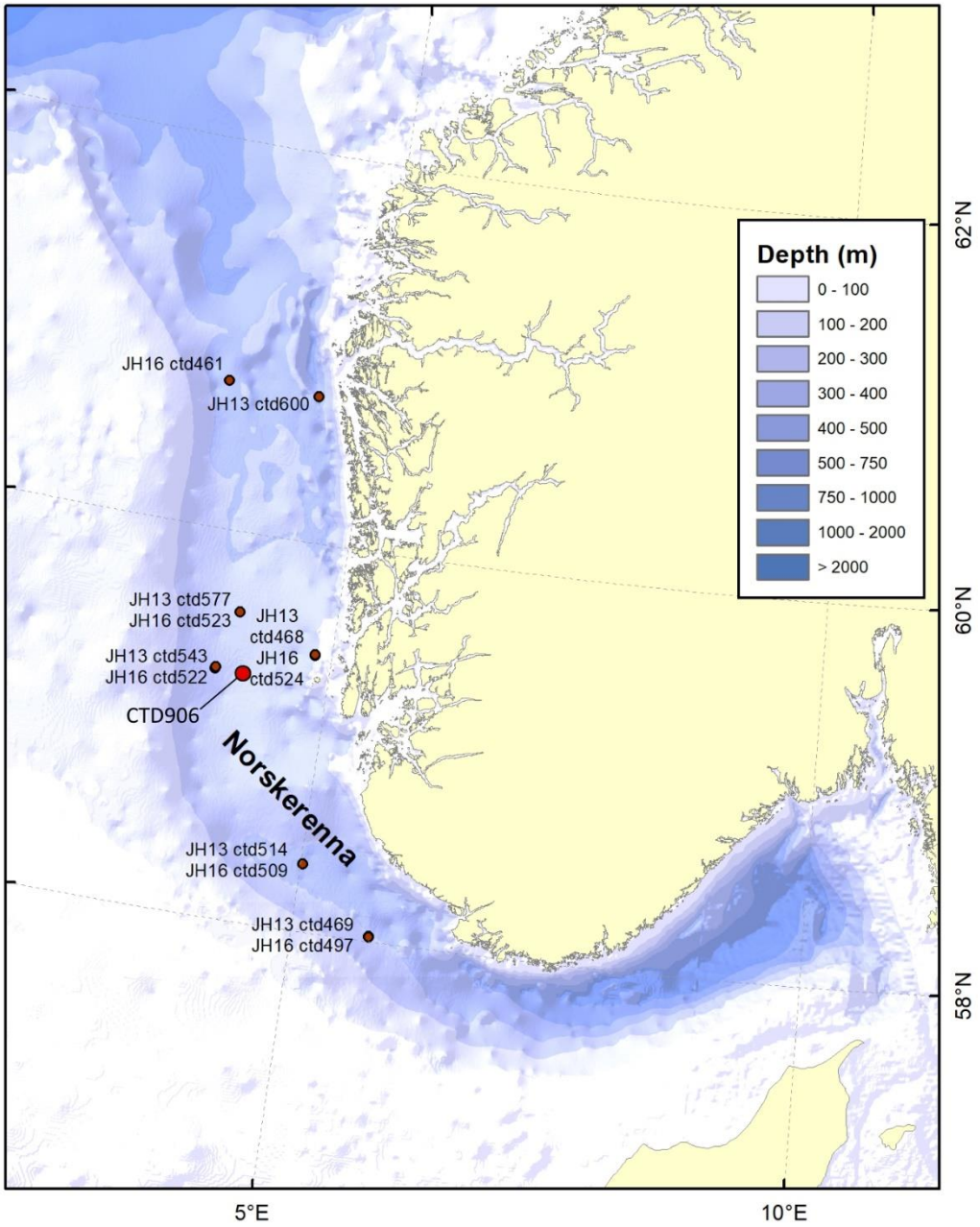

Figure 5.1: Sample stations were sediment cores have been taken and analysed for ^{137}Cs in 2013 and 2016. The results are given in Figure 5.2. The larger bright red dot indicates where sediment cores in this thesis were taken. (Figure: K. Bakkeplass, IMR).

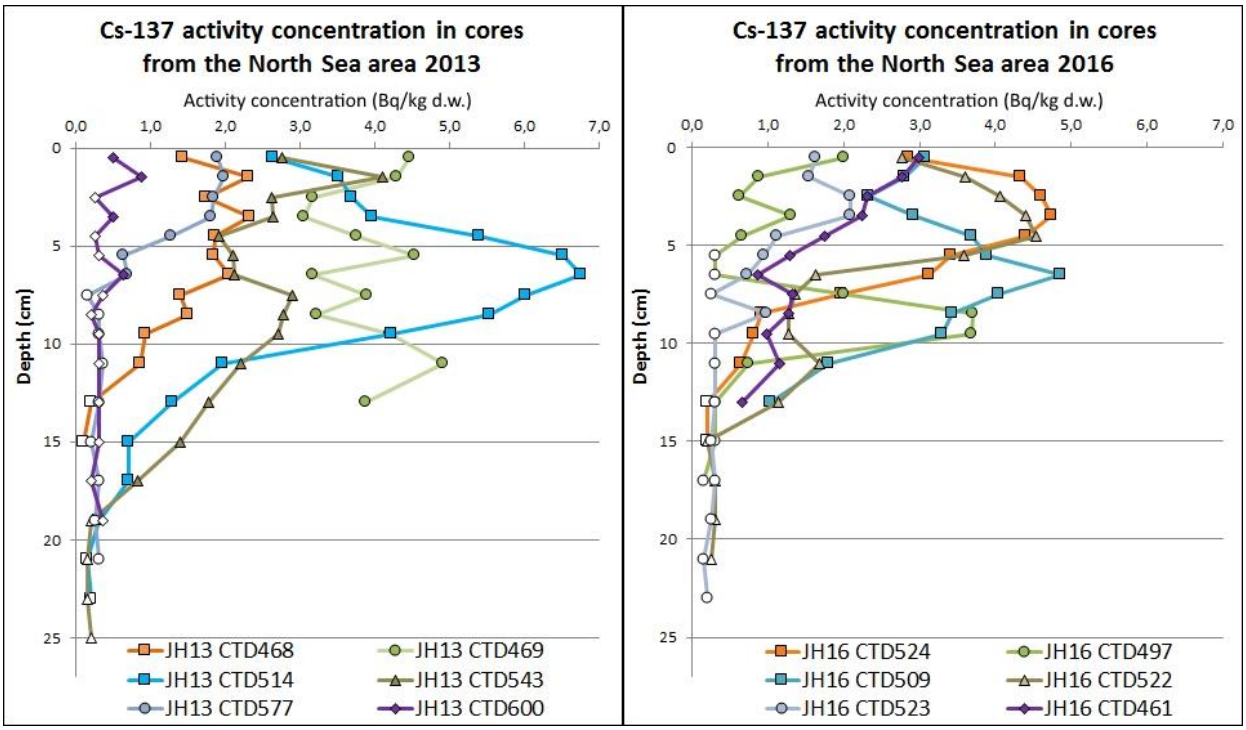

Figure 5.2: ^{137}Cs in sediment cores from the North Sea area (Figure 5.1) in 2013 and 2016 (Unpublished data from IMR/ RAME). The colours in the two figures represent cores taken from the same location. Markers without filling indicate concentrations below the detection limit, and the results are given as half the detection limit.

Rudjord et al. (1999) analysed in 1995 surface samples (0-2 cm) from two locations, one in the North Sea and one in the Norwegian Sea, where the ^{137}Cs levels were 13.1 and 24.7 Bq/kg d.w, respectively. Also, Grøttheim (1998) has analysed surface samples (0-2 cm) in the North Sea area in 1995, and finding ^{137}Cs levels from 3.4 to 13.1 Bq/kg d.w. By comparing these results to the results found in this thesis, and results in Figure 5.2, it seems like the levels in surface sediments in the area has decreased the last years. The decreasing levels of ^{137}Cs is in agreement with the reduced discharges from Sellafield (UNSCEAR, 2000a., Vintró et al., 2000) and La Hauge (UNSCEAR, 2000a), as well as decreasing levels in the Baltic Sea (Herrman et al., 2013).

The levels of ^{137}Cs found in sediments in the Norwegian Sea and the North Sea are comparable with levels found in the Barents Sea. Measurements of surface sediments (0-2 cm) done by RAME in 2012 showed ^{137}Cs levels in the range of 1 to 4 Bq/kg d.w. (Skjerdal et al., 2017). In earlier analyses from 2007-2010, the levels ranged from <0.8 to 14 Bq/kg d.w. in the Barents Sea, with the highest levels near the Norwegian Coast (Gäfvert et al., 2009; 2011; 2012).

The levels found in the Norwegian Sea and the North Sea are lower compared to the adjacent areas of the Irish Sea and the Baltic Sea. In the Irish Sea Charlesworth et al. (2006) measured ^{137}Cs levels in the range of 3 to 164 Bq/kg d.w., with the highest levels correlated to fine-grained sediments. A sample from the mud basin close to the Cumbrian coast (close to Sellafield) measured 275 Bq/kg d.w. (Charlesworth et al., 2006). The same tendencies are found in work conducted by MacKenzie et al. (1999), were ^{137}Cs levels in surface sediments measured close to Sellafield were in the range of approximately 300 to 600 Bq/kg. A clear correlation between fine-grained sediments like mud and clay, and high levels of ^{137}Cs is also found in this work. The "Sellafield mudpatch", an area of fine sediments outside the Cumbrian coast, acted as a sink for approximately 10% of the ^{137}Cs during the period of maximum discharge. From here, major redistribution of ^{137}Cs have occurred since (MacKenzie, 1999). Redistribution of ^{137}Cs may follow the ocean currents, and contaminate other sea areas, like the North Sea, Norwegian Sea and Barents Sea (Figure 2.6).

The Baltic Sea is one of the most contaminated sea areas in the world with regards to ^{137}Cs, and it is estimated that over 80% of the ^{137}Cs originates from the Chernobyl accident (Herrmann et al., 2009; 2013). The estimated inventory of ^{137}Cs in seawater of the Baltic sea was about 1540 TBq in 1999, and have steadily decreased to 730 TBq in 2010 (Herrmann et al., 2013). It is estimated that the pre-Chernobyl levels of 15 Bq/m^3 in seawater will be reached within 2023 (Herrmann et al., 2013). The inventory of ^{137}Cs in sediments in the Baltic Sea was about 2100-2400 TBq at the beginning of the 2000s, a number which is 8-9 times higher compared to levels pre-Chernobyl (Herrmann et al., 2009). Sediment samples measured in the Gulf of Finland, east in the Baltic Sea, in 1986-2002 is given in Figure 5.3 (Ilus, 2007). It shows that the sediments in 2002 still are highly elevated with regards to ^{137}Cs, with maximum levels at about 5000-6000 Bq/kg d.w within the core, but decreasing levels in surface sediments with time, suggesting a decrease in supply of ^{137}Cs to the sediments.

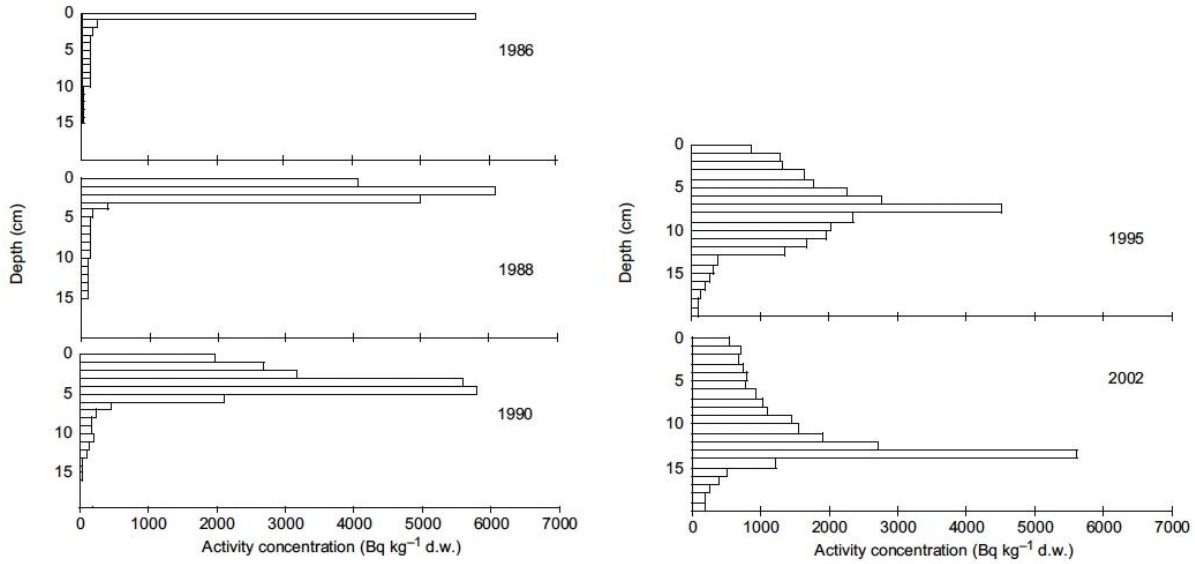

Figure 5.3: Vertical distribution of ^{137}Cs in sediment cores from a coastal station in the Gulf of Finland in 1986-2002 (Ilus, 2007).

5.3.2. ^{228}Ra, ^{226}Ra and ^{210}Pb

The ^{226}Ra values do not vary much downwards the core (Figure 4.3-4.4). Non-elevated levels in the uppermost layers may indicate no significant supply of ^{226}Ra from the oil and gas industry (chapter 2.3.2). The ^{228}Ra results seem to slightly increase down the core more or less for all cores (Figure 4.5-4.6). The results for both radium isotopes are comparable with results found by Dowdall and Lepland (2012). The profiles are comparable, with the exception of some surface samples, which have elevated levels up to 252 Bq/kg d.w. for ^{226}Ra and 110 Bq/kg d.w. for ^{228}Ra (Table 3, Dowdall & Lepland (2012)). Dowdall & Lepland could not conclude on the origin of the elevated levels, but did not exclude the oil and gas industry as a potential source. A trend in both samples analysed by Dowdall and Lepland, and in this thesis, is that the levels of ^{228}Ra are generally higher than the ^{226}Ra levels. The different levels may be due to different concentrations of the mother nuclides ^{232}Th and ^{238}U (in which ^{228}Ra and ^{226}Ra originate from) in the sediments. Also, ^{232}Th and ^{238}U behave differently from one another. Thorium is much less soluble than uranium in seawater (K_d $5*10^2$ for U and $5*10^6$ for Th (chapter 2.1.1)), indicating that thorium is much more retained in sediments (Strålberg et al., 2003).

Beks (2000) found ^{226}Ra inventories in sediment cores from the Norwegian Trench and Skagerrak area in the range 13 to 49 Bq/kg (depth not specified). At two locations

adjacent to the location in this thesis, Beks found ^{226}Ra levels to be 28 and 32 Bq/kg, which is in good agreement with the results found in this thesis.

For ^{210}Pb, all four cores analysed were comparable (Figure 4.3 and 4.4). The ^{210}Pb profiles in sediment cores from the North Sea area found in Beks (2000), shows comparable results, but higher levels in the surface sediments in some cores, up to about 800 Bq/kg d.w. The results from Beks also shows that the ^{210}Pb does not always follow an ideal exponential decline. In an ideal sediment core, there should be an exponential decline in ^{210}Pb and a constant ^{226}Ra concentration with increasing depth. At a certain depth, the concentration of ^{210}Pb should be equal to the concentration of ^{226}Ra due to radioactive decay (Appleby & Oldfield, 1978) (chapter 2.6). In cores were this is not the case, it is not always feasible to use the cores for dating, as discussed further in chapter 5.5.1. In all cores in this thesis, the ^{210}Pb levels reach the ^{226}Ra levels. However, in some samples, the ^{210}Pb levels are lower than the ^{226}Ra levels, which should not be the case. This is affecting the CRS method, due to the calculations relying on a positive amount of ^{210}Pb-excess (chapter 2.6.1). The reason for ^{210}Pb levels being lower than ^{226}Ra may be uncertainties in measurements, which also may be the reason why the ^{210}Pb levels are not completely stable downward the core. Some sort of disturbance (e.g. bioturbation, chapter 5.1), or uneven ^{210}Pb supply to the sediments may also have caused these uneven levels.

Other studies of ^{210}Pb in sediments in the North Trench than those mentioned above was not found.

5.3.3. ^{40}K

The results found in this work (Figure 4.7 and 4.8) are comparable, but somewhat higher, than results from Dowdall & Lepland (2012) from the Norwegian Trench and Skagerrak area (Figure 2.8 and Table 3), where levels were in the range from 518 to 834 Bq/kg d.w. for all samples. Other results of ^{40}K in the area was not found in the literature.

As for other radionuclides (e.g. ^{137}Cs), the results for core 2 seem to vary slightly from the other three cores (Figure 4.8 and chapter 5.1). Potassium is found in many minerals, divided into three categories; clay minerals, rock-forming minerals and evaporates (where potassium occurs as salt) (Schön, 2011). It is likely that the potassium found in this study origins from clay minerals as the sediments were fine-grained (determined by studying the

sediments when sampling). Illite is an example of a mineral which has a high potassium content (3.5-8.3%) (Schön, 2011). Local variations in sediment composition may result in varying content of radionuclides like ^{40}K. Analyses of sediment composition could be done to further investigate this. However, all the results have an uncertainty, and taking it into account, the results do not differ much. The uncertainties for the ^{40}K this case were 9-10% for all samples.

5.4. Activity concentrations in sediment samples from the Vefsnfjord

5.4.1. ^{137}Cs

The ^{137}Cs activity concentrations in surface samples (0-1 cm) in the present study (Figure 4.9) are comparable to levels in surface samples (0-2 cm) observed in the monitoring program RAME in the time period 2002-2017 (Figure 2.11). The RAME results from the outer part of the fjord (equivalent to CTD 1121) have ranged from 137 to 256 Bq/kg d.w. in the time period 2002-2017, and from the inner part of the fjord (equivalent to CTD1124) from 189 to 348 Bq/kg d.w. in the same time period. The variation between the RAME results and results in this thesis probably arise from variation in sampling location. The surface samples collected within RAME are also from the upper 0-2 cm of the sediments, whereas the samples in this thesis are from the 0-1 cm layer. Results from RAME may indicate that the levels are declining by time (Figure 2.11), and this may be due to radioactive decay, or from decreased supply of ^{137}Cs to the fjord from run-off. Further investigations are needed to confirm this.

Investigations of ^{137}Cs levels in Norwegian fjords done by RAME in the time period from 2008 to 2017 are shown in Figure 5.4. The figure show analyses deducted in the inner and outer part of the fjords. The Namsenfjord and Trondheimsfjord are located south of the Vefsnfjord, in mid-Norway, and did also receive fallout of caesium from the Chernobyl accident, but to lesser extent (Figure 2.2 and 2.12), and continues to receive ^{137}Cs as run-off from contaminated land areas. The Laksefjord, located entirely north in Norway, was not exposed to the Chernobyl fallout to the same degree, which is reflected by the measured ^{137}Cs in the fjord.

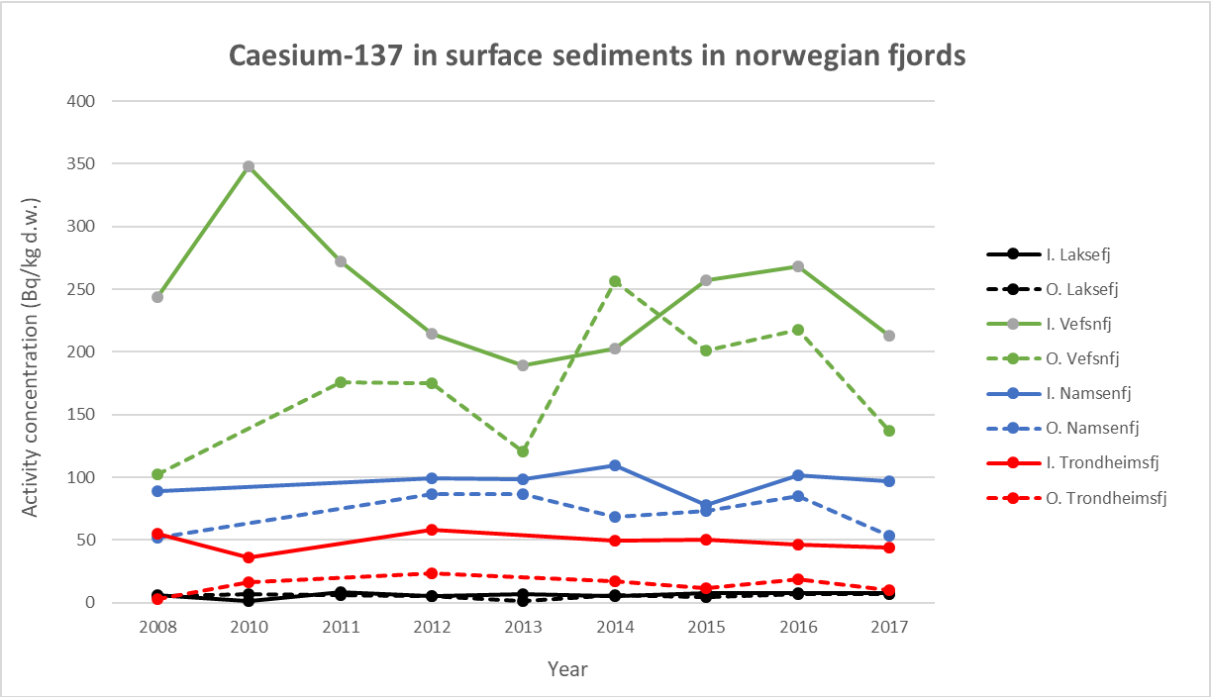

Figure 5.4: Activity concentrations (Bq/kg d.w.) in surface sediments (0-2 cm) from the inner (I) and outer (O) part of the Laksefjord, the Vefsnfjord, the Namsenfjord and the Trondheimsfjord in Norway (Unpublished data from RAME).

Results from the RAME program and this thesis show that the Vefsnfjord is still supplied with ^{137}Cs. Transfer from land to sea can occur by different processes (chapter 2.4.1). Contamination includes run-off from contaminated land areas (chapter 2.3.1), both from weathering and from freshwater supply from rivers in the area (mostly Vefsna) (chapter 2.4.2). The rivers may transport ^{137}Cs as dissolved in the water masses, or as particulate matter. Variation in run-off may be seasonal, or affected by differences in e.g. rainfall. Other contamination sources to the fjord (chapter 2.2) are assumed to be of minor relevance today. This is evident from marine areas near the Vefsnfjord, which have much lower levels in seawater and sediments than within the fjord. Samples of surface seawater collected in the Norwegian Sea in 2014 within RAME ranged from 1.7 to 2.9 Bq/m^3, and surface sediments ranged from below the detection limit (<0.2) to 9.7 Bq/kg d.w (Skjerdal et al., 2017). ^{137}Cs levels in seawater samples from the Vefsnfjord from 2012-2014 showed 4.1 and 3.6 Bq/m^3 (Skjerdal et al., 2017). It indicates that ^{137}Cs levels in surface seawater in the Vefsnfjord are somewhat higher than in the Norwegian sea, but not very elevated, while levels of ^{137}Cs in sediment samples in the Vefsnfjord is much higher than adjacent areas. The high levels of ^{137}Cs found in sediments in the Vefsnfjord compared to adjacent areas, may suggest that the

^{137}Cs is removed from the water column, and retained in sediments, as suggested in chapter 2.1.1.

The cores from CTD1121-CTD1123 show similar vertical ^{137}Cs-trends, with clear peaks in activity concentrations. The peak was least clear for core CTD1124-2 (Figure 4.9d). The maximum peak is most likely to originate from the Chernobyl accident, based on the accident being the major contributor to contamination of ^{137}Cs to the fjord and the area around (see chapter 2.4.2). Comparing sedimentation rates calculated based on ^{137}Cs and ^{210}Pb (Table 15) show good agreement, thus supporting the assumption. In the cores from CTD1122 to CTD1124, the maximum peak is found at about 8-11 cm depth. For both cores at CTD1121, the outermost station in the fjord, the peak is present further down the core, at about 13 and 18 cm depth. In the cores from CTD1121, as well as CTD1122-2, the highest activity concentrations are found. The fact that the highest levels are found in the outer part of the fjord is unexpected, since former surface samples from RAME generally found the highest levels in the inner part of the fjord (e.g. Figure 5.4), and this is the trend also in surface samples from other fjords (e.g. Sværen, 2010). It was expected that the levels should be highest at the inner part of the fjord due to run-off from Vefsna (as well as other rivers), which has its outlet at the innermost part of the fjord. Limitation of water exchange due to a threshold in the inlet of the fjord (chapter 2.4.2.) may cause ^{137}Cs to concentrate at the outlet, but this is not investigated. The maximum-peaks in the cores from CTD1121 is also present deeper in the cores than for the other stations. This irregularity may be due to errors during sampling, preparing and measuring the samples, or due to some disturbance of the sediments, as discussed for other results in this thesis as well (chapter 5.7 and chapter 5.1).

The two cores from the inner part of the fjord, CTD1123 and CTD1124, agrees well in terms of activity concentration down the core, while there is some variation between the two cores taken at the outer part of the fjord, CTD1121 and CTD1122. The cores follow the same pattern in activity concentration down the core, but one of the cores is offset from the other (Figure 4.9a-b). A possible explanation for these results may be errors during sediment sampling or disturbance of the sediments (chapter 5.7 and chapter 5.1). Another explanation may be errors when weighing the samples, causing errors in the density corrected depths.

5.4.2. ^{228}Ra, ^{226}Ra and ^{210}Pb

The two cores taken from the same box corer show good agreement at all four locations for ^{226}Ra and ^{228}Ra, while some variations within the fjord are found (Figure 4.10 and 4.11). For ^{228}Ra, the uppermost layers show elevated levels, before the levels are stabilizing down the core. This pattern is seen in the cores from CTD1122, CTD1123, and to some extent in CTD1124, but not in the cores from CTD1121 (Figure 4.11). The same tendency is also found for ^{226}Ra in the same cores, just to a lower extent (Figure 4.10). The elevated levels may come from run-off from land. CTD1123 is located not far from the outlet of the river Hundålå, and CTD1124 is located at the innermost part of the fjord, not far from the outlet of Vefsna, Fusta and Drevja (figure 3.3). Again, if this is the cause, one might expect the highest levels at CTD1124 and not CTD1123 and CTD1122. Further investigation should be done to be able to determine the source of these results.

It was not possible to find results from other studies of ^{226}Ra and ^{228}Ra in sediments in the Vefsnfjord in the literature. However, Sværen (2010) analysed sediment cores in two other Norwegian fjords: Laksefjorden (Finnmark) and Sognefjorden (Sogn og Fjordane). The cores were analysed for ^{226}Ra and ^{210}Pb, for ^{210}Pb dating purposes. The ^{226}Ra levels in the Laksefjord ranged from 22 to 29 Bq/kg d.w. in the outer part of the fjord, and from 19 to 26 Bq/kg d.w. in the inner part of the fjord. In the Sognefjord, the ^{226}Ra levels were in the range from 25 to 35 Bq/kg d.w. in the outer part of the fjord, and from 34 to 43 Bq/kg d.w. in the inner part of the fjord. These results are comparable to the results found in this thesis. In the Sognefjord, the highest levels were found in the inner part of the fjord, as also seen in the Vefsnfjord. Neither the results from the Laksefjord nor the Sognefjord showed elevated levels in uppermost layers, as seen in the Vefsnfjord.

The activity concentration of ^{210}Pb (Figure 4.10) is comparable to the results found by Haugen et al. (1981) in the inner part of the Vefsnfjord, where ^{210}Pb-levels ranged from approximately 8.5 to1 pCi/g (~315 to 37 Bq/kg) down the core. It was not possible to find other ^{210}Pb results from the Vefsnfjord in the literature. However, Sværen (2010) have investigated ^{210}Pb levels in the Laksefjord and the Sognefjord. In the inner part of the Laksefjord, the levels ranged from 289 to 19 Bq/kg d.w. with the highest levels at the uppermost layers, and declining levels down the core, as for the cores in this thesis. In the outer part the levels ranged from 319 to 18 Bq/kg d.w. In the outlet of the Sognefjord the ^{210}Pb levels ranged from 397 to 29 Bq/kg d.w., and at the head of the fjord the levels ranged from 161 to 42 Bq/kg d.w. These levels are comparable with the ones found in this thesis.

Some of the cores found in Sværen (2010) have an uneven decrease in ^{210}Pb levels down the core, as also observed in cores examined in this thesis.

Figure 4.10 shows that the ^{210}Pb levels do not decline exponentially as they should, and do not reach the ^{226}Ra levels, as expected (chapter 2.6). There are, as also pointed out in chapter 5.3.2, several possible reasons for this, including procedures in sampling, sample preparation and measurements of samples (chapter 5.7), disturbance in sediments due to e.g. bioturbation (chapter 5.1) or bottom trawling (needs to be investigated further), or contribution of ^{210}Pb from land by run-off causing an uneven flux to the sediments. The uneven decrease in ^{210}Pb is especially seen in the cores from CTD1121.

5.4.3. ^{40}K

The two cores from the same box corer agree well in terms of activity concentration down the core, while some variation within the fjord is found (Figure 4.12). Local variation in sediment composition may explain the results (chapter 5.1). Also, sample preparation and measurements may give rise to some variation in results. However, including the uncertainties (9-10% for all ^{40}K results), all samples are within uncertainty calculations, and local variations may be arbitrary. Cores from CTD1121 and CTD1123 show relatively stable activity concentration downward the cores, and so does CTD1122, except for a slight increase in the uppermost sediment layers. The cores at CTD1124 stands out from the rest of the cores, with decreasing activity concentrations downward the cores, before increasing again. Again, the variations may arise from sediment composition, or from disturbance of the sediment (e.g. bioturbation, chapter 5.1). No data on ^{40}K levels from the Vefsnfjord was found in the literature. The levels within the fjord did, however, compare with the results found in the Norwegian Trench. The similarity in ^{40}K levels may be due to the sediment samples from both marine environments consisted of fine-grained sediments. Analyses of the sediment composition could be done to further investigate this.

5.5. Dating results

5.5.1. The Norwegian Trench

The sedimentation rates determined according to Tadjiki & Erten (1994) (chapter 2.6.2), without taking effects of potential mixing into account or doing any corrections, were found

to be 0.07, 0.11, 0.09 and 0.12 for the four cores taken from the same box corer (Table 13). From the results one can see that there are some variations between the cores. These variations most likely originate from uncertainty related to sampling, preparation and analysis of the samples, but local variations cannot be ruled out.

Sedimentation rates found by Bø et al. (1996) in the Skagerrak area were typically 10-20 cm/100 years (0.1-0.2 cm/year), increasing to more than 30 cm/100 year in the southeastern parts and at some locations in the northwest part of Skagerrak. Also, sedimentation rates exceeding 50 cm/100 years on the southeastern slope of the Norwegian Trench, and in the northeasternmost part of the Norwegian Trench were found (Bøe et al., 1996). High sediment flux and sedimentation rates have been reported in the area by Erlenkeuser and Pederstad (1984), and based on mineralogical studies thought to originate from the North Sea or Baltic Sea. It is reasonable to believe that the highest sedimentation rates found are not representative for the Norwegian Trench area as a whole. Sedimentation rates have also been found to be 0.1 cm/year and 0.5 cm/year for two locations south and east in the Skagerrak area (NSTF, 1993). Few studies on sedimentation rates further north in the Norwegian Trench (where samples from this thesis are collected) is performed. However, Rise et al. (2008) have found sedimentation rates at a location near the one in this thesis, to be in the range 0.04- 0.7 cm/year.

The sedimentation rates found in the Norwegian Trench this thesis is similar to sedimentation rates found in Jensen et al. (2018) from the MAREANO program, in the Norwegian Sea and the Barents Sea (Figure 5.5).

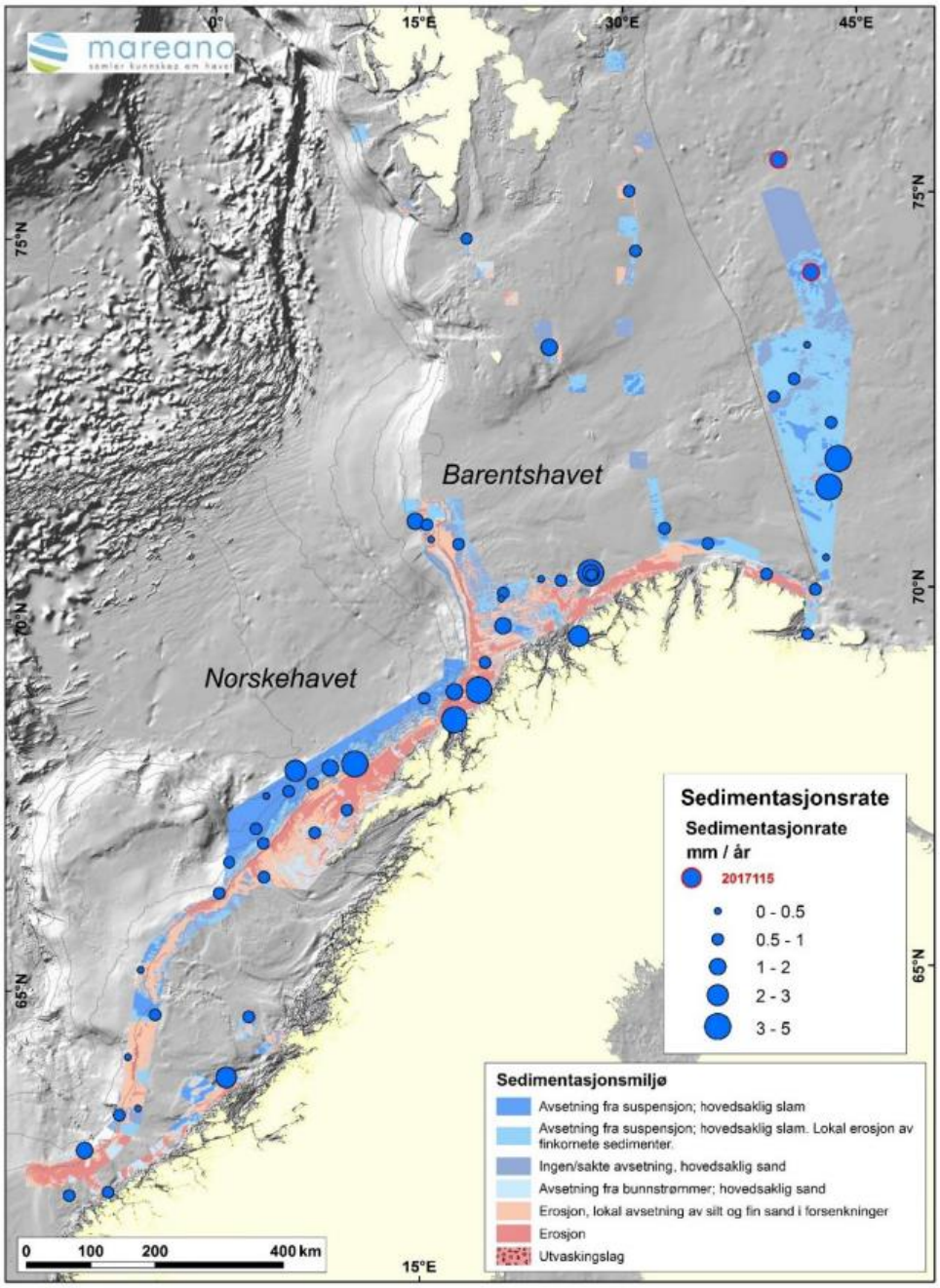

Figure 5.5: Sedimentation rates in the Norwegian Sea and the Barents Sea based on ^{210}Pb analyses from 2006 to 2017 from the MAREANO chemistry reports (Jensen et al., 2018).

The age of the sediment layers calculated using the CRS method, gave quite different results, and especially core 2 stood out. It is not clear why it is so different from the other three cores when applying the CRS method. When comparing this core to the three others, the decrease in ^{210}Pb is rather rapid in the uppermost layers. The rapid decrease might suggest bioturbation or some other disturbance of the upper layers in the core (chapter 5.1). However,

Core 2 is different from the other three cores with regards to other results as well (^{137}Cs, ^{40}K, see figure 4.2 and 4.8). Also, the dating results have significant uncertainties, and can only be looked at as estimates. In addition, no clear ^{137}Cs peaks that could contribute to validate the results are found in any of the cores.

Sedimentation rates were also calculated from the CRS method, to easier compare the two methods (Table 14). The results were 0.09, 0.03, 0.06 and 0.12 cm/year. Core 2 stands out with a lower sedimentation rate of only 0.03 cm/year, due to the large difference from the CRS results. As mentioned above, it was not possible to determine why this core stood out. The sedimentation rates for the other three cores are comparable with the sedimentation rates found by ^{210}Pb according to Tadjiki & Erten (1994).

5.5.2. The Vefsnfjord

The cores from CTD1121 were not included in the dating study, as the cores were not suitable for dating, due to its uneven decrease in ^{210}Pb (Figure 4.10a). The reason for this disturbance is unknown, but may be due to a non-constant atmospheric flux of ^{210}Pb as a result of variation in e.g. rainfall. Heavy rainfall could also increase the supply of ^{210}Pb from run-off from rivers (Appleby, 1998). Also, bioturbation may have occurred (chapter 5.1). Errors during sampling and sample preparation may also be an explanation, even though this seems not to be the case since the same pattern is present in both cores from the location. In an ideal sediment core, there should be an exponential decline in unsupported ^{210}Pb with increasing depth and a constant ^{226}Ra concentration with increasing depth (chapter 2.6), and at a certain depth, the concentration of unsupported ^{210}Pb should be equal to the concentration of ^{226}Ra due to radioactive decay (Appleby& Oldfield, 1978). This is not the case for the cores analysed in the Vefsnfjord. As seen in figure 4.10a-d, the ^{210}Pb does not decrease exponentially with depth, and does not reach the ^{226}Ra values at the depth analysed in these cores, as expected. Also, in the two cores from CTD1123, the ^{226}Ra values are not constant, but elevated in the uppermost part of the core. This inconsistency is contributing to the cores not being ideal for use in dating analysis, and must be taken into account when assessing the results.

The sedimentation rates calculated according to Tadjiki & Erten (1994) are comparable within the fjord, even though some variation is found (Table 15). The most considerable difference is found between a core from CTD1122 (0.18 cm/year) and CTD1123

(0.27 cm/year) in the middle part of the fjord. The results from the two cores sampled from the same box corer were in good agreement for CTD1122 and CTD1124. Some variation was found between the two cores at CTD1123, but the results were still comparable. Whether this difference is due to actual variation within the fjord, or due to the uncertainty in sampling and measuring, is uncertain. There are large uncertainties related to the ^{210}Pb dating method, so the results should only be considered as estimates. Comparing the results with other results, from e.g. ^{137}Cs (chapter 2.6.3), can help to validate the ^{210}Pb dating results (Tadjiki & Erten, 1994).

The sedimentation rates found by using ^{137}Cs peaks, were based on in which layer the maximum ^{137}Cs peak was found, and dating the middle of this layer to the year of the Chernobyl accident, 1986. Core 2 from CTD1124 did not have as clear ^{137}Cs-peak as the other cores, and this may add to the uncertainty for the sedimentation rate for this core, which does tend to be a bit lower than the other sedimentation rates. The maximum ^{137}Cs peak is thought to originate from the Chernobyl accident based on the fact that the accident is the major contributor to ^{137}Cs in the Vefsnfjord (e.g. Skjerdal et al., 2017). The fact that the sedimentation rates match the ones calculated by ^{210}Pb fairly well, is also a good indicator. To help identify the source of ^{137}Cs, analyses of plutonium-isotope ratios can be determined (e.g. Oughton et al., 2004) or measurements of ^{241}Am could be done (Appelby, 1998), but this is not studied in this thesis.

The age of the different sediment layers was determined using the CRS method (Table 16). The dating results correspond well between the cores from the same location, especially in the upper part of the core. The difference gets larger further down the core, which is expected because of higher uncertainties for older sediments. From the different age layers, sedimentation rates were calculated to easier compare the CRS method to the calculated sedimentation rates (Table 16). When comparing these results to the results using ^{210}Pb and ^{137}Cs, one can see that they are comparable for all cores (Table 15). However, the results showed slightly lower sedimentation rates than calculated from ^{210}Pb and ^{137}Cs. The biggest difference is in core 2 at CTD1122, were the difference between the three methods (^{210}Pb, ^{137}Cs and the CRS method) were 0.13 cm/year. The CRS method is a simple method, and may come to short in environments with complex transport processes (Appleby, 1998). The fact that these samples are taken in a marine environment, and not in a closed system of a lake, may suggest this. The model does, however, often give more accurate results than another commonly used and simple method, the CIC (Constant Initial Concentration) model, in such

environments, due to the robustness of the dating parameter. This is because integration is a relatively reliable numerical procedure, and also has the effect of smoothing out minor irregularities (Appleby, 1998). Also, if the accumulation rate of sediment has not been constant over time, the CRS method should be preferred (Appleby & Oldfield, 1978).

The results on sedimentation rates in this thesis correspond fairly well with the results found in Haugen et al. (1981), where the sedimentation rates in two cores taken from the inner part of the fjord were found to be 0.20 cm/year and 0.17 cm/year. The sedimentation rates were found using ^{210}Pb. The results from Haugen et al. is the only literature found on sedimentation rates from the Vefsnfjord, but investigations have been conducted in other Norwegian fjords. Sternal et al. (2017) have investigated sedimentation rates in the Repparfjord located in Tromsø in northern Norway. They found sedimentation rates based on ^{210}Pb in the inner part of the fjord ranging from 0.06 to 0.47 cm/year, and in the outer part of the fjord ranging from 0.04 to 0.18 cm/year. Sedimentation rates based on ^{137} for the same locations were found in the range >0.11 to >0.29 and 0.08 to 0.15 cm/year, respectively. From the results, one can see that the sedimentation rate varies, both between different sampling locations within the fjord, and by using different calculation methods. Sværen (2010) have dated sediments from two fjords in Norway, the Laksefjord in northern Norway, and the Sognefjord in southern Norway. In the study, the CRS and CIC methods were used, and sedimentations rates were not calculated.

When comparing the age determination results from the CRS method (Table 16) with ^{137}Cs levels in the cores (4.9a-d), one can see that the oldest sediment, which was dated to be a hundred years old, contains ^{137}Cs. This is not a good indication of the credibility in these analyses, as ^{137}Cs was not present in the environment at that time. Bioturbation may cause vertical transport of ^{137}Cs, as well as the migration of ^{137}Cs to increasing depth (chapter 5.1), and is most likely the cause of these results. Another reason for the content of ^{137}Cs in deeper sediment layers may be due to contamination during sampling and slicing of the sediments (chapter 5.7). Detecting ^{137}Cs at sediment layers deeper than expected has been reported in earlier studies as well (e.g. Holby & Evans, 1996., Sværen, 2010).

Overall, the sedimentation rate for all three methods was in the range of 0.14 to 0.27 cm/year for all cores. From these results it is not possible to see any clear trends within the fjord. It is not possible to determine whether the difference between cores from the same location comes from actual local variations, or uncertainty from sampling, preparation and

measurements. The last option is most likely, but further investigation must be done to confirm this.

5.6. LECO analyses

LECO analyses was performed by NGU to determine the content of sulphur, carbon and total organic carbon in samples from the Vefsnfjord. One core from the same box corer as the cores analysed for radionuclides was analysed (Table 11 and 12).

The content of sulphur ranges from 0.10 to 0.49 %, which is in good agreement with sulphur content found in the Norwegian Sea and the Barents Sea, ranging from 0.1 to 0.3 % (NGU, 2018). From the core sampled at the outer part of the fjord (CTD1121), and to some extent at CTD1123, the sulphur content is increasing down the core. The increasing levels is, however, not seen in the two other cores.

The content of total carbon ranges from 1.4 to 2.9 % and total organic carbon (TOC) content ranges from 1.0 to 2.0 % for all samples analysed. The TOC content is similar to levels found in the Barents Sea in 2017, ranging from 1.9 to 3.6 %, and with earlier studies from the Barents Sea and the Norwegian Sea (Figure 5.6) (Jensen et al., 2018). As seen in Figure 5.6, the two northern samples from 2017 show somewhat lower TOC content than the three samples located further south in the Barents Sea. The lower content is thought to be due to the samples in the south consisting of more fine-grained sediments (Jensen et al., 2018). Variation in sediment composition may also be a reason for the minor variations in TOC found in this thesis.

Some minor variations within the cores, as well as some variations between the different stations, were found for both sulphur, total carbon and total organic carbon. The levels were, however, very low and no clear trends were found that may explain other results found in this thesis. However, by looking at the results found in this thesis, it may seem like the levels of both sulphur, total carbon and total organic carbon is slightly higher at the outermost part of the fjord. Further studies must be done to confirm this, as well as explain the possible variations.

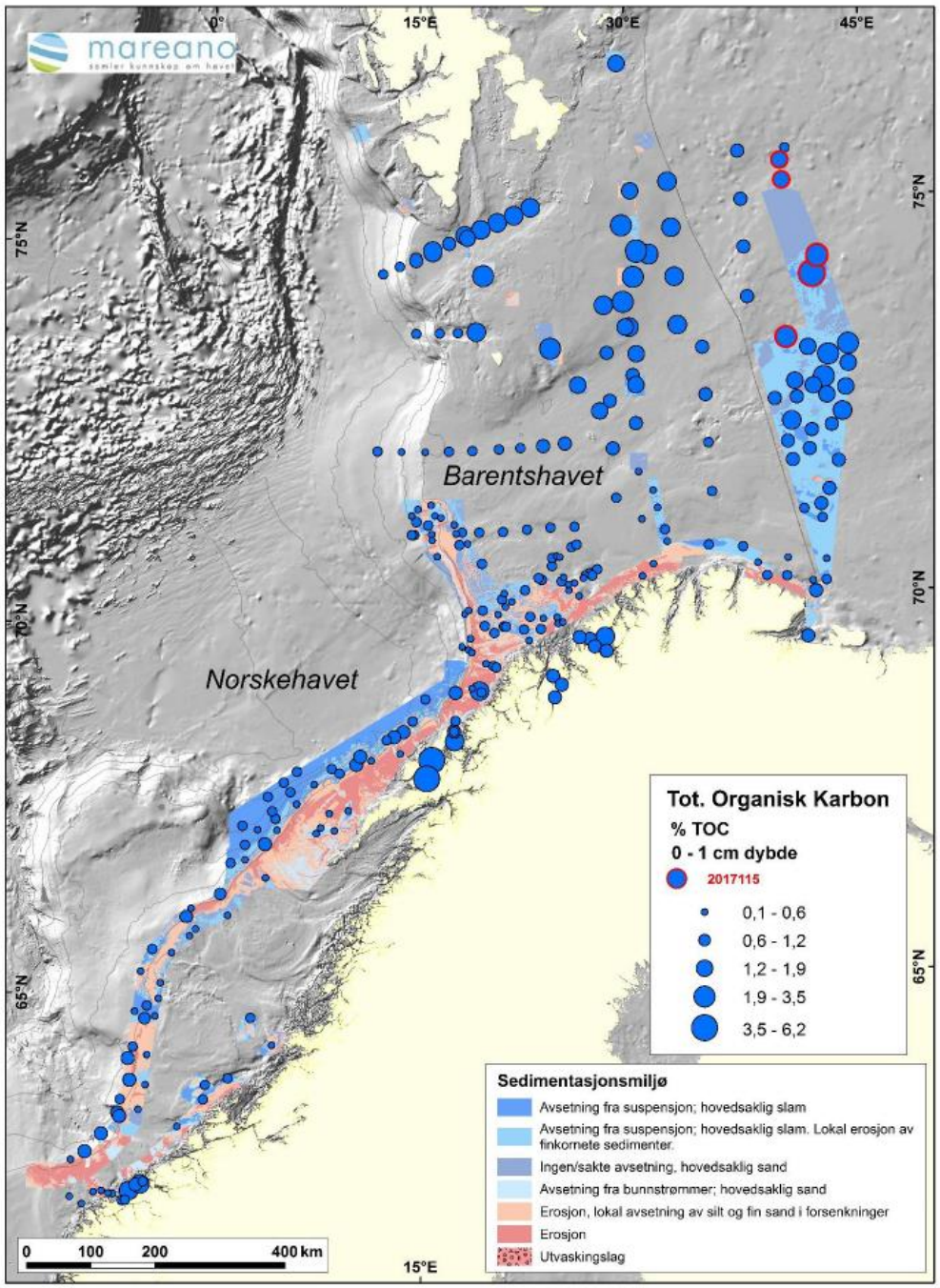

Figure 5.6: TOC content in surface samples of sediment (0-1 cm) in the Norwegian Sea and the Barents Sea from the MAREANO program (Jensen et al., 2018). The five samples in the Barents Sea, given with a red ring, are samples from 2017. The other samples are compiled from earlier studies in MAREANO.

The LECO analyses was supposed to supply grain size analyses of the samples in the Vefsnfjord. By studying the results from the LECO analysis and the grain size analyses together, maybe some trends to help explain the results found in this thesis could be found.

The grain size analyses were unfortunately delayed due to problems at the NGU laboratory, and was not analysed in time for this thesis. However, it was decided to include the LECO analyses in this thesis, even though the results came shortly before the thesis was due, and it was not time enough to study the results sufficiently.

5.7. Inaccuracy in sample collection and sample preparation

When obtaining sediment samples with a Smøgen box corer (chapter 3.1), the box corer should penetrate the seabed perpendicularly. It may, however, penetrate the seabed with an angle (Figure 5.7). The result will then be sediment cores and sediment slices, non-parallel to the seabed, and that one sediment slice could contain sediment from more than one layer. The problem could also result in different length on the sediment cores. This may be a reason for the different length of the cores from the Norwegian Trench. Ideally, all the cores should have equal lengths as they were taken from the same box corer, but this is not the case, as the four cores vary from 12 to 19 cm in length. Another source to disturbance of the sediment within the box corer could occur if the box corer does not fully close after obtaining the sediments. This could happen if a stone is trapped in the closing mechanism, or the closing mechanism does not function as it should. A malfunction could lead to water entering the box corer as it is moved to the surface, and wash some of the sediments out.

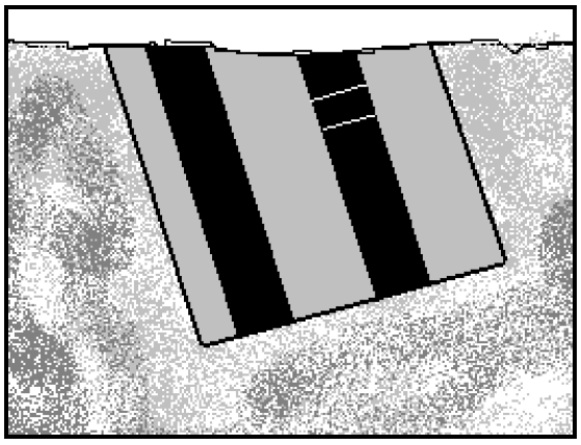

Figure 5.7: Illustration of a box corer sampling, and subsampling of cores (black tubes) (Sværen, 2010).

The box corer could also compress the sediment when sampling, and this compression would not necessarily be uniform within the box corer. Compression of sediment samples

when obtaining the cores using PVC tubes may also occur. To minimize the compression from the tubes on the sediment samples, the end of the tube was sharpened, and the tubes carefully pressed into the sediment. Both when pressing the tube into the sediment, and when pushing the core out when slicing, some material may stick to the walls of the PVC tubes, causing some contamination between the sediment slices. This problem was minimized by using rather large tubes (10 cm diameter), making the relative amount of sediment from the tube walls smaller compared to tubes with a smaller diameter.

When slicing the cores, the thickness (1 or 2 cm) was determined by eye using a ruler, which may cause some inaccuracy in sample thickness. Also, the top layer for all cores was more or less uneven, making it difficult to slice a representative layer of 1 cm. None of the samples contained large fragments (stones e.g.), so a loss in sample size because of that was prevented. However, a small loss of sediment sample due to transfer from the tube to the aluminium containers may occur, and contribute to the overall inaccuracy. This problem was more present when slicing the thawed-up cores from the Norwegian Trench than for the fresh sediment cores from the Vefsnfjord, due to the sediments being easier to cut without falling apart. The sediment cores from the Vefsnfjord having a different composition than the ones from the Norwegian Trench could also have contributed to the cores being easier to slice. The samples from the Vefsnfjord were sliced aboard the research vessel, instead of in a laboratory, and this may have contributed to some inaccuracy when slicing the samples. However, it is estimated that this is a minor contributor, due to suitable conditions aboard the research vessel when slicing the cores from the Vefsnfjord. A possible error for both the samples from the Norwegian Trench and the Vefsnfjord is mixing the samples or labelling the samples wrong. This mistake should not occur, but may happen when many samples are handled at the same time.

Loss of sample, as well as possible cross-contamination between samples, could occur while freeze-drying the sediments. Cross-contamination was tried prevented by packing the samples in special cloth-bags during freeze-drying, and to only have sediment slices from the same core in the freeze dryer. The freeze dryer was cleaned, and the cloth-bags washed between each time it was used. When grinding the samples, a new risk of sample-loss and cross-contamination occurred. The loss of sample is however estimated to be low, and to prevent cross-contamination, the equipment was cleaned between each sample (chapter 3.2.2).

6. SUGGESTIONS FOR FUTURE WORK

In this thesis variations in radionuclide levels between sediment cores collected within a box corer was studied. To help understand and explain the observed variations, analyses of grain size and sediment composition should be done. Such studies could help explain the observed variation in radionuclide levels within the Vefsnfjord. Analysis of soil samples in the area, and analysis of water and sediments in rivers with outlet in the Vefsnfjord could also give information on distribution of radionuclides to the fjord.

Few results from studies on naturally occurring radionuclides in sediments in Norwegian marine areas are available in the literature. Such results are of great importance to better understand the impact of discharges of produced water from the oil and gas industry, and more data are needed to shed light on this subject. It is also important to have a benchmark for natural radionuclides in different marine areas, so that any potential increase in the levels can be detected. The naturally occurring radionuclides investigated in this thesis are considered to be radiotoxic, especially lead and radium. Transfer from sediments to benthic organisms introduces these radionuclides to marine food webs. More data will contribute to a better assessment on the uptake of these radionuclides in marine food webs.

In this thesis, the age of the sediment slices was determined using the ^{210}Pb CRS method. The CRS method gave comparable results for the samples in the Vefsnfjord, while variation was found between different cores from the same box corer in the Norwegian Trench. More advanced dating methods than the CRS method is available, and could be applied, especially when dating sediments taken in open marine environment, where it may occur more advanced processes than in a closed system of a lake. This needs further attention.

The different sources of radioactive contamination have different isotope ratios. Information about plutonium isotope ratios (e.g. ^{238}Pu/ ^{239,240}Pu) in the cores analysed in the present study would give more information about the origin of the ^{137}Cs peaks. It would also help validate the ^{210}Pb dating method, to confirm the origin of the ^{137}Cs maximum peak.

Radionuclide speciation was not investigated in this thesis. By including this, one could be able to predict whether the radionuclides are mobile or irreversible bound to sediments. Remobilization of ^{137}Cs from sediments to seawater is happening both in the Irish Sea and the Baltic Sea. If this is happening also in the Vefsnfjord, or the ^{137}Cs within the fjord is irreversible bound to the sediments, could be studied further by applying radionuclide speciation techniques.

7. CONCLUSIONS

The two study areas were quite different from each other with regards to ^{137}Cs levels. The ^{137}Cs levels found in the Norwegian Trench ranged from below the detection limit (<0.4) to 3.0 Bq/kg dry weight, while the levels found in the Vefsnfjord ranged from 13 to 432 Bq/kg dry weight. The levels found in the Vefsnfjord show that still over 30 years after the Chernobyl accident, elevated levels of ^{137}Cs are present in sediments in the fjord. Levels of the other radionuclides studied in this work were comparable for the two study areas. Radium levels in sediment cores from the Norwegian Trench and the Vefsnfjord ranged from 23 to 53 Bq/ kg d.w. and from 28 to 79 Bq/kg d.w. for ^{226}Ra and ^{228}Ra, respectively. ^{210}Pb levels ranged from 24 to 279 Bq/kg d.w., and ^{40}K levels ranged from 581 to 949 Bq/kg d.w.

Investigations of local variations of ^{137}Cs, ^{226}Ra, ^{228}Ra, ^{210}Pb and ^{40}K within a box corer showed that the variations mostly were within the calculated uncertainties for all sediment cores. However, for some radionuclides there were some variation at some of the locations.

Regional variations of ^{137}Cs, ^{226}Ra, ^{228}Ra, ^{210}Pb and ^{40}K within the Vefsnfjord was studied by sampling at four different locations in a gradient from the outermost to the innermost part of the fjord. The results were mostly comparable within the fjord, but some variations were found. No clear trends were found between radionuclide content in sediment cores in the inner and the outer part of the fjord.

The sediment cores were dated using ^{210}Pb and the CRS method. Sediment layers from the same depth in different cores collected from the same box corer in the Norwegian Trench showed quite different ages. None of the cores from the Norwegian Trench had a clear ^{137}Cs peaks that could be used to verify the ^{210}Pb dating results. Age determination of the sediments from the Vefsnfjord using the CRS method gave results that were in good agreement with each other, both between cores from the same box corer, and between the different sampling locations.

The sedimentation rates determined by ^{210}Pb in the Norwegian Trench ranged from 0.07 to 0.12 cm/year, and the sedimentation rates determined both by ^{210}Pb and ^{137}Cs in the Vefsnfjord ranged from 0.17 to 0.27 cm/year.

To better compare the CRS dating results to the sedimentation rates calculated according to Tadjiki & Erten (1994), and from ^{137}Cs, the ages of the different slices were

converted to sedimentation rates. The results from the Norwegian Trench ranged from 0.03 to 0.12 cm/year, while the results from the Vefsnfjord ranged from 0.14 to 0.21 cm/year.

8. REFERENCES

Appleby, P G. (1998). *Dating Recent Sediments By ^{210}pb: Problems and Solutions.* STUK-A145: Helsinki.

Appleby, P G. (2008). *Three decades of dating recent sediments by fallout radionuclides: a review*. The Holocene. Vol. 18, pp. 83-93. Sage.

Appleby, P G & Oldfield, F. (1978). *The calculation of lead-210 dates assuming a constant rate of supply of unsupported ^{210}pb to the sediment.* Catena. Vol 5, pp. 1-8.

Albretsen, J. (2014). *Sirculation and water masses.* Institute of Marine Research. Available from:http://www.imr.no/temasider/havomrader_og_okosystem/nordsjoen_og_skagerrak/sirkulasjon_og_vannmasser/nb-no (Downloaded 10.10.2018).

Asplin, L. (2014). *The Norwegian Coastal Current*. Institute of Marine Research. Available from: https://www.imr.no/temasider/kyst_og_fjord/den_norske_kyststrommen/en (Downloaded 09.10.2018).

Bache, S., Bjerke, H., Rudjord, A L., Ugletveit, F. (1986). *Cesium Fallout in Norway after the Chernobyl Accident.* National Institute of Radiation Hygiene. SIS rapport 1986:5. (In Norwegian).

Baxter M S., Harms I., Osvath I., Povinec P P., Scott EM. (1998). *Modelling the potential radiological consequences of radioactive waste dumping in the Kara Sea.* Journal of Environmental Radioactivity. Vol. 39, pp. 161–181.

Beks, J P. (2000). *Storage and distribution of plutonium, ^{241}Am, ^{137}Cs and $^{210}Pb_{XS}$ in North Sea sediments.* Continental Shelf Research 20. Elsevier.

Binford, M W. (1990). *Calculation and uncertainty analysis of ^{210}Pb dates for PIRLA project lake sediment cores.* Journal of Paleolimnology. Vol. 3, pp. 253-267. Kluwer Academic Publishers: Belgium.

Bøe, R. (1993). *Sedimentology and geotechnical research on sediment cores from Skagerrak.* Report nr. 93.050. Geological Survey of Norway: Trondheim.

Bøe, R., Rise, L., Thorsnes, T H., de Haas, H., Seether, O M., Kunzendorf, H. (1996). *Sea-bed sediments and sediment accumulation rates in the Norwegian part of the Skagerrak.* Geological Survey of Norway Bulletin. Vol. 430, pp. 75-84.

Charlesworth, M E., Service, M., Gibson, C E. (2006). *The distribution and transport of Sellafield derived ^{137}Cs and ^{241}Am to western Irish Sea sediments.* Science of The Total Environment. Vol. 354, pp. 83-92. Elsevier.

Choppin, G., Ekberg, C., Liljenzin, J.O., Rydberg, J. (2013). *Radiochemistry and Nuclear Chemistry*, 4th edition. Academic Press: Oxford.

Cournane, S., Vintró, L L., Mitchell, P I. (2010). *Modelling the reworking effects of bioturbation on the incorporation of radionuclides into the sediment column: implications for the fate of particle-reactive radionuclides in Irish Sea sediments.* Journal of Environmental Radioactivity. Vol. 101, pp. 985-991. Elsevier.

Crusius, J., Bothner, M H., Sommerfield, C K. (2004). *Bioturbation depths, rates and process in Massachusetts Bay sediments inferred from modelling of ^{210}Pb and $^{239+240}Pu$ profiles.* Estuarine Coastal and Shelf Science. Vol. 61, pp. 643-655.

Cutshall, N H., Larsen, I L., Olsen, C R. (1983). *Direct analysis of ^{210}Pb in sediment samples: self-absorption corrections.* Nuclear Instruments and Methods. Vol. 206, pp. 309-312. 309 North-Holland Publishing Company. Environmental Sciences Division, Oak Ridge National Laboratory.

Dowdall, M & Lepland, A. (2012). *Elevated levels of radium-226 and radium-228 in marine sediments of the Norwegian Trench (''Norskrenna'') and Skagerrak.* Marine Pollution Bulletin. Vol. 64, pp. 2069–2076. Elsevier.

Dreher, R., Magill, J., Pfennig, G., Sóti, Z. (2015). *Karlsruher Nuklidkarte (Chart of the nuclides)*. 9th edition. Germany.

Dulaiova, H & Burnett, W C. (2004). *An efficient method for γ-spectrometric determination of radium-226,228 via manganese fibers.* Limnology and Oceanography: Methods. Vol 2, pp. 256–261. The American Society of Limnology and Oceanography, Inc.

Erlenkeuser, H & Pederstad, K. (1984). *Recent sediment accumulation in Skagerrak as depicted by 210pb-dating.* Norwegian Journal of Geology. Vol. 64, pp. 135-152. Oslo.

GammaVision. (2017). *Gamma-Ray Spectrum Analysis and MCA Emulator for Microsoft® Windows® 7, 8.1, and 10 Professional.* Software User's Manual. Software version 8.1. ORTEC: U.S.A.

Geological Survey of Norway (NGU). (2018). *Combustion analysis: C-S-N.* Webpage. Available from: https://www.ngu.no/fagomrade/forbrenningsanalyse-c-s-n (Downloaded 25.04.2019). (In Norwegian).

Gilmore, G R. (2008). *Practical Gamma-ray Spectrometry.* 2nd edition. John Wiley & Sons, Ltd. England. ISBN 978-0-470-86196-7.

Gjelsvik, R & Steinnes, E. (2013). *Geographical trends in ^{137}Cs fallout from the Chernobyl accident and leaching from natural surface soil in Norway*. Journal of Environmental Radioactivity. Vol. 126, pp. 99-103. Elsevier.

Goldberg, E D. (1963). *Geochronology with Pb-210 in radioactive dating*. International Atomic Energy Agency. Symposium Proceedings. pp. 121-131. Vienna.

Grøttheim, S. (1998). *A preliminary report on radioactive contamination in the northern marine environment – studies on distribution of radiocaesium, plutonium and americium in sea water and sediments.* Norwegian Radiation Protection Authority.

Gwynn, J. (2018). *Radionuclides in the marine environment: Sources.* Norwegian Radiation Protection Authority. The Fram Centre, Tromsø. (PowerPoint).

Gäfvert, T, and Mauring, A. (2013). *Radon tightness of different sample sealing methods for gamma spectrometric measurements of ^{226}Ra*. Applied Radiation and Isotopes. Vol. 81, pp. 92-95. Elsevier.

Gäfvert T., Føyn L., Brungot A L., Kolstad A K., Lind B., Christensen G C., Strålberg E., Drefvelin J., Rudjord A L. (2003). *Radioactivity in the marine environment 2000 and 2001. Results from the Norwegian National Monitoring Programme (RAME).* Report 2003:8. Norwegian Radiation Protection Authority: Østerås.

Gäfvert T., Sværen I., Brungot A L., Kolstad A K., Lind B, Gwynn J., Alvestad P., Heldal H E., Føyn L., Strålberg E., Christensen G C., Skipperud L., Salbu B., Drefvelin J., Dowdall M., Rudjord A L. (2006). *Radioactivity in the marine environment 2004. Results from the Norwegian National Monitoring Programme (RAME).* Report 2006:14. Norwegian Radiation Protection Authority: Østerås.

Gäfvert T., Sværen I., Gwynn J., Brungot A L., Kolstad A K., Lind B., Alvestad P., Heldal H E., Strålberg E., Christensen G C., Drefvelin J., Dowdall M., Rudjord A L. (2007). *Radioactivity in the marine environment 2005. Results from the Norwegian National Monitoring Programme (RAME).* Report 2007:10. Norwegian Radiation Protection Authority: Østerås.

Gäfvert T., Heldal H E., Brungot A L., Gwynn J., Sværen I., Kolstad A K., Møller B., Strålberg E., Christensen G C., Drefvelin J., Dowdall M., Lind B., Rudjord A L. (2009). *Radioactivity in the marine environment 2007. Results from the Norwegian National Monitoring Programme (RAME).* Report 2009:15. Norwegian Radiation Protection Authority: Østerås.

Gäfvert T., Heldal H E., Brungot A L., Gwynn J., Sværen I., Kolstad A K., Møller B., Strålberg E., Christensen G C., Drefvelin J., Dowdall M., Lind B., Rudjord A L. (2011). *Radioactivity in the marine environment 2008 and 2009. Results from the Norwegian National Monitoring Programme (RAME).* Report 2011:4. Norwegian Radiation Protection Authority: Østerås.

Gäfvert, T., Heldal, H E., Brungot, A L., Gwynn, J., Strålberg, E., Sværen, I., Strømsnes, H., Kolstad, A K., Møller, B., Komperød, M., Lind, B., Rudjord, A L. (2012). *Radioactivity in the marine environment 2010. Results from the Norwegian National Monitoring Programme (RAME).* Report 2012:10. Norwegian Radiation Protection Authority: Østerås.

Haugen, I., Kirkerud, L., Kvalvågnæs, K., Magnusson, J., Rygg, B., Skei, J. (1981). *Vefsnfjorden as a recipient for waste from Mosjøen Aluminumworks*. Surveys 1978-1980. Report no. 1330. Norwegian institute for water research (NIVA): Oslo. (In Norwegian).

Harbitz, O. & Skuterud, Lavrans. (1999). *Radioactive contamination - importance for agriculture, the environment and the population.* Landbruksforlaget: Oslo. (In Norwegian).

Heldal, H E., Vikebø, F., Johansen G O. (2013). *Dispersal of the radionuclide caesium-137 (^{137}Cs) from point sources in the Barents and Norwegian Seas and its potential contamination of the Arctic marine food chain: Coupling numerical ocean models with geographical fish distribution data.* Environmental Pollution. Vol. 180, pp. 190-198. Elsevier.

Herrmann, J., Ikäheimonen, T K., Ilus, E., Kanisch, G., Lüning, M., Mattila, J., Nielsen, S P., Osvath, I., Outola, I. (2009). *Radioactivity in the Baltic Sea, 1999-2006.* Baltic Sea Environment Proceedings No. 117. HELCOM. ISSN 0357-2994.

Herrmann, J., Hutri, K L., Ikäheimonen, T K., Kanisch, G., Lüning, Nielsen, S P., Pham M K., Vartti, V P. (2013). *Thematic assessment of long-term changes in radioactivity in the Baltic Sea, 2007-2010.* Baltic Sea Environment Proceedings No. 135. HELCOM. ISSN 0537-2994.

Holby, O & Evans, S. (1996). *The Vertical Distribution of Chernobyl-Derived Radionuclides in a Baltic Sea Sediment.* Journal of Environmental Radioactivity. Vol. 33, pp. 129-145. Elsevier.

Ilus, E. (2007). *The Chernobyl accident and the Baltic Sea.* Boreal Environmental Research. Vol. 12, pp. 1-10. ISSN 1239-6095.

International Atomic Energy Agency Power Reactor Information System. (2019). IAEA PRIS. Webpage, available from: https://pris.iaea.org/PRIS/home.aspx (Downloaded: 26.02.2019).

International Atomic Energy Agency (IAEA). (2014). *The Environmental Behaviour of Radium: Revised Edition*. Technical Reports Series No. 476. IAEA: Vienna.

International Atomic Energy Agency (IAEA). (2005). *Worldwide marine radioactivity studies (WOMARS) Radionuclide levels in oceans and seas.* TECDOC-1429. IAEA: Vienna.

International Atomic Energy Agency (IAEA). (2004). *Sediment distribution coefficients and concentration factors for biota in the marine environment*. Technical Reports Series No. 422. IAEA: Vienna.

International Atomic Energy Agency (2003). *Extent of Environmental Contamination by Naturally Occurring Radioactive Material (NORM) and Technological Options for Mitigation.* Technical Reports Series No. 419. IAEA: Vienna.

International Atomic Energy Agency (IAEA). (1990). *The environmental behaviour of radium*. Vol. 1. Technical Reports Series No. 310. IAEA: Vienna.

Jensen. H, K B., Knies, J., Bellec, V. (2018). *Environmental geochemical data and dating results from MAREANO East – MAREANO.* Geological Survey of Norway (NGU) Report: Trondheim. ISSN 2387-3515.

Khalturin, I V., Rautian, T G., Richards, P G., and Leith, W S. (2005). *A Review of Nuclear Testing by the Soviet Union at Novaya Zemlya, 1955-1990.* Science and Global Security. Vol. 13, pp. 1–42. Taylor & Francis Inc. ISSN: 0892-9882 print.

Kinn, G & Gjelsvik, R. (2017). *Radioactivity in animals grazing on uncultivated pastures 2016. Summer monitoring and sheep classification zones 2016.* Report 2017:11. Norwegian Radiation Protection Authority: Østerås. (In Norwegian).

Kofstad, Per K & Pedersen, B. (2018). *Cesium.* From Store norske leksikon. Webpage, available from: https://snl.no/cesium (Downloaded 15.10.2018). (In Norwegian).

Liland, A., Hosseini, A., Losjpe, M., Nilsen, K A., Gäfvert T., Skjerdal, H. (2012). *Radioactive substances - fluxes, concentrations and possible effects in the Norwegian Sea.* Report 2016:6. Norwegian Radiation Protection Authority: Østerås. (In Norwegian).

Lind, O. C. (2018). *Sources; Past, present and future sources of radionuclides in the environment. CERAD* CoE. Norwegian University of Life Sciences: Isotope laboratory, Ås. (PowerPoint).

Lubis, A A. (2006). *Constant rate of supply (CRS) model for determining the sediment accumulation rates in the coastal area using ^{210}Pb.* Journal of Coastal Development. Vol. 10, pp. 9-18. ISSN 1410-5217.

LnHB. (2012a). *Atomic and nuclear data.* $^{210}_{82}Pb_{128}$. Webpage, available from: http://www.lnhb.fr/nuclides/Pb-210_tables.pdf (downloaded 18.09.2018).

LnHB. (2012b). *Atomic and nuclear data.* $^{228}_{88}Ra_{140}$. Webpage, available from: http://www.lnhb.fr/nuclides/Ra-228_tables.pdf (downloaded 15.10.2018).

LnHB. (2012c). *Atomic and nuclear data.* $^{40}_{19}K_{21}$. Webpage, available from: http://www.lnhb.fr/nuclides/K-40_tables.pdf (downloaded 02.05.2019).

LnHM. (2008a). *Atomic and nuclear data.* $^{137}_{55}Cs_{82}$. Webpage, available from: http://www.lnhb.fr/nuclides/Cs-137_tables.pdf (downloaded 15.10.2018).

LnHB. (2008b). *Atomic and nuclear data.* $^{226}_{88}Ra_{138}$. Webpage, available from: http://www.lnhb.fr/nuclides/Ra-226_tables.pdf (downloaded 15.10.2018).

MacKenzie, A B., Cook, G T., McDonald, P. (1999). *Radionuclide distribution and particle size association in Irish Sea surface sediments: implications for actinide dispersion.* Journal of Environmental Radioactivity. Vol. 44, pp. 275-296. Elsevier.

MacKenzie, A B., Hardie, S M L., Farmer J G., Eades L J., Pulford, I D. (2011). *Analytical and sampling constraints in ^{210}Pb dating.* Science of The Total Environment. Vol. 409, pp. 1298-1304. Elsevier.

North Sea Task Force (NSTF). (1993). *North Sea Quality Status Report 1993*. Oslo and Paris Commissions, London. Edited by: International Council of the Exploration of the Sea. Olsen & Olsen, Fredensborg, Denmark. ISBN: 87-85215-26-0.

Norwegian Mapping Authority. (-). *Maps of Norway*. Available from: https://www.norgeskart.no/?_ga=2.133304910.1339888707.1538652621-72359207.1538652621#!?project=seeiendom&layers=1002,1015&zoom=13&lat=7311356.88&lon=391169.09&sok=vefsnf (downloaded 04.10.2018).

Norwegian Radiation and Nuclear Safety Authority (DSA). (2019). *Joint Norwegian-Russian expedition to the sunken nuclear submarine Komsomolets in the Norwegian Sea*. DSA-information No. 07:2019. Østerås. (In Norwegian).

Norwegian Radiation and Nuclear Safety Authority (DSA). (in prep). *Radioactivity in the marine environment 2015, 2016 and 2017.* Results from the Norwegian National Monitoring Programme (RAME). In prep.

Norwegian Radiation Protection Authority (NRPA). (2018). *No leakage from the sunken nuclear submarine K-159.* NRPA Bulletin No. 07:2018. Østerås.

Norwegian Radiation Protection Authority (NRPA). (2012). *Joint Norwegian-Russian mission to investigate dumped atomic waste in the Kara Sea.* NRPA Bulletin. No. 2012:13. Østerås.

Norwegian Radiation Protection Authority (NRPA). (2006). *Radioactive contamination of Norwegian foodstuffs after the Chernobyl accident.* NRPA Bulletin. No. 2006:19. Østerås.

Olid, C., Diego, D., Orellana, J G., Cortizas, A M., Klaminder, J. (2016*). Modeling the downward transport of 210Pb in Peatlands: Initial Penetration-Constant Rate of Supply (IP-CRS) model.* Science of The Total Environment. Vol. 541, pp. 1222-1231. Elsevier.

Ottersen, G., Postmyr, E., Irgens, M. (2010). *Academic basis for a management plan for the North Sea and Skagerrak: Area report.* "Fisken og havet". No. 6:2010. Institute of Marine Research. TA-2681/2010. (In Norwegian).

Ottesen, D., Rise, L., Bøe, R., Longva, O., Olsen, H A., Thorsnes, T. (2000). *Geological atlas of the southern part of the Norwegian Trench and the northeastern North Sea.* NGU Report No. 104:2000. Geological Survey of Norway: Trondheim.

Oughton, D H., Skipperud, L., Fifield, L K., Cresswell, R G., Salbu, B., Day, P. (2004). *Accelerator mass spectrometry measurements of $^{240}Pu/^{239}Pu$ isotope ratios in Novaya Zemlya and Kara Sea sediments.* Applied radiation and Isotopes. Vol. 61, pp. 249-253. Elsevier.

Quality assurance data sheet. (2005) RAD12. Internal at the IMR.

Quality assurance data sheet. (2015) RAD14. Internal at the IMR.

Rise, L., Bøe, R., Ottesen, D., Longva, O., Olsen, H A. (2008). *Postglacial depositional environments and sedimentation rates in the Norwegian Channel off southern Norway.* Marine Geology. Vol. 251, pp.124-138. Elsevier.

Robu, E & Giovani, C. (2009). *Gamma-ray self-attenuation corrections in environmental samples.* Romanian Reports in Physics. Vol. 61, pp. 295-300.

Rudjord, A L., Oughton, D., Bergan, T D., Christensen, G. (1999). *Radionuclides in marine sediments – Distribution and processes*. In: Final reports from the sub-projects within the Nordic Nuclear Safety research Project EKO-1, pp. 72-95. ISBN 87-7893-056-1.

Schneider, M & Marignac, Y. (2008). *Spent Nuclear Fuel Reprocessing in France*. Research report no. 4. International Panel on Fissile Materials.

Schön, S J. (2011). *Physical Properties of Rocks*. Handbook of Petroleum Exploration and Production. Vol. 8, pp. 107-148. Elsevier.

Selnæs, Ø G., Eikelmann, I M., Amundsen, I. (2018). *Endringer i trusselbildet. Trusselvurdering for Kriseutvalget for atomberedskap, 2018*. Report 2018:10. Norwegian Radiation Protection Authority. Østerås. (In Norwegian).

Skipperud, L., Oughton, D H., Salbu, B. (2000). *The impact of plutonium speciation on the distribution coefficients in a sediment-sea water system, and radiological assessments of doses to humans.* Health Physics. Vol. 79, pp. 147-153.

Skjerdal, H., Heldal, H E., Gäfvert, T., Gwynn, J., Strålberg, E., Sværen, I., Liebig, P L., Kolstad, AK., Møller, B., Komperød, M., Lind, B., Rudjord, A L. (2015). *Radioactivity in the marine environment 2011. Results from the Norwegian National Monitoring Programme (RAME).* Report 2015:3. Norwegian Radiation Protection Authority: Østerås.

Skjerdal, H., Heldal, H E., Gwynn, J., Strålberg, E., Møller, B., Liebig, P L., Sværen, I., Rand, A., Gäfvert, T., Haanes, H. (2017). *Radioactivity in the Marine Environment 2012, 2013 and 2014. Results from the Norwegian National Monitoring Programme (RAME).* Report 2017:13. Norwegian Radiation Protection Authority: Østerås.

Stenius, S. (2017). *Revised flood calculation for the Vefsna and Skjerva rivers.* Report no. 17:2017. The Norwegian Water Resources and Energy Directorate (NVE). (In Norwegian). ISBN-978-82-410-1569-4.

Sternal, B., Junttila, J., Skirbekk, K., Forwick, M., Carroll, J., Pedersen, K B. (2017). *The immpact of submarine copper mine tailing disposal from the 1970s on Repparfjorden, northern Norway.* Marine Pollution Bulletin. Vol. 120, pp. 136-153. Elsevier.

Strålberg, E., Varskog, A T. S., Raaum, A., Varskog, P. (2003). *Naturally occurring radionuclides in the marine environment – an overview of current knowledge with emphasis the North Sea area.* Edited by P. Varskog. Report: ND/E-19/03. Norse Decom AS: Kjeller. ISBN 82-92538-01-1.

Sværen, I., Volynkin, A. (2019). *08r instructions for use and operation of ortec poptop HPGe-detectors; rad 12, rad14 and rad15.* Internal method at IMR. (In Norwegian).

Sværen, I. (2010). *Caesium-137 in sediments from two Norwegian fjords – including dating sediment cores.* Master of Science Thesis in Environmental Chemistry. Department of Chemistry, University of Bergen, Norway.

Tadjiki, S., Erten, H. N. (1994). *Radiochronology of sediments from the Mediterranean Sea using natural ^{210}Pb and fallout ^{137}Cs.* Journal of radioanalytical and nuclear chemistry, Vol. 181, pp. 447-459.

The Norwegian Directorate for Civil Protection (DSB). (2014). *National risk picture 2014.* Report from DSB. (In Norwegian). ISBN: 978-82-7768-352-2.

The Organisation for Economic Co-operation and Development (OECD). (2002). *Chernobyl: Assessment of Radiological and Health Impacts. 2002 Update of Chernobyl: Ten Years On.* Available from: https://www.oecd-nea.org/rp/pubs/2003/3508-chernobyl.pdf (Downloaded 15.10.2018).

Thørring, H., Hosseini A., Skuterud, L., Bergan, T D. (2014). *Radioactive contamination in population groups in 1999 and 2002. Reindeer herders in Central and Northern Norway.* Report 2004:12. Norwegian Radiation Protection Authority: Østerås. (In Norwegian).

United Nations Scientific Committee on the Effects of Atomic Radiation (UNSCEAR). (2000a). *ANNEX C: Exposures to the public from man-made sources of radiation.* Report. Available from: http://www.unscear.org/docs/publications/2000/UNSCEAR_2000_Report_Vol.I.pdf (Downloaded 21.02.2019). ISBN 92-1-142238-8.

United Nations Scientific Committee on the Effects of Atomic Radiation (UNSCEAR). (2000b). *ANNEX J: Exposures and effects of the Chernobyl accident.* Report. Available from: http://www.unscear.org/docs/reports/2000/Volume%20II_Effects/AnnexJ_pages%20451-566.pdf (Downloaded 15.10.2018). ISBN 92-1-142200-0.

United States Environmental Protection Agency (US EPA). (2018). Technologically Enhanced Naturally Occurring Radioactive Materials (TENORM). Available from: https://www.epa.gov/radiation/technologically-enhanced-naturally-occurring-radioactive-materials-tenorm. (Downloaded 06.05.2019).

Volynkin, A. (2019). *464 - Determination of radionuclides in sediments and biota, measured by gamma spectroscopy on the HPGe detector.* Internal method at IMR. (In Norwegian).

Zaborska, A., Carroll, J., Papucci C., Torricelli, L., Carroll, M.L., Walkusz-Miotk, J., Pempkowiak, J. (2008). *Recent sediment accumulation rates for the Western margin of the Barents Sea*. Deep Sea Research Part II. Vol. 55, pp. 2352-2360.

APPENDICES

Appendix A: Sample weights, porosities and density corrected depths

Table A1: Sample weights (g), porosities (%) and density corrected depths (cm) in sediment samples from core 1 from the Norwegian Trench (CTD906).

Sample-id: 906-1									
Sampling date: 13.11.2017									
Layer	Empty cups (g)	Gross wet weight (g)	Gross dry weight (g)	Net wet weight (g)	Net dry weight (g)	Porosity (%)	Nom. Thickness (cm)	Corr. Thicknes s/Cti	Corr. Depth/Cdi (cm)
0-1 cm	3,8	109,9	63,3	106,1	59,5	43,92	1,0	1,0	0,5
1-2 cm	3,8	121,1	71,8	117,3	68	42,03	1,0	1,0	1,5
2-3 cm	3,8	109,9	64,1	106,1	60,3	43,17	1,0	1,0	2,5
3-4 cm	3,8	135,3	77,1	131,5	73,3	44,26	1,0	1,0	3,5
4-5 cm	3,8	107,9	61,9	104,1	58,1	44,19	1,0	1,0	4,5
5-6 cm	3,8	121,7	68,3	117,9	64,5	45,29	1,0	1,0	5,5
6-7 cm	3,8	103,1	56,5	99,3	52,7	46,93	1,0	0,9	6,5
7-8 cm	3,9	112,3	58,8	108,4	54,9	49,35	1,0	0,9	7,4
8-9 cm	3,9	114,3	58,3	110,4	54,4	50,72	1,0	0,9	8,3
9-10 cm	3,9	134,0	68,0	130,1	64,1	50,73	1,0	0,9	9,2
10-12 cm	3,9	233,8	119,2	229,9	115,3	49,85	2,0	1,8	10,5
12-14 cm	3,8	251,4	130,5	247,6	126,7	48,83	2,0	1,8	12,3
14-16 cm	3,8	234,1	122,2	230,3	118,4	48,59	2,0	1,8	14,1
16-18 cm	3,8	284,8	152,3	281	148,5	47,15	2,0	1,9	16,0
18-19 cm	3,9	142,1	85,8	138,2	81,9	40,74	1,0	1,1	17,5

Table A2: Sample weights (g), porosities (%) and density corrected depths (cm) in sediment samples from core 2 from the Norwegian Trench (CTD906).

Sample-id: 906-2									
Sampling date: 13.11.2017									
Layer	Empty cups (g)	Gross wet weight (g)	Gross dry weight (g)	Net wet weight (g)	Net dry weight (g)	Porosity (%)	Nom. Thickness (cm)	Corr. Thicknes s/Cti	Corr. Depth/Cdi (cm)
0-1 cm	3,8	118,0	56,2	114,2	52,4	54,1	1,0	1,0	0,5
1-2 cm	3,8	120,9	59,2	117,1	55,4	52,7	1,0	1,0	1,5
2-3 cm	3,8	123,5	59,4	119,7	55,6	53,6	1,0	1,0	2,5
3-4 cm	3,8	119,4	59,1	115,6	55,3	52,2	1,0	1,0	3,6
4-5 cm	3,8	120,7	62,5	116,9	58,7	49,8	1,0	1,1	4,6
5-6 cm	3,8	115,4	58,7	111,6	54,9	50,8	1,0	1,1	5,7
6-7 cm	3,8	110,9	54,6	107,1	50,8	52,6	1,0	1,0	6,8
7-8 cm	3,9	120,9	59,0	117,0	55,1	52,9	1,0	1,0	7,8
8-9 cm	3,8	123,4	61,3	119,6	57,5	51,9	1,0	1,0	8,8
9-10 cm	3,9	138,8	72,1	134,9	68,2	49,4	1,0	1,1	9,9
10-12 cm	3,8	275,0	154,5	271,2	150,7	44,4	2,0	2,4	11,7

Table A3: Sample weights (g), porosities (%) and density corrected depths (cm) in sediment samples from core 3 from the Norwegian Trench (CTD906).

Sample-id: 906-3									
Sampling date: 13.11.2017									
Layer	Empty cups (g)	Gross wet weight (g)	Gross dry weight (g)	Net wet weight (g)	Net dry weight (g)	Porosity (%)	Nom. Thickness (cm)	Corr. Thicknes s/Cti	Corr. Depth/Cdi (cm)
0-1 cm	3,8	112,6	53,3	108,8	49,5	54,5	1,0	1,0	0,5
1-2 cm	3,8	122,3	60,0	118,5	56,2	52,6	1,0	1,0	1,5
2-3 cm	3,8	133,5	67,2	129,7	63,4	51,1	1,0	1,1	2,6
3-4 cm	3,8	133,2	69,5	129,4	65,7	49,2	1,0	1,1	3,7
4-5 cm	3,8	136,8	72,7	133,0	68,9	48,2	1,0	1,1	4,8
5-6 cm	3,8	135,4	73,3	131,6	69,5	47,2	1,0	1,2	6,0
6-7 cm	3,8	129,5	69,0	125,7	65,2	48,1	1,0	1,1	7,1
7-8 cm	3,8	129,9	68,6	126,1	64,8	48,6	1,0	1,1	8,2
8-9 cm	3,9	140,3	74,7	136,4	70,8	48,1	1,0	1,1	9,4
9-10 cm	3,8	139,1	76,6	135,3	72,8	46,2	1,0	1,2	10,5
10-12 cm	3,8	267,4	154,5	263,6	150,7	42,8	2,0	2,5	12,4
12-14 cm	3,8	197,4	114,9	193,6	111,1	42,6	2,0	2,5	14,9

Table A4: Sample weights (g), porosities (%) and density corrected depths (cm) in sediment samples from core 4 from the Norwegian Trench (CTD906).

Sample-id: 906-4									
Sampling date: 13.11.2017									
Layer	Empty cups (g)	Gross wet weight (g)	Gross dry weight (g)	Net wet weight (g)	Net dry weight (g)	Porosity (%)	Nom. Thickness (cm)	Corr. Thicknes s/Cti	Corr. Depth/Cdi (cm)
0-1 cm	3,8	123,7	58,0	119,9	54,2	54,8	1,0	1,0	0,5
1-2 cm	3,8	119,1	59,4	115,3	55,6	51,8	1,0	1,1	1,5
2-3 cm	3,8	118,1	61,0	114,3	57,2	50,0	1,0	1,1	2,6
3-4 cm	3,9	126,6	66,3	122,7	62,4	49,1	1,0	1,1	3,7
4-5 cm	3,8	132,1	71,0	128,3	67,2	47,6	1,0	1,2	4,9
5-6 cm	3,8	135,6	72,9	131,8	69,1	47,6	1,0	1,2	6,0
6-7 cm	3,8	136,9	75,7	133,1	71,9	46,0	1,0	1,2	7,2
7-8 cm	3,8	146,0	84,8	142,2	81,0	43,0	1,0	1,3	8,4
8-9 cm	3,9	131,9	79,6	128,0	75,7	40,9	1,0	1,3	9,7
9-10 cm	3,9	129,5	79,1	125,6	75,2	40,1	1,0	1,3	11,0
10-12 cm	3,9	275,2	169,8	271,3	165,9	38,8	2,0	2,7	13,1
12-14 cm	3,8	278,6	174,2	274,8	170,4	38,0	2,0	2,7	15,8
14-16 cm	3,8	222,4	138,2	218,6	134,4	38,5	2,0	2,7	18,5
16-18 cm	3,8	235,9	142,3	232,1	138,5	40,3	2,0	2,6	21,2

Table A5: Sample weights (g), porosities (%) and density corrected depths (cm) in sediment samples from 2 cores from Vefsnfjord (CTD1121).

Sample-id: 1121-1										Sample-id: 1121-2									
Sampling date: 28.10.2018										Sampling date: 28.10.2018									
Layer	Empty cups (g)	Gross wet weight (g)	Gross dry weight (g)	Net wet weight (g)	Net dry weight (g)	Porosity (%)	Nom. Thickness (cm)	Corr. Thickness /Cti (cm)	Corr. Depth/Cdi (cm)	Layer	Empty cups (g)	Gross wet weight	Gross dry weight	Net wet weight (g)	Net dry weight (g)	Porosity (%)	Nom. Thickness (cm)	Corr. Thickness /Cti (cm)	Corr. Depth/Cdi (cm)
0-1 cm	2,5	167,5	67,3	165,0	64,8	60,7	1,0	1,0	0,5	0-1 cm	2,5	183,0	76,3	180,5	73,8	59,1	1,0	1,0	0,5
1-2 cm	2,5	152,0	69,2	149,5	66,7	55,4	1,0	1,1	1,6	1-2 cm	2,5	149,0	65,7	146,5	63,2	56,9	1,0	1,1	1,5
2-3 cm	2,5	119,0	57,5	116,5	55,0	52,8	1,0	1,2	2,7	2-3 cm	2,5	173,5	82,2	171,0	79,7	53,4	1,0	1,1	2,6
3-4 cm	2,5	135,0	67,0	132,5	64,5	51,3	1,0	1,2	4,0	3-4 cm	2,5	169,0	83,6	166,5	81,1	51,3	1,0	1,2	3,8
4-5 cm	2,5	128,0	63,8	125,5	61,3	51,2	1,0	1,2	5,2	4-5 cm	2,5	172,5	86,2	170,0	83,7	50,8	1,0	1,2	5,0
5-6 cm	2,5	126,5	63,1	124,0	60,6	51,1	1,0	1,2	6,4	5-6 cm	2,5	193,0	96,2	190,5	93,7	50,8	1,0	1,2	6,2
6-7 cm	2,5	141,5	70,2	139,0	67,7	51,3	1,0	1,2	7,7	6-7 cm	2,5	165,0	81,9	162,5	79,4	51,1	1,0	1,2	7,4
7-8 cm	2,5	112,0	54,8	109,5	52,3	52,2	1,0	1,2	8,9	7-8 cm	2,5	120,0	59,2	117,5	56,7	51,7	1,0	1,2	8,6
8-9 cm	2,5	106,0	51,7	103,5	49,2	52,5	1,0	1,2	10,1	8-9 cm	2,5	156,5	76,6	154,0	74,1	51,9	1,0	1,2	9,8
9-10 cm	2,5	98,5	48,0	96,0	45,5	52,6	1,0	1,2	11,3	9-10 cm	2,5	137,5	66,6	135,0	64,1	52,5	1,0	1,2	10,9
10-12 cm	2,5	201,5	97,4	199,0	94,9	52,3	2,0	2,4	13,2	10-12 cm	2,5	216,0	103,8	213,5	101,3	52,6	2,0	2,3	12,7
12-14 cm	2,5	201,5	97,9	199,0	95,4	52,1	2,0	2,4	15,6	12-14 cm	2,5	250,0	120,9	247,5	118,4	52,2	2,0	2,3	15,0
14-16 cm	2,5	219,0	106,6	216,5	104,1	51,9	2,0	2,4	18,0	14-16 cm	2,5	228,5	113,2	226,0	110,7	51,0	2,0	2,4	17,4
16-18 cm	2,5	241,5	120,3	239,0	117,8	50,7	2,0	2,5	20,5	16-18 cm	2,5	206,0	103,7	203,5	101,2	50,3	2,0	2,4	19,8
18-20 cm	2,5	226,0	113,9	223,5	111,4	50,2	2,0	2,5	23,0	18-19 cm*	2,5	124,0	64,2	121,5	61,7	49,2	1,0	1,2	21,6
										* last slice (12-13 cm) only 1 cm.									

Table A6: Sample weights (g), porosities (%) and density corrected depths (cm) in sediment samples from 2 cores from Vefsnfjord (CTD1122).

Sample-id: 1122-1										Sample-id: 1122-2									
Sampling date: 28.10.2018										Sampling date: 28.10.2018									
Layer	Empty cups (g)	Gross wet weight	Gross dry weight	Net wet weight (g)	Net dry weight (g)	Porosity (%)	Nom. Thickness (cm)	Corr. Thickness/Cti	Corr. Depth/Cdi (cm)	Layer	Empty cups (g)	Gross wet weight	Gross dry weight	Net wet weight (g)	Net dry weight (g)	Porosity (%)	Nom. Thickness (cm)	Corr. Thickness/Cti	Corr. Depth/Cdi (cm)
0-1 cm	2,5	136,5	60,9	134,0	58,4	56,4	1,0	1,0	0,5	0-1 cm	2,5	185,0	78,6	182,5	76,1	58,3	1,0	1,0	0,5
1-2 cm	2,5	137,0	63,8	134,5	61,3	54,4	1,0	1,0	1,5	1-2 cm	2,5	136,0	62,4	133,5	59,9	55,1	1,0	1,1	1,5
2-3 cm	2,5	149,5	73,7	147,0	71,2	51,6	1,0	1,1	2,6	2-3 cm	2,5	156,5	78,8	154,0	76,3	50,5	1,0	1,2	2,7
3-4 cm	2,5	171,0	87,9	168,5	85,4	49,3	1,0	1,2	3,7	3-4 cm	2,5	175,5	91,3	173,0	88,8	48,7	1,0	1,2	3,9
4-5 cm	2,5	136,5	71,7	134,0	69,2	48,4	1,0	1,2	4,9	4-5 cm	2,5	167,5	89,6	165,0	87,1	47,2	1,0	1,3	5,1
5-6 cm	2,5	144,5	77,1	142,0	74,6	47,5	1,0	1,2	6,1	5-6 cm	2,5	157,0	85,2	154,5	82,7	46,5	1,0	1,3	6,4
6-7 cm	2,5	140,0	76,5	137,5	74,0	46,2	1,0	1,2	7,3	6-7 cm	2,5	190,0	106,3	187,5	103,8	44,6	1,0	1,3	7,7
7-8 cm	2,5	142,5	77,8	140,0	75,3	46,2	1,0	1,2	8,6	7-8 cm	2,5	151,0	86,4	148,5	83,9	43,5	1,0	1,4	9,0
8-9 cm	2,5	142,0	79,9	139,5	77,4	44,5	1,0	1,3	9,8	8-9 cm	2,5	158,5	92,7	156,0	90,2	42,2	1,0	1,4	10,4
9-10 cm	2,5	153,0	90,0	150,5	87,5	41,9	1,0	1,3	11,1	9-10 cm	2,5	160,0	96,5	157,5	94,0	40,3	1,0	1,4	11,8
10-12 cm	2,5	257,5	153,1	255,0	150,6	40,9	2,0	2,7	13,1	10-12 cm	2,5	266,5	160,6	264,0	158,1	40,1	2,0	2,9	14,0
12-14 cm	2,5	273,5	163,8	271,0	161,3	40,5	2,0	2,7	15,9	12-14 cm*	2,5	159,0	96,5	156,5	94,0	39,9	1,5	2,2	16,5
										* last slice (12-14 cm) not completly 2 cm.									

Table A7: Sample weights (g), porosities (%) and density corrected depths (cm) in sediment samples from 2 cores from Vefsnfjord (CTD1123).

Sample-id: 1123-1										Sample-id: 1123-2									
Sampling date: 28.10.2018										Sampling date: 28.10.2018									
Layer	Empty cups (g)	Gross wet weight	Gross dry weight	Net wet weight (g)	Net dry weight (g)	Porosity (%)	Nom. Thickness (cm)	Corr. Thickness /Cti (cm)	Corr. Depth/Cd i (cm)	Layer	Empty cups (g)	Gross wet weight	Gross dry weight	Net wet weight (g)	Net dry weight (g)	Porosity (%)	Nom. Thickness (cm)	Corr. Thickness/ Cti (cm)	Corr. Depth/C di (cm)
0-1 cm	2,5	130,0	48,7	127,5	46,2	63,8	1,0	1,0	0,5	0-1 cm	2,5	191,0	73,2	188,5	70,7	62,5	1,0	1,0	0,5
1-2 cm	2,5	155,5	66,2	153,0	63,7	58,4	1,0	1,1	1,6	1-2 cm	2,5	140,5	65,5	138,0	63,0	54,3	1,0	1,2	1,6
2-3 cm	2,5	139,0	67,6	136,5	65,1	52,3	1,0	1,3	2,8	2-3 cm	2,5	153,5	76,8	151,0	74,3	50,8	1,0	1,3	2,9
3-4 cm	2,5	140,0	74,1	137,5	71,6	47,9	1,0	1,4	4,2	3-4 cm	2,5	170,0	90,4	167,5	87,9	47,5	1,0	1,4	4,2
4-5 cm	2,5	152,0	83,6	149,5	81,1	45,8	1,0	1,5	5,7	4-5 cm	2,5	177,0	97,3	174,5	94,8	45,7	1,0	1,4	5,7
5-6 cm	2,5	163,0	90,4	160,5	87,9	45,2	1,0	1,5	7,2	5-6 cm	2,5	137,5	74,5	135,0	72,0	46,7	1,0	1,4	7,1
6-7 cm	2,5	145,0	80,0	142,5	77,5	45,6	1,0	1,5	8,7	6-7 cm	2,5	139,5	76,0	137,0	73,5	46,4	1,0	1,4	8,5
7-8 cm	2,5	136,5	75,8	134,0	73,3	45,3	1,0	1,5	10,2	7-8 cm	2,5	124,0	67,9	121,5	65,4	46,2	1,0	1,4	9,9
8-9 cm	2,5	139,5	78,3	137,0	75,8	44,7	1,0	1,5	11,7	8-9 cm	2,5	156,0	87,2	153,5	84,7	44,8	1,0	1,5	11,4
9-10 cm	2,5	130,0	74,4	127,5	71,9	43,6	1,0	1,6	13,2	9-10 cm	2,5	155,5	88,1	153,0	85,6	44,1	1,0	1,5	12,9
10-12 cm	2,5	226,5	132,4	224,0	129,9	42,0	2,0	3,2	15,6	10-12 cm	2,5	285,0	167,2	282,5	164,7	41,7	2,0	3,1	15,2
12-14 cm	2,5	234,0	141,2	231,5	138,7	40,1	2,0	3,3	18,9	12-14 cm	2,5	306,0	180,7	303,5	178,2	41,3	2,0	3,1	18,3
14-16 cm	2,5	258,0	155,1	255,5	152,6	40,3	2,0	3,3	22,2	14-16 cm	2,5	254,5	150,8	252,0	148,3	41,2	2,0	3,1	21,4
16-18 cm	2,5	258,0	154,6	255,5	152,1	40,5	2,0	3,3	25,5										

Table A8: Sample weights (g), porosities (%) and density corrected depths (cm) in sediment samples from 2 cores from Vefsnfjord (CTD1124).

Sample-id: 1124-1										Sample-id: 1124-2									
Sampling date: 28.10.2018										Sampling date: 28.10.2018									
Layer	Empty cups (g)	Gross wet weight	Gross dry weight	Net wet weight (g)	Net dry weight (g)	Porosity (%)	Nom. Thickness (cm)	Corr. Thickness /Cti (cm)	Corr. Depth/Cd i (cm)	Layer	Empty cups (g)	Gross wet weight	Gross dry weight	Net wet weight (g)	Net dry weight (g)	Porosity (%)	Nom. Thickness (cm)	Corr. Thickness/ Cti (cm)	Corr. Depth/C di (cm)
0-1 cm	2,5	176,0	80,9	173,5	78,4	54,8	1,0	1,0	0,5	0-1 cm	2,5	150,5	66,4	148,0	63,9	56,8	1,0	1,0	0,5
1-2 cm	2,5	140,0	70,6	137,5	68,1	50,5	1,0	1,1	1,5	1-2 cm	2,5	144,5	70,6	142,0	68,1	52,0	1,0	1,1	1,6
2-3 cm	2,5	130,5	70,8	128,0	68,3	46,6	1,0	1,2	2,7	2-3 cm	2,5	149,5	80,2	147,0	77,7	47,1	1,0	1,2	2,7
3-4 cm	2,5	138,0	78,7	135,5	76,2	43,8	1,0	1,2	3,9	3-4 cm	2,5	153,5	88,4	151,0	85,9	43,1	1,0	1,3	4,0
4-5 cm	2,5	147,5	87,3	145,0	84,8	41,5	1,0	1,3	5,2	4-5 cm	2,5	151,5	92,4	149,0	89,9	39,7	1,0	1,4	5,4
5-6 cm	2,5	152,0	94,6	149,5	92,1	38,4	1,0	1,4	6,5	5-6 cm	2,5	156,0	98,1	153,5	95,6	37,7	1,0	1,4	6,8
6-7 cm	2,5	161,0	102,4	158,5	99,9	37,0	1,0	1,4	7,9	6-7 cm	2,5	156,5	100,7	154,0	98,2	36,2	1,0	1,5	8,2
7-8 cm	2,5	146,5	92,4	144,0	89,9	37,6	1,0	1,4	9,3	7-8 cm	2,5	158,5	102,9	156,0	100,4	35,6	1,0	1,5	9,7
8-9 cm	2,5	134,0	84,7	131,5	82,2	37,5	1,0	1,4	10,6	8-9 cm	2,5	148,0	96,0	145,5	93,5	35,7	1,0	1,5	11,2
9-10 cm	2,5	164,0	104,2	161,5	101,7	37,0	1,0	1,4	12,0	9-10 cm	2,5	159,5	103,5	157,0	101,0	35,7	1,0	1,5	12,7
10-12 cm	2,5	279,0	175,7	276,5	173,2	37,4	2,0	2,8	14,1	10-12 cm	2,5	300,0	193,1	297,5	190,6	35,9	2,0	3,0	14,9
										12-13 cm*	2,5	153,0	97,4	150,5	94,9	36,9	1,0	1,5	17,1
										* last slice (12-13 cm) only 1 cm.									

Appendix B: Data from detector control, background measurements and calibration measurements

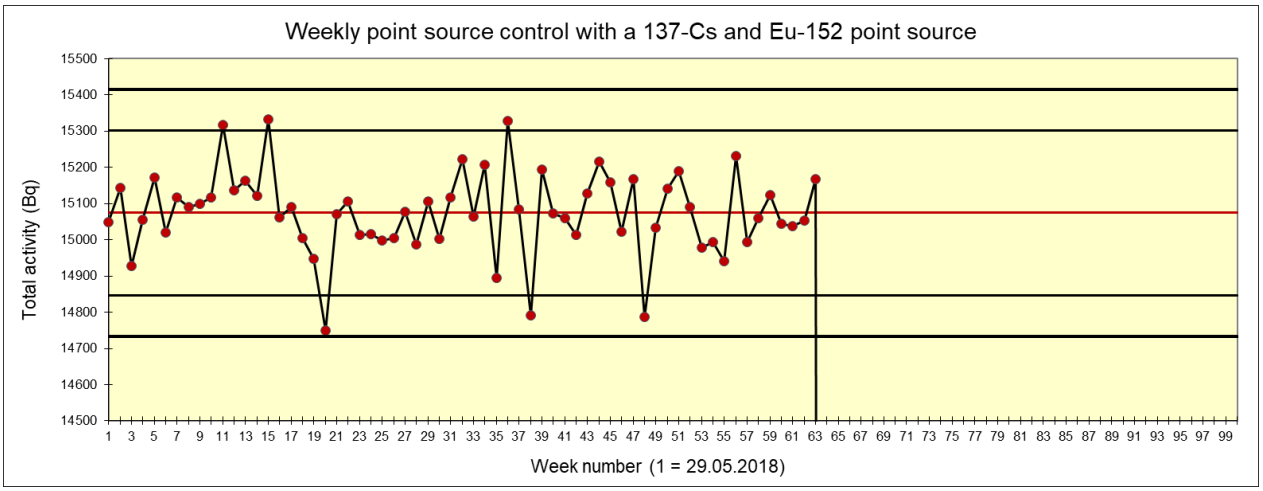

Figure B1: Weekly measurements of a ^{137}Cs (661.7 keV) +^{152}Eu (244.7 keV and 1408.0 keV) point source from 29.05.2018 (1) to 20.05.2019 (63) on detector RAD12. The red line is mean value, and the black lines represent mean ± 2 and 3 std.dev.

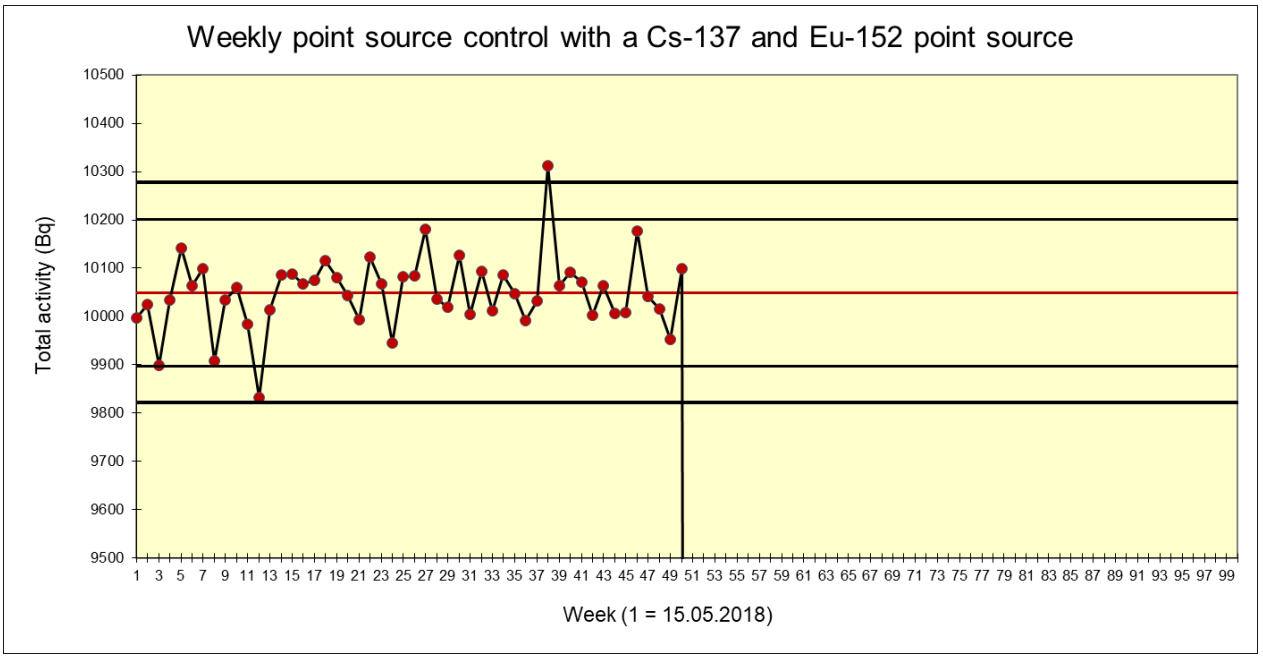

Figure B2: Weekly measurements of a ^{137}Cs (661.7 keV) +^{152}Eu (244.7 keV and 1408.0 keV) point source from 15.05.2018 (1) to 20.05.2019 (50) on detector RAD14. The red line is mean value, and the black lines represent mean ± 2 and 3 std.dev.

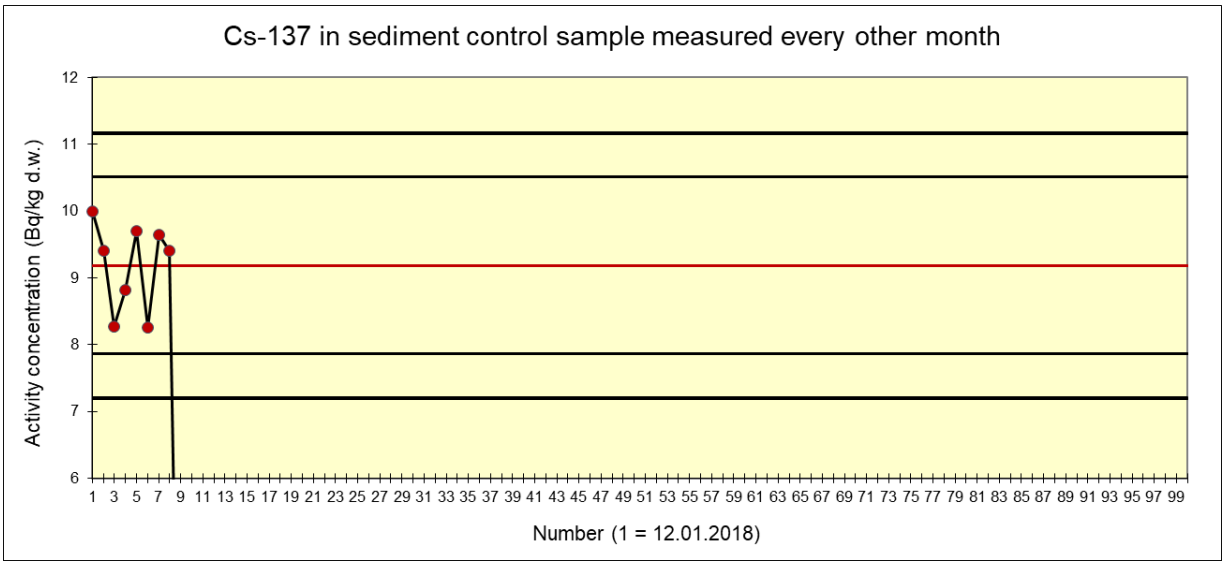

Figure B3: Every other month measurement of a ^{137}Cs in a sediment control sample "Kara" on detector RAD12 from 12.01.2018 to 21.12.2018. The red line is mean value, and the black lines represent mean ± 2 and 3 std.dev.

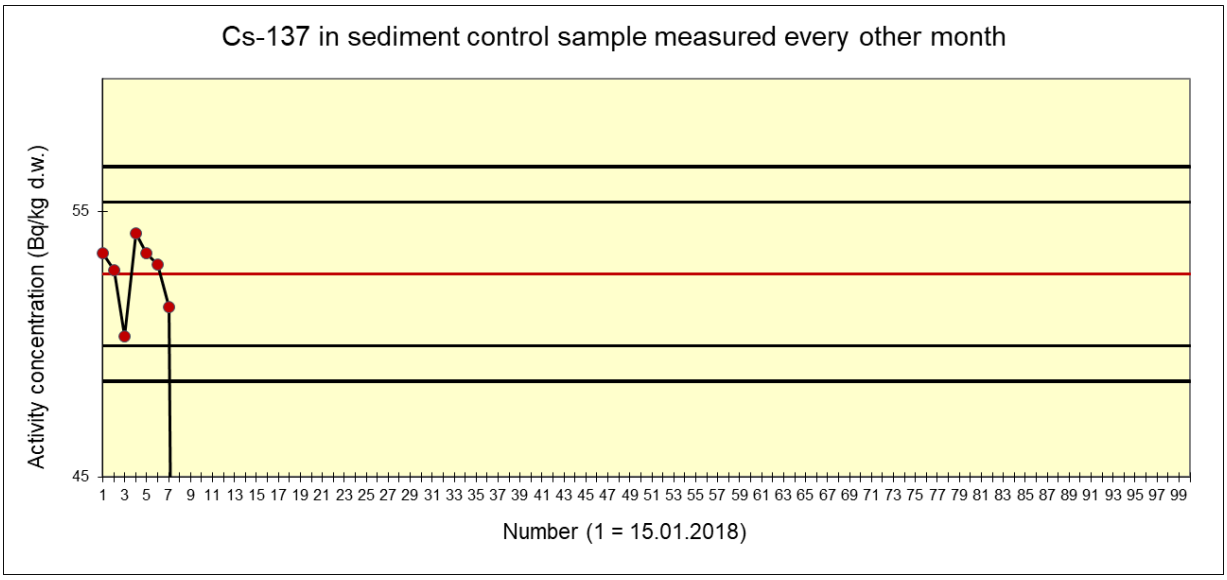

Figure B4: Every other month measurement of a ^{137}Cs in a sediment control sample "Murmansk" on detector RAD12 from 15.01.2018 to 19.12.2018. The red line is mean value, and the black lines represent mean ± 2 and 3 std.dev.

Appendix C: Data and results from measuring Cs-137, Ra-226, Ra-228 and K-40

Table C1: Data and results of Cs-137, Ra-226, Ra-228 and K-40 measurements in core 1/4 from the Norwegian Trench (CTD906-1).

Sample-id: 906-1												
Layer	Sampling date	Date of sealing sample	Date of measurement	Sample weight (g)	Counting time (sec)	Cs-137 (Bq/kg d.w.)	Uncertainty (Bq/kg d.w.)	Bi-214/Ra-226 (Bq/kg	Uncertainty (Bq/kg d.w.)	Ac-228/Ra-228	Uncertainty (Bq/kg d.w.)	K-40 (Bq/kg d.w.)	Uncertainty (Bq/kg d.w)
0-1 cm	13.11.2017	23.04.2018	07.06.2018	57,4	81830	2,7	0,8	31,9	3,8	48,5	6,4	761,5	74,9
1-2 cm	13.11.2017	23.04.2018	08.06.2018	58,4	88510	2,7	0,8	31,9	3,8	48,5	6,4	761,5	74,9
2-3 cm	13.11.2017	23.04.2018	11.06.2018	58,2	261799	2,5	0,4	27,0	2,8	38,3	4,7	809,4	77,3
3-4 cm	13.11.2017	23.04.2018	21.06.2018	59,9	77448	2,4	0,8	28,8	3,5	42,4	5,9	832,2	81,5
4-5 cm	13.11.2017	23.04.2018	22.06.2018	57,6	85451	2,1	0,6	28,5	3,5	42,6	5,7	863,0	84,2
5-6 cm	13.11.2017	23.04.2018	08.08.2018	59,8	84748	1,8	0,5	30,4	3,8	44,6	5,9	858,8	83,8
6-7 cm	13.11.2017	25.04.2018	09.08.2018	52,8	84945	1,9	0,7	29,8	3,8	49,9	6,6	873,6	85,6
7-8 cm	13.11.2017	25.04.2018	10.08.2018	54,9	88532	2,2	0,9	30,2	3,7	50,1	6,6	817,9	85,2
8-9 cm	13.11.2017	25.04.2018	13.08.2018	54,7	256844	0,9	0,3	31,8	3,3	48,8	5,9	877,4	83,8
9-10 cm	13.11.2017	25.04.2018	14.08.2018	59,4	76894	0,6 (b.d.)	-	31,4	3,8	51,3	6,6	889,9	87,0
10-12 cm	13.11.2017	25.04.2018	15.08.2018	57,3	86267	0,7 (b.d.)	-	34,0	4,0	52,1	6,8	906,1	88,4
12-14 cm	13.11.2017	26.04.2018	16.08.2018	58,2	88110	0,6 (b.d.)	-	33,6	4,0	51,8	6,5	906,3	88,2
14-16 cm	13.11.2017	26.04.2018	21.08.2018	55,3	71701	0,7 (b.d.)	-	33,7	4,1	52,1	6,9	932,8	91,9
16-18 cm	13.11.2017	26.04.2018	22.08.2018	60,4	85264	0,6 (b.d.)	-	36,7	4,1	53,6	6,7	927,9	90,3
18-19 cm	13.11.2017	26.04.2018	23.08.2018	59,9	80189	0,4 (b.d.)	-	37,3	4,0	54,7	7,0	915,2	89,3

Table C2: Data and results of Cs-137, Ra-226, Ra-228 and K-40 measurements in core 2/4 from the Norwegian Trench (CTD906-2).

Sample-id: 906-2													
Layer	Sampling date	Date of sealing sample	Date of measurement	Sample weight (g)	Counting time (sec)	Cs-137 (Bq/kg d.w.)	Uncertainty (Bq/kg d.w.)	Bi-214/Ra-226 (Bq/kg	Uncertainty (Bq/kg d.w.)	Ac-228/Ra-228	Uncertainty (Bq/kg d.w.)	K-40 (Bq/kg d.w.)	Uncertainty (Bq/kg d.w)
0-1 cm	13.11.2017	26.04.2018	23.07.2018	51,8	224022	2,4	0,4	31,5	3,3	45,8	5,7	780,8	74,9
1-2 cm	13.11.2017	26.04.2018	30.07.2018	55,3	236461	1,9	0,4	28,9	3,0	40,7	5,1	816,0	78,1
2-3 cm	13.11.2017	26.04.2018	24.07.2018	55,7	87359	1,8	0,8	29,7	3,8	44,3	5,9	875,7	85,5
3-4 cm	13.11.2017	26.04.2018	27.08.2018	55,2	255383	1,0	0,3	29,9	3,1	45,8	5,6	890,7	84,9
4-5 cm	13.11.2017	27.04.2018	28.08.2018	58,8	83031	0,5 (b.d.)	-	32,2	3,6	47,4	6,2	912,2	88,9
5-6 cm	13.11.2017	27.04.2018	29.08.2018	55	84398	0,9 (b.d.)	-	32,9	3,9	49,4	6,7	917,8	89,7
6-7 cm	13.11.2017	27.04.2018	30.08.2018	50,7	85686	0,6 (b.d.)	-	32,2	4,1	49,5	6,6	941,7	92,2
7-8 cm	13.11.2017	27.04.2018	31.08.2018	55,1	87305	0,8	0,5	34,3	4,0	51,0	6,5	918,7	89,7
8-9 cm	13.11.2017	27.04.2018	03.09.2018	57,4	251506	0,4 (b.d.)	-	33,0	3,4	50,7	6,1	926,6	88,3
9-10 cm	13.11.2017	27.04.2018	04.09.2018	61,4	74514	0,7 (b.d.)	-	34,4	4,1	51,9	6,7	937,3	91,5
10-12 cm	13.11.2017	27.04.2018	05.09.2018	57,6	80474	0,5 (b.d.)	-	37,5	4,3	52,5	6,8	935,7	91,3

Table C3: Data and results of Cs-137, Ra-226, Ra-228 and K-40 measurements in core 3/4 from the Norwegian Trench (CTD906-3).

Sample-id: 906-3													
Layer	Sampling date	Date of sealing sample	Date of measurement	Sample weight (g)	Counting time (sec)	Cs-137 (Bq/kg d.w.)	Uncertainty (Bq/kg d.w.)	Bi-214/Ra-226 (Bq/kg	Uncertainty (Bq/kg d.w.)	Ac-228/Ra-228	Uncertainty (Bq/kg d.w.)	K-40 (Bq/kg d.w.)	Uncertainty (Bq/kg d.w)
0-1 cm	13.11.2017	08.06.2018	06.09.2018	50,1	81940	2,5	0,8	32,5	3,9	45,2	6,1	766,7	76,1
1-2 cm	13.11.2017	08.06.2018	07.09.2018	56,7	85913	2,8	0,8	30,4	3,7	46,5	6,2	754,2	74,1
2-3 cm	13.11.2017	08.06.2018	10.09.2018	62,2	95883	2,7	0,5	27,7	3,4	38,4	5,1	785,3	76,5
3-4 cm	13.11.2017	08.06.2018	11.09.2018	62,1	80226	3,0	0,8	27,7	3,4	39,0	5,3	790,4	77,4
4-5 cm	13.11.2017	08.06.2018	12.09.2018	62,0	86068	2,3	0,4	29,6	3,2	40,9	5,1	788,2	75,8
5-6 cm	13.11.2017	08.06.2018	13.09.2018	57,9	85683	2,0	0,5	28,8	3,8	43,3	5,8	837,7	81,9
6-7 cm	13.11.2017	08.06.2018	14.09.2018	60,0	75003	1,7	0,7	27,3	3,3	43,1	5,9	839,4	82,3
7-8 cm	13.11.2017	08.06.2018	17.09.2018	60,3	252899	1,0	0,3	28,3	2,9	45,8	5,6	856,0	81,6
8-9 cm	13.11.2017	08.06.2018	18.09.2018	61,5	68214	0,7	0,4	31,3	4,0	49,8	6,6	858,6	84,2
9-10 cm	13.11.2017	08.06.2018	19.09.2018	60,5	89627	0,7 (b.d.)	-	32,7	3,9	50,7	6,6	897,1	87,1
10-12 cm	13.11.2017	20.06.2018	20.09.2018	56,0	84844	0,5 (b.d.)	-	34,4	4,2	52,8	6,9	898,3	87,7
12-14 cm	13.11.2017	20.06.2018	21.09.2018	55,1	78236	0,5 (b.d.)	-	38,6	4,4	54,9	7,2	877,7	86,2

Table C4: Data and results of Cs-137, Ra-226, Ra-228 and K-40 measurements in core 4/4 from the Norwegian Trench (CTD906-4).

Sample-id: 906-4													
Layer	Sampling date	Date of sealing sample	Date of measurement	Sample weight (g)	Counting time (sec)	Cs-137 (Bq/kg d.w.)	Uncertainty (Bq/kg d.w.)	Bi-214/Ra-226 (Bq/kg	Uncertainty (Bq/kg d.w.)	Ac-228/Ra-228	Uncertainty (Bq/kg d.w.)	K-40 (Bq/kg d.w.)	Uncertainty (Bq/kg d.w)
0-1 cm	13.11.2017	20.06.2018	24.09.2018	57,4	234356	2,5	0,4	35,5	3,6	48,0	5,9	755,9	72,4
1-2 cm	13.11.2017	20.06.2018	26.09.2018	58,4	70290	2,6	0,6	33,5	3,8	46,4	6,3	761,9	75,6
2-3 cm	13.11.2017	20.06.2018	27.09.2018	58,2	86942	2,7	0,8	29,9	3,7	39,0	5,2	775,6	76,0
3-4 cm	13.11.2017	20.06.2018	28.09.2018	59,9	81774	2,7	0,8	29,4	3,6	40,1	5,4	815,2	79,7
4-5 cm	13.11.2017	20.06.2018	01.10.2018	57,6	256820	1,8	0,3	28,3	3,0	40,2	5,0	817,3	77,9
5-6 cm	13.11.2017	20.06.2018	02.10.2018	59,8	84414	2,2	0,7	29,4	3,6	44,8	5,9	832,0	81,3
6-7 cm	13.11.2017	20.06.2018	03.10.2018	52,8	81275	1,6	0,6	32,1	3,6	48,3	6,4	849,8	83,1
7-8 cm	13.11.2017	20.06.2018	04.10.2018	54,9	82768	0,7 (b.d.)	-	29,9	3,8	46,8	6,1	885,7	86,2
8-9 cm	13.11.2017	20.06.2018	05.10.2018	54,7	89293	1,0	0,4	31,0	3,7	48,6	6,3	903,5	87,9
9-10 cm	13.11.2017	20.06.2018	08.10.2018	59,4	254627	0,4	0,2	30,3	3,0	47,7	5,7	916,1	87,2
10-12 cm	13.11.2017	20.06.2018	09.10.2018	57,3	74070	0,6 (b.d.)	-	32,9	4,1	49,2	6,5	913,0	89,4
12-14 cm	13.11.2017	20.06.2018	10.10.2018	58,2	86609	0,8 (b.d.)	-	31,8	3,6	53,7	7,0	918,4	89,6
14-16 cm	13.11.2017	20.06.2018	11.10.2018	55,3	86678	0,6 (b.d.)	-	35,5	4,0	52,6	6,8	903,7	88,1
16-18 cm	13.11.2017	20.06.2018	12.10.2018	60,4	85064	0,7 (b.d.)	-	34,9	4,0	53,8	7,0	949,1	92,5

Table C5: Data and results of Cs-137, Ra-226, Ra-228 and K-40 measurements in core 1/2 from the Vefsnfjord (CTD1121-1).

Sample-id: 1121-1													
Layer	Sampling date	Date of sealing sample	Date of measurement	Sample weight (g)	Counting time (sec)	Cs-137 (Bq/kg d.w.)	Uncertainty (Bq/kg d.w.)	Bi-214/Ra-226 (Bq/kg	Uncertainty (Bq/kg d.w.)	Ac-228/Ra-228	Uncertainty (Bq/kg d.w.)	K-40 (Bq/kg d.w.)	Uncertainty (Bq/kg d.w)
0-1 cm	28.10.2018	14.11.2018	13.02.2019	50,0	88125	158,9	14,5	25,8	3,5	30,9	4,7	685,8	68,1
1-2 cm	28.10.2018	14.11.2018	14.02.2019	51,8	77667	173,1	15,8	23,1	3,8	27,6	4,5	700,2	69,7
2-3 cm	28.10.2018	14.11.2018	10.01.2019	52,2	79844	188,4	17,2	25,6	3,6	32,8	5,0	709,4	70,5
3-4 cm	28.10.2018	14.11.2018	15.02.2019	49,8	89024	204,2	18,6	24,4	3,5	31,9	4,7	719,3	71,3
4-5 cm	28.10.2018	14.11.2018	18.02.2019	50,3	256952	215,1	19,4	25,7	3,0	33,2	4,2	703,6	67,5
5-6 cm	28.10.2018	14.11.2018	19.02.2019	50,0	90116	210,4	19,1	25,3	3,5	36,7	5,4	722,6	71,5
6-7 cm	28.10.2018	14.11.2018	20.02.2019	50,1	83059	173,7	15,8	25,9	4,0	41,4	5,9	698,7	69,5
7-8 cm	28.10.2018	14.11.2018	11.01.2019	47,8	74904	148,9	13,6	26,0	4,1	40,7	5,9	726,9	72,9
8-9 cm	28.10.2018	14.11.2018	14.01.2019	48,0	256373	168,5	15,2	25,4	2,8	41,2	5,1	719,6	69,2
9-10 cm	28.10.2018	14.11.2018	17.01.2019	45,4	160068	200,9	18,2	25,3	3,2	42,1	5,6	715,4	69,9
10-12 cm	28.10.2018	14.11.2018	21.02.2019	50,9	77905	301,6	27,3	25,8	4,1	43,7	6,0	714,6	71,3
12-14 cm	28.10.2018	14.11.2018	22.02.2019	50,4	97715	373,3	33,7	23,3	3,3	40,8	5,7	698,3	68,9
14-16 cm	28.10.2018	14.11.2018	25.02.2019	48,0	250019	432,0	38,9	26,0	3,1	43,6	5,5	713,1	68,5
16-18 cm	28.10.2018	14.11.2018	26.02.2019	50,8	73763	42,7	4,1	27,0	3,8	46,0	6,2	719,7	71,7
18-20 cm	28.10.2018	14.11.2018	27.02.2019	49,9	85874	22,3	2,3	24,1	3,3	44,9	6,2	711,3	70,8

Table C6: Data and results of Cs-137, Ra-226, Ra-228 and K-40 measurements in core 2/2 from the Vefsnfjord (CTD1121-2).

Sample-id: 1121-2													
Layer	Sampling date	Date of sealing sample	Date of measurement	Sample weight	Counting time (sec)	Cs-137 (Bq/kg	Uncertainty (Bq/kg	Bi-214/Ra-226	Uncertainty (Bq/kg	Ac-228/Ra-	Uncertainty (Bq/kg	K-40 (Bq/kg	Uncertainty (Bq/kg d.w)
0-1 cm	28.10.2018	16.11.2018	26.02.2019	51,6	73657	155,9	14,2	26,8	3,2	31,7	4,4	698,5	68,5
1-2 cm	29.10.2018	16.11.2018	27.02.2019	51,4	85526	160,2	14,5	26,4	3,2	31,7	4,3	687,1	67,3
2-3 cm	30.10.2018	16.11.2018	28.02.2019	51,7	84598	174,7	15,9	27,8	3,5	33,0	4,4	708,3	69,3
3-4 cm	31.10.2018	20.11.2018	28.02.2019	50,1	84781	172,9	15,8	22,5	3,6	33,1	5,6	674,1	67,2
4-5 cm	01.11.2018	20.11.2018	01.03.2019	51,5	86639	168,0	15,3	22,9	3,3	33,7	4,9	695,8	69,1
5-6 cm	02.11.2018	20.11.2018	01.03.2019	51,7	86282	164,2	14,9	25,8	3,2	40,9	5,2	699,4	68,5
6-7 cm	03.11.2018	20.11.2018	06.03.2019	50,8	90080	145,9	13,2	26,2	3,0	43,6	5,7	721,0	70,3
7-8 cm	04.11.2018	20.11.2018	07.03.2019	49,9	72617	129,6	11,8	25,2	3,2	40,3	5,2	706,2	69,6
8-9 cm	05.11.2018	20.11.2018	09.03.2019	49,0	200000	144,4	13,0	25,7	2,8	42,2	5,2	712,6	68,3
9-10 cm	06.11.2018	22.11.2018	12.03.2019	52,7	74212	300,6	27,2	28,5	4,0	44,3	6,3	731,7	72,9
10-12 cm	07.11.2018	22.11.2018	12.03.2019	52,8	73888	336,8	30,4	29,0	3,8	45,8	5,9	728,5	71,4
12-14 cm	08.11.2018	22.11.2018	13.03.2019	54,0	86802	209,9	19,0	28,1	3,4	44,3	6,0	733,8	71,5
14-16 cm	09.11.2018	22.11.2018	13.03.2019	51,5	93916	32,1	3,1	28,8	3,7	43,3	5,8	699,1	69,1
16-18 cm	10.11.2018	22.11.2018	15.03.2019	52,9	82126	20,5	2,2	26,4	3,3	44,2	6,1	706,8	70,2
18-19 cm	11.11.2018	22.11.2018	15.03.2019	51,2	81938	14,5	1,5	26,1	3,2	47,2	6,1	734,0	72,0

Table C7: Data and results of Cs-137, Ra-226, Ra-228 and K-40 measurements in core 1/2 from the Vefsnfjord (CTD1122-1).

Sample-id: 1122-1													
Layer	Sampling date	Date of sealing sample	Date of measurement	Sample weight	Counting time (sec)	Cs-137 (Bq/kg	Uncertainty (Bq/kg	Bi-214/Ra-226	Uncertainty (Bq/kg	Ac-228/Ra-	Uncertainty (Bq/kg	K-40 (Bq/kg	Uncertainty (Bq/kg d.w)
0-1 cm	28.10.2018	22.11.2018	18.01.2019	56,8	76440	141,0	12,9	41,2	4,6	55,0	7,2	679,9	67,6
1-2 cm	28.10.2018	22.11.2018	08.02.2019	55,1	91769	150,2	13,6	43,7	4,5	57,6	7,1	721,6	70,2
2-3 cm	28.10.2018	22.11.2018	11.02.2019	56,6	259420	170,3	15,3	37,4	3,6	48,4	5,7	724,1	69,0
3-4 cm	28.10.2018	22.11.2018	12.02.2019	58,0	84858	197,0	17,8	31,3	3,3	39,1	5,1	755,1	73,4
4-5 cm	28.10.2018	22.11.2018	13.02.2019	56,6	87889	246,7	22,3	32,5	3,5	39,3	5,1	736,9	71,6
5-6 cm	28.10.2018	22.11.2018	14.02.2019	57,9	77445	314,1	28,4	31,7	3,5	43,0	5,5	728,1	70,9
6-7 cm	28.10.2018	22.11.2018	15.02.2019	56,7	88784	371,6	33,5	31,4	3,6	44,0	5,5	725,5	70,6
7-8 cm	28.10.2018	22.11.2018	18.02.2019	57,7	256429	358,5	32,3	30,9	3,0	43,9	5,2	722,6	68,6
8-9 cm	28.10.2018	22.11.2018	19.02.2019	57,4	90589	223,4	20,2	31,5	3,6	44,9	5,7	723,3	70,2
9-10 cm	28.10.2018	22.11.2018	20.02.2019	60,2	83013	115,1	10,5	30,4	3,3	45,0	5,6	712,1	69,3
10-12 cm	28.10.2018	22.11.2018	21.02.2019	60,2	77835	47,9	4,5	31,0	3,4	46,5	5,8	718,5	70,0
12-14 cm	28.10.2018	22.11.2018	22.02.2019	61,1	97513	24,5	2,4	29,4	3,0	45,3	5,6	693,4	67,2

Table C8: Data and results of Cs-137, Ra-226, Ra-228 and K-40 measurements in core 2/2 from the Vefsnfjord (CTD1122-2).

Sample-id: 1122-2													
Layer	Sampling date	Date of sealing sample	Date of measurement	Sample weight	Counting time (sec)	Cs-137 (Bq/kg	Uncertainty (Bq/kg	Bi-214/Ra-226	Uncertainty (Bq/kg	Ac-228/Ra-	Uncertainty (Bq/kg	K-40 (Bq/kg	Uncertainty (Bq/kg d.w)
0-1 cm	28.10.2018	06.12.2018	23.01.2019	54,1	85041	124,6	11,3	42,7	4,4	61,5	7,5	680,6	66,5
1-2 cm	28.10.2018	06.12.2018	24.01.2019	56,0	82667	153,5	14,0	37,2	4,4	47,6	6,2	698,2	69,2
2-3 cm	28.10.2018	06.12.2018	25.01.2019	55,8	86147	161,8	14,7	33,2	3,5	38,1	4,8	717,4	69,8
3-4 cm	28.10.2018	06.12.2018	28.01.2019	56,4	259903	172,3	15,5	31,2	3,0	39,9	4,8	733,0	69,8
4-5 cm	28.10.2018	06.12.2018	29.01.2019	54,8	87248	222,4	20,1	31,9	3,5	40,4	5,1	738,9	71,9
5-6 cm	28.10.2018	06.12.2018	30.01.2019	54,4	74565	247,1	22,3	32,8	3,7	40,8	5,3	722,1	70,7
6-7 cm	28.10.2018	27.11.2018	31.01.2019	58,6	89530	243,1	22,0	30,5	3,3	43,6	5,4	711,2	69,1
7-8 cm	28.10.2018	27.11.2018	01.02.2019	59,0	80557	247,0	22,3	30,7	3,3	42,1	5,4	724,8	70,6
8-9 cm	28.10.2018	27.11.2018	04.02.2019	57,4	285562	294,5	26,5	30,7	3,0	44,8	5,3	727,3	69,2
9-10 cm	28.10.2018	27.11.2018	05.02.2019	57,6	65008	150,0	13,6	31,5	3,7	45,1	5,7	722,5	70,9
10-12 cm	28.10.2018	27.11.2018	06.02.2019	60,1	80962	34,5	3,3	31,7	3,5	45,4	5,6	731,9	71,2
12-14 cm	28.10.2018	27.11.2018	07.02.2019	57,9	85779	16,2	1,7	31,6	3,4	44,4	5,4	716,0	69,6

Table C9: Data and results of Cs-137, Ra-226, Ra-228 and K-40 measurements in core 1/2 from the Vefsnfjord (CTD1123-1).

Sample-id: 1123-1													
Layer	Sampling date	Date of sealing sample	Date of measurement	Sample weight	Counting time (sec)	Cs-137 (Bq/kg	Uncertainty (Bq/kg	Bi-214/Ra-226	Uncertainty (Bq/kg	Ac-228/Ra-	Uncertainty (Bq/kg	K-40 (Bq/kg	Uncertainty (Bq/kg d.w)
0-1 cm	28.10.2018	05.11.2018	05.12.2018	43,6	80341	166,9	15,3	53,1	5,9	78,5	10,2	743,3	75,0
1-2 cm	28.10.2018	05.11.2018	06.12.2018	52,7	76858	169,1	15,4	40,0	4,6	61,4	8,2	726,8	72,4
2-3 cm	28.10.2018	05.11.2018	07.12.2018	55,8	87817	165,9	15,1	32,1	3,8	40,2	5,6	729,6	72,0
3-4 cm	28.10.2018	05.11.2018	10.12.2018	53,8	250756	170,1	15,4	29,4	3,2	34,1	4,5	736,2	70,6
4-5 cm	28.10.2018	05.11.2018	11.12.2018	54,5	79453	159,2	14,5	28,2	3,5	37,1	5,5	725,0	71,9
5-6 cm	28.10.2018	09.11.2018	12.12.2018	59,2	84308	148,0	13,5	28,4	3,5	40,3	5,5	705,6	69,5
6-7 cm	28.10.2018	09.11.2018	13.12.2018	59,1	88237	210,4	19,1	28,1	3,5	42,4	5,8	714,1	70,1
7-8 cm	28.10.2018	09.11.2018	18.12.2018	55,6	80108	225,6	20,5	29,9	4,2	43,4	5,9	724,2	71,7
8-9 cm	28.10.2018	09.11.2018	19.12.2018	56,4	83180	188,7	17,1	28,7	3,6	45,9	6,1	737,7	72,8
9-10 cm	28.10.2018	09.11.2018	24.12.2018	55,9	200000	171,4	15,5	28,8	3,2	43,9	5,5	726,4	69,8
10-12 cm	28.10.2018	09.11.2018	30.12.2018	59,1	200000	108,8	9,8	29,7	3,3	45,2	5,6	712,2	68,4
12-14 cm	28.10.2018	09.11.2018	07.01.2019	57,2	255804	45,5	4,2	29,0	3,0	44,7	5,5	730,0	69,8
14-16 cm	28.10.2018	09.11.2018	08.01.2019	56,8	80378	27,6	2,7	28,4	3,7	48,5	6,4	725,0	71,6
16-18 cm	28.10.2018	09.11.2018	09.01.2019	53,2	83572	13,2	1,6	30,1	3,8	51,8	6,7	775,4	76,7

Table C10: Data and results of Cs-137, Ra-226, Ra-228 and K-40 measurements in core 2/2 from the Vefsnfjord (CTD1123-2).

Sample-id: 1123-2													
Layer	Sampling date	Date of sealing sample	Date of measurement	Sample weight	Counting time (sec)	Cs-137 (Bq/kg	Uncertainty (Bq/kg	Bi-214/Ra-226	Uncertainty (Bq/kg	Ac-228/Ra-	Uncertainty (Bq/kg	K-40 (Bq/kg	Uncertainty (Bq/kg d.w)
0-1 cm	28.10.2018	07.11.2018	05.12.2018	52,3	80256	166,0	15,1	54,1	5,5	79,0	9,5	767,1	75,2
1-2 cm	28.10.2018	07.11.2018	06.12.2018	54,7	76616	170,5	15,5	36,1	3,9	46,4	5,8	738,3	72,2
2-3 cm	28.10.2018	07.11.2018	07.12.2018	56,4	87658	177,4	16,1	30,5	3,4	36,7	4,8	752,6	73,1
3-4 cm	28.10.2018	07.11.2018	10.12.2018	53,3	250185	190,6	17,2	31,2	3,1	36,4	4,4	754,9	72,0
4-5 cm	28.10.2018	09.11.2018	11.12.2018	56,6	79350	181,5	16,4	30,0	3,3	39,6	5,1	739,1	72,2
5-6 cm	28.10.2018	07.11.2018	12.12.2018	56,8	84514	163,1	14,8	31,2	3,3	41,7	5,3	742,2	72,3
6-7 cm	28.10.2018	07.11.2018	13.12.2018	54,1	87779	168,9	15,3	31,9	3,6	43,9	5,5	747,7	72,9
7-8 cm	28.10.2018	07.11.2018	18.12.2018	54,4	80091	211,1	19,1	32,4	3,8	47,5	6,0	752,8	73,4
8-9 cm	28.10.2018	07.11.2018	19.12.2018	57,2	82704	232,3	21,0	31,0	3,3	45,5	5,7	774,6	75,2
9-10 cm	28.10.2018	08.11.2018	30.12.2018	58,1	200000	159,6	14,4	31,2	3,0	45,5	5,5	748,0	71,4
10-12 cm	28.10.2018	08.11.2018	03.01.2019	58,4	95477	84,0	7,7	30,5	3,3	44,8	5,5	730,8	70,7
12-14 cm	28.10.2018	09.11.2018	04.01.2019	57,9	76733	29,3	2,8	30,5	3,4	48,4	6,0	756,3	73,7
14-16 cm	28.10.2018	08.11.2018	07.01.2019	58,1	254578	15,7	1,5	29,1	2,8	48,6	5,7	747,9	71,2

Table C11: Data and results of Cs-137, Ra-226, Ra-228 and K-40 measurements in core 1/2 from the Vefsnfjord (CTD1124-1).

Sample-id: 1124-1													
Layer	Sampling date	Date of sealing sample	Date of measurement	Sample weight	Counting time (sec)	Cs-137 (Bq/kg	Uncertainty (Bq/kg	Bi-214/Ra-226	Uncertainty (Bq/kg	Ac-228/Ra-	Uncertainty (Bq/kg	K-40 (Bq/kg	Uncertainty (Bq/kg d.w)
0-1 cm	28.10.2018	06.12.2018	25.01.2019	56,5	85360	179,3	16,3	32,8	4,1	43,7	5,9	666,6	66,1
1-2 cm	28.10.2018	06.12.2018	28.01.2019	58,7	260578	183,5	16,5	31,5	3,3	37,5	4,7	661,0	63,3
2-3 cm	28.10.2018	30.11.2018	29.01.2019	63,6	71073	178,3	16,2	29,8	3,8	37,2	5,1	647,0	64,4
3-4 cm	28.10.2018	30.11.2018	30.01.2019	65,4	74005	172,0	15,6	28,1	3,6	31,3	4,6	609,2	60,6
4-5 cm	28.10.2018	30.11.2018	31.01.2019	67,2	89392	179,1	16,2	26,5	3,3	31,1	4,4	585,9	57,8
5-6 cm	28.10.2018	30.11.2018	05.02.2019	67,9	78231	210,0	19,0	25,0	3,2	35,4	5,1	580,7	57,6
6-7 cm	28.10.2018	30.11.2018	06.02.2019	65,3	84327	242,1	21,9	27,0	3,7	36,8	5,1	592,5	58,6
7-8 cm	28.10.2018	30.11.2018	07.02.2019	65,5	86035	196,1	17,8	27,2	3,5	36,0	4,8	589,5	58,3
8-9 cm	28.10.2018	06.12.2018	08.02.2019	63,2	91938	136,6	12,4	25,2	3,0	33,6	4,6	618,1	60,9
9-10 cm	28.10.2018	06.12.2018	11.02.2019	62,1	260200	104,6	9,5	25,3	2,7	36,3	4,6	619,0	59,3
10-12 cm	28.10.2018	06.12.2018	12.02.2019	64,5	84861	80,4	7,4	25,4	3,2	41,2	5,4	635,6	62,6

Table C12: Data and results of Cs-137, Ra-226, Ra-228 and K-40 measurements in core 2/2 from the Vefsnfjord (CTD1124-2).

Sample-id: 1124-2													
Layer	Sampling date	Date of sealing sample	Date of measurement	Sample weight	Counting time (sec)	Cs-137 (Bq/kg	Uncertainty (Bq/kg	Bi-214/Ra-226	Uncertainty (Bq/kg	Ac-228/Ra-	Uncertainty (Bq/kg	K-40 (Bq/kg	Uncertainty (Bq/kg d.w)
0-1 cm	28.10.2018	08.11.2018	08.01.2019	58,1	80850	185,3	16,8	36,2	3,9	49,8	6,3	700,2	68,4
1-2 cm	28.10.2018	08.11.2018	09.01.2019	61,3	83467	191,7	17,3	32,8	3,4	46,5	5,7	692,8	67,5
2-3 cm	28.10.2018	08.11.2018	10.01.2019	62,0	79303	180,3	16,3	29,3	3,2	36,4	4,7	663,1	64,7
3-4 cm	28.10.2018	08.11.2018	11.01.2019	64,5	80985	181,2	16,4	28,8	3,3	33,8	4,3	636,9	62,1
4-5 cm	28.10.2018	08.11.2018	25.02.2019	65,2	249132	197,3	17,8	26,1	2,5	32,9	4,0	615,2	58,6
5-6 cm	28.10.2018	13.11.2018	14.01.2019	67,0	259714	203,5	18,3	26,7	2,6	34,0	4,0	606,2	57,7
6-7 cm	28.10.2018	13.11.2018	15.01.2019	69,3	87032	199,2	18,0	27,3	3,0	34,8	4,4	598,3	58,1
7-8 cm	28.10.2018	13.11.2018	17.01.2019	70,7	170962	165,3	14,9	27,2	2,7	35,8	4,3	585,3	56,0
8-9 cm	28.10.2018	13.11.2018	18.01.2019	65,2	83640	142	12,9	27,9	3,1	38,1	4,7	609,9	59,5
9-10 cm	28.10.2018	13.11.2018	21.01.2019	66,0	252508	126,8	11,4	25,7	2,5	38,0	4,5	612,3	58,3
10-12 cm	28.10.2018	13.11.2018	22.01.2019	69,6	77195	76	7,0	28,0	3,0	38,9	4,8	619,5	60,4
12-13 cm	28.10.2018	13.11.2018	23.01.2019	63,0	83698	63,2	5,8	28,3	3,0	42,8	5,3	660,6	64,3

Appendix D: Data and results from Pb-210 measurements and self-absorption correction.

Table D1: Pb-210 measurements and correction for self absorption in core 1/4 from the Norwegian Trench (CTD906-1).

Sample-id: 906-1												
Sample				Measuring sample				Measuring sample with Pb-210 point-source on top		Correction factor for self-absoption	Results	
Layer	Sampling date	Date of measurement	Sample weight (g)	Mark peak channel	Net counts in 46,5keV	s(Net counts in 46,5keV	Counting time (sec)	Net counts in 46,5keV	Counting time (sec)		Pb-210 (Bq/kg d.w.)	Uncertainty (Bq/kg d.w.)
0-1 cm	13.11.2017	07.06.2018	57,4	329-349	3480	92	81830	157397	600	1,50	179,2	10,1
1-2 cm	13.11.2017	08.06.2018	58,4	329-349	2671	89	88510	156294	600	1,50	125,0	7,5
2-3 cm	13.11.2017	11.06.2018	58,2	329-349	6796	142	261799	162853	600	1,48	105,9	5,7
3-4 cm	13.11.2017	21.06.2018	59,9	329-349	1520	75	77448	156243	600	1,50	78,9	5,5
4-5 cm	13.11.2017	22.06.2018	57,6	329-349	1271	74	85451	159775	600	1,49	61,3	4,7
5-6 cm	13.11.2017	08.08.2018	59,8	329-349	939	76	84748	158360	600	1,50	44,0	4,2
6-7 cm	13.11.2017	09.08.2018	52,8	329-349	918	72	84945	183029	600	1,40	45,6	4,3
7-8 cm	13.11.2017	10.08.2018	54,9	329-349	850	75	88532	172362	600	1,44	39,9	4,1
8-9 cm	13.11.2017	13.08.2018	54,7	329-349	2773	125	256844	165779	600	1,47	46,0	3,1
9-10 cm	13.11.2017	14.08.2018	59,4	329-349	699	70	76894	142721	600	1,56	37,8	4,3
10-12 cm	13.11.2017	15.08.2018	57,3	329-349	759	72	86267	163336	600	1,48	35,8	3,9
12-14 cm	13.11.2017	16.08.2018	58,2	329-349	886	74	88110	155253	600	1,51	41,3	4,0
14-16 cm	13.11.2017	21.08.2018	55,3	329-349	560	65	71701	173782	600	1,44	31,9	4,1
16-18 cm	13.11.2017	22.08.2018	60,4	329-349	852	75	85264	156892	600	1,50	39,4	4,0
18-19 cm	13.11.2017	23.08.2018	59,9	329-349	855	74	80189	161294	600	1,48	42,0	4,2

Table D2: Pb-210 measurements and correction for self absorption in core 2/4 from the Norwegian Trench (CTD906-2).

Sample-id: 906-2												
Sample				Measuring sample				Measuring sample with Pb-210 point-source on top			Results	
Layer	Sampling date	Date of measurement	Sample weight (g)	Mark peak channel	Net counts in 46,5keV	s(Net counts in 46,5keV	Counting time (sec)	Net counts in 46,5keV	Counting time (sec)	Correction factor for self-absoption	Pb-210 (Bq/kg d.w.)	Uncertainty (Bq/kg d.w.)
0-1 cm	13.11.2017	23.07.2018	51,8	329-349	9307	149	224022	192400	600	1,37	178,4	9,4
1-2 cm	13.11.2017	30.07.2018	55,3	329-349	5669	135	236461	168995	600	1,45	101,6	5,6
2-3 cm	13.11.2017	24.07.2018	55,7	329-349	1330	79	87359	168785	600	1,45	63,6	4,9
3-4 cm	13.11.2017	27.08.2018	55,2	329-349	3372	130	255383	175659	600	1,43	54,7	3,4
4-5 cm	13.11.2017	28.08.2018	58,8	329-349	929	72	83031	164452	600	1,47	44,6	4,1
5-6 cm	13.11.2017	29.08.2018	55	329-349	740	71	84398	175259	600	1,43	36,0	3,9
6-7 cm	13.11.2017	30.08.2018	50,7	329-349	723	70	85686	184861	600	1,40	36,7	4,0
7-8 cm	13.11.2017	31.08.2018	55,1	329-349	803	73	87305	172090	600	1,44	38,1	4,0
8-9 cm	13.11.2017	03.09.2018	57,4	329-349	2012	125	251506	163868	600	1,47	32,3	2,6
9-10 cm	13.11.2017	04.09.2018	61,4	329-349	765	68	74514	141983	600	1,57	41,6	4,3
10-12 cm	13.11.2017	05.09.2018	57,6	329-349	578	75	80474	162501	600	1,48	28,9	4,1

Table D3: Pb-210 measurements and correction for self absorption in core 3/4 from the Norwegian Trench (CTD906-3).

Sample-id: 906-3												
Sample				Measuring sample				Measuring sample with Pb-210 point-source on top			Results	
Layer	Sampling date	Date of measurement	Sample weight (g)	Mark peak channel	Net counts in 46,5keV	s(Net counts in 46,5keV	Counting time (sec)	Net counts in 46,5keV	Counting time (sec)	Correction factor for self-absoption	Pb-210 (Bq/kg d.w.)	Uncertainty (Bq/kg d.w.)
0-1 cm	13.11.2017	06.09.2018	50,1	329-349	3517	88	81940	190513	600	1,38	192,2	10,7
1-2 cm	13.11.2017	07.09.2018	56,7	329-349	3390	90	85913	169716	600	1,45	164,2	9,2
2-3 cm	13.11.2017	10.09.2018	62,2	329-349	2873	90	95883	144782	600	1,55	121,4	7,1
3-4 cm	13.11.2017	11.09.2018	62,1	329-349	1542	80	80226	153435	600	1,52	75,6	5,4
4-5 cm	13.11.2017	12.09.2018	62,0	329-349	1364	78	86068	144628	600	1,55	63,8	4,8
5-6 cm	13.11.2017	13.09.2018	57,9	329-349	1217	75	85683	165010	600	1,47	57,8	4,6
6-7 cm	13.11.2017	14.09.2018	60,0	329-349	685	71	75003	160816	600	1,49	35,8	4,1
7-8 cm	13.11.2017	17.09.2018	60,3	329-349	2768	127	252899	156014	600	1,50	43,5	2,9
8-9 cm	13.11.2017	18.09.2018	61,5	329-349	708	66	68214	148996	600	1,53	41,2	4,4
9-10 cm	13.11.2017	19.09.2018	60,5	329-349	679	76	89627	155106	600	1,51	29,7	3,7
10-12 cm	13.11.2017	20.09.2018	56,0	329-349	684	73	84844	172556	600	1,44	32,7	3,9
12-14 cm	13.11.2017	21.09.2018	55,1	329-349	602	70	78236	175426	600	1,43	31,5	4,0

Table D4: Pb-210 measurements and correction for self absorption in core 4/4 from the Norwegian Trench (CTD906-4).

Sample-id: 906-4												
Sample				Measuring sample				Measuring sample with Pb-210 point-source on top			Results	
Layer	Sampling date	Date of measurement	Sample weight (g)	Mark peak channel	Net counts in 46,5keV	s(Net counts in 46,5keV	Counting time (sec)	Net counts in 46,5keV	Counting time (sec)	Correction factor for self-absoption	Pb-210 (Bq/kg d.w.)	Uncertainty (Bq/kg d.w.)
0-1 cm	13.11.2017	24.09.2018	57,4	329-349	11727	158	234356	168943	600	1,45	206,7	10,6
1-2 cm	13.11.2017	26.09.2018	58,4	329-349	2998	84	70290	169403	600	1,45	172,8	9,8
2-3 cm	13.11.2017	27.09.2018	58,2	329-349	2718	86	86942	161551	600	1,48	129,4	7,6
3-4 cm	13.11.2017	28.09.2018	59,9	329-349	2029	82	81774	153302	600	1,52	101,8	6,5
4-5 cm	13.11.2017	01.10.2018	57,6	329-349	5103	136	256820	154237	600	1,51	84,3	4,7
5-6 cm	13.11.2017	02.10.2018	59,8	329-349	1496	76	84414	161001	600	1,48	71,0	5,0
6-7 cm	13.11.2017	03.10.2018	52,8	329-349	1118	75	81275	159457	600	1,49	62,3	5,2
7-8 cm	13.11.2017	04.10.2018	54,9	329-349	678	74	82768	152721	600	1,52	35,8	4,3
8-9 cm	13.11.2017	05.10.2018	54,7	329-349	855	74	89293	156758	600	1,50	41,8	4,2
9-10 cm	13.11.2017	08.10.2018	59,4	329-349	2617	130	254627	152301	600	1,52	41,9	2,9
10-12 cm	13.11.2017	09.10.2018	57,3	329-349	584	70	74070	159062	600	1,49	32,4	4,2
12-14 cm	13.11.2017	10.10.2018	58,2	329-349	927	75	86609	165935	600	1,47	43,0	4,1
14-16 cm	13.11.2017	11.10.2018	55,3	329-349	950	73	86678	165517	600	1,47	46,4	4,2
16-18 cm	13.11.2017	12.10.2018	60,4	329-349	857	72	85064	164348	600	1,47	39,1	3,8

Table D5: Pb-210 measurements and correction for self absorption in core 1/2 from the Vefsnfjord (CTD1121-1).

Sample-id: 1121-1												
Sample				Measuring sample				Measuring sample with Pb-210 point-source on top			Results	
Layer	Sampling date	Date of measurement	Sample weight (g)	Mark peak channel	Net counts in 46,5keV roi	s(Net counts in 46,5keV	Counting time (sec)	Net counts in 46,5keV roi	Counting time (sec)	Correction factor for self-absoption	Pb-210 (Bq/kg d.w.)	Uncertainty (Bq/kg d.w.)
0-1 cm	28.10.2018	13.02.2019	50,0	329-349	3572	93	88125	180635	600	1,41	183,2	10,4
1-2 cm	28.10.2018	14.02.2019	51,8	329-349	3020	87	77667	170904	600	1,45	173,7	10,1
2-3 cm	28.10.2018	10.01.2019	52,2	329-349	2778	86	79844	164505	600	1,47	156,2	9,3
3-4 cm	28.10.2018	15.02.2019	49,8	329-349	2507	85	89024	178999	600	1,42	127,9	7,8
4-5 cm	28.10.2018	18.02.2019	50,3	329-349	6175	140	256952	173375	600	1,44	109,4	6,1
5-6 cm	28.10.2018	19.02.2019	50,0	329-349	1968	82	90116	176836	600	1,43	99,0	6,5
6-7 cm	28.10.2018	20.02.2019	50,1	329-349	1516	77	83059	175526	600	1,43	82,6	5,9
7-8 cm	28.10.2018	11.01.2019	47,8	329-349	1610	69	74904	190008	600	1,38	98,4	6,6
8-9 cm	28.10.2018	14.01.2019	48,0	329-349	4889	135	256373	189564	600	1,38	86,9	5,0
9-10 cm	28.10.2018	17.01.2019	45,4	329-349	2976	107	160068	200884	600	1,35	87,3	5,4
10-12 cm	28.10.2018	21.02.2019	50,9	329-349	1671	80	77905	174270	600	1,43	96,1	6,7
12-14 cm	28.10.2018	22.02.2019	50,4	329-349	2288	91	97715	179476	600	1,42	104,8	6,7
14-16 cm	28.10.2018	25.02.2019	48,0	329-349	4873	143	250019	185750	600	1,40	90,0	5,3
16-18 cm	28.10.2018	26.02.2019	50,8	329-349	775	64	73763	172404	600	1,44	46,7	4,6
18-20 cm	28.10.2018	27.02.2019	49,9	329-349	667	66	85874	179185	600	1,42	34,2	3,9

Table D6: Pb-210 measurements and correction for self absorption in core 2/2 from the Vefsnfjord (CTD1121-2).

Sample-id: 1121-2												
Sample				Measuring sample				Measuring sample with Pb-210 point-source on top			Results	
Layer	Sampling date	Date of measurement	Sample weight (g)	Mark peak channel	Net counts in 46,5keV roi	s(Net counts in 46,5keV	Counting time (sec)	Net counts in 46,5keV roi	Counting time (sec)	Correction factor for self-absoption	Pb-210 (Bq/kg d.w.)	Uncertainty (Bq/kg d.w.)
0-1 cm	28.10.2018	26.02.2019	51,6	327-347	5204	108	73657	263629	600	1,52	190,5	10,4
1-2 cm	28.10.2018	27.02.2019	51,4	327-347	6299	119	85526	261294	600	1,53	200,2	10,8
2-3 cm	28.10.2018	28.02.2019	51,7	327-347	5578	114	84598	268666	600	1,51	176,0	9,6
3-4 cm	28.10.2018	28.02.2019	50,1	329-349	2475	84	84781	180278	600	1,41	131,5	8,0
4-5 cm	28.10.2018	01.03.2019	51,5	329-349	1922	81	86639	171864	600	1,44	99,0	6,5
5-6 cm	28.10.2018	01.03.2019	51,7	327-347	1467	85	86282	264057	600	1,52	79,8	5,0
6-7 cm	28.10.2018	06.03.2019	50,8	327-347	4122	141	90080	267417	600	1,51	65,7	4,4
7-8 cm	28.10.2018	07.03.2019	49,9	327-347	2662	103	72617	273170	600	1,50	54,9	4,2
8-9 cm	28.10.2018	09.03.2019	49,0	327-347	2854	103	200000	276253	600	1,49	56,8	3,5
9-10 cm	28.10.2018	12.03.2019	52,7	329-349	1361	78	74212	165995	600	1,47	71,7	5,8
10-12 cm	28.10.2018	12.03.2019	52,8	327-347	2662	103	73888	257350	600	1,54	95,6	6,1
12-14 cm	28.10.2018	13.03.2019	54,0	327-347	2854	103	86802	246066	600	1,57	86,9	5,4
14-16 cm	28.10.2018	13.03.2019	51,5	327-347	949	73	93916	172398	600	1,44	44,3	4,1
16-18 cm	28.10.2018	15.03.2019	52,9	327-347	576	67	82126	162802	600	1,48	30,3	3,9
18-20 cm	28.10.2018	15.03.2019	51,2	329-349	731	82	81938	264962	600	1,52	23,5	2,9

Table D7: Pb-210 measurements and correction for self absorption in core 1/2 from the Vefsnfjord (CTD1122-1).

Sample-id: 1122-1												
Sample				Measuring sample				Measuring sample with Pb-210 point-source on top			Results	
Layer	Sampling date	Date of measurement	Sample weight (g)	Mark peak channel	Net counts in 46,5keV roi	s(Net counts in 46,5keV	Counting time (sec)	Net counts in 46,5keV roi	Counting time (sec)	Correction factor for self-absoption	Pb-210 (Bq/kg d.w.)	Uncertainty (Bq/kg d.w.)
0-1 cm	28.10.2018	18.01.2019	56,8	329-349	4167	97	76440	151461	600	1,52	233,9	13,0
1-2 cm	28.10.2018	08.02.2019	55,1	327-347	8425	135	91769	245197	600	1,57	238,9	12,7
2-3 cm	28.10.2018	11.02.2019	56,6	327-347	21745	222	259420	234867	600	1,60	216,2	11,1
3-4 cm	28.10.2018	12.02.2019	58,0	327-347	5606	120	84858	226861	600	1,62	168,5	9,2
4-5 cm	28.10.2018	13.02.2019	56,6	327-347	5328	120	87889	237623	600	1,59	155,4	8,6
5-6 cm	28.10.2018	14.02.2019	57,9	327-347	4124	113	77445	230839	600	1,61	135,0	7,7
6-7 cm	28.10.2018	15.02.2019	56,7	327-347	3868	121	88784	242509	600	1,58	110,3	6,5
7-8 cm	28.10.2018	18.02.2019	57,7	327-347	10639	201	256429	234649	600	1,60	104,7	5,6
8-9 cm	28.10.2018	19.02.2019	57,4	327-347	3134	111	90589	236707	600	1,59	87,3	5,4
9-10 cm	28.10.2018	20.02.2019	60,2	327-347	2387	99	83013	224627	600	1,63	70,6	4,6
10-12 cm	28.10.2018	21.02.2019	60,2	327-347	1727	89	77835	226600	600	1,62	54,1	3,9
12-14 cm	28.10.2018	22.02.2019	61,1	327-347	1970	95	97513	225050	600	1,63	48,6	3,4

Table D8: Pb-210 measurements and correction for self absorption in core 2/2 from the Vefsnfjord (CTD1122-2).

Sample-id: 1122-2												
Sample				Measuring sample				Measuring sample with Pb-210 point-source on top			Results	
Layer	Sampling date	Date of measurement	Sample weight (g)	Mark peak channel	Net counts in 46,5keV roi	s(Net counts in 46,5keV	Counting time (sec)	Net counts in 46,5keV roi	Counting time (sec)	Correction factor for self-absoption	Pb-210 (Bq/kg d.w.)	Uncertainty (Bq/kg d.w.)
0-1 cm	28.10.2018	23.01.2019	54,1	327-347	7332	127	85041	245158	600	1,57	228,2	12,2
1-2 cm	28.10.2018	24.01.2019	56,0	329-349	4245	98	82667	157314	600	1,50	220,0	12,2
2-3 cm	28.10.2018	25.01.2019	55,8	327-347	6942	125	86147	244034	600	1,57	207,1	11,1
3-4 cm	28.10.2018	28.01.2019	56,4	327-347	18358	211	259903	242393	600	1,58	180,1	9,3
4-5 cm	28.10.2018	29.01.2019	54,8	327-347	4489	116	87248	253946	600	1,55	132,2	7,5
5-6 cm	28.10.2018	30.01.2019	54,4	327-347	3380	107	74565	259449	600	1,53	116,2	6,9
6-7 cm	28.10.2018	31.01.2019	58,6	327-347	3632	116	89530	228391	600	1,62	101,7	6,1
7-8 cm	28.10.2018	01.02.2019	59,0	327-347	2949	107	80557	225611	600	1,62	91,6	5,7
8-9 cm	28.10.2018	04.02.2019	57,4	327-347	9345	202	285562	235916	600	1,59	82,5	4,5
9-10 cm	28.10.2018	05.02.2019	57,6	327-347	1604	88	65008	238622	600	1,59	61,5	4,6
10-12 cm	28.10.2018	06.02.2019	60,1	327-347	1727	91	80962	227624	600	1,62	51,9	3,8
12-14 cm	28.10.2018	07.02.2019	57,9	327-347	1513	89	85779	239842	600	1,58	43,5	3,4

Table D9: Pb-210 measurements and correction for self absorption in core 1/2 from the Vefsnfjord (CTD1123-1).

Sample-id: 1123-1												
Sample				Measuring sample				Measuring sample with Pb-210 point-source on top			Results	
Layer	Sampling date	Date of measurement	Sample weight (g)	Mark peak channel	Net counts in 46,5keV roi	s(Net counts in 46,5keV	Counting time (sec)	Net counts in 46,5keV roi	Counting time (sec)	Correction factor for self-absoption	Pb-210 (Bq/kg d.w.)	Uncertainty (Bq/kg d.w.)
0-1 cm	28.10.2018	05.12.2018	43,6	329-349	4523	102	80341	198727	600	1,35	278,6	15,5
1-2 cm	28.10.2018	06.12.2018	52,7	329-349	4277	99	76858	165878	600	1,47	246,7	13,8
2-3 cm	28.10.2018	07.12.2018	55,8	329-349	4085	99	87817	163492	600	1,48	195,8	11,0
3-4 cm	28.10.2018	10.12.2018	53,8	329-349	9210	156	250756	173689	600	1,44	155,9	8,4
4-5 cm	28.10.2018	11.12.2018	54,5	329-349	2360	83	79453	169136	600	1,45	125,7	7,8
5-6 cm	28.10.2018	12.12.2018	59,2	329-349	2217	85	84308	149040	600	1,53	108,0	6,9
6-7 cm	28.10.2018	13.12.2018	59,1	329-349	2170	88	88237	149246	600	1,53	101,0	6,6
7-8 cm	28.10.2018	18.12.2018	55,6	329-349	1805	83	80108	158960	600	1,49	95,7	6,6
8-9 cm	28.10.2018	19.12.2018	56,4	329-349	1858	84	83180	156731	600	1,50	94,1	6,4
9-10 cm	28.10.2018	24.12.2018	55,9	329-349	4367	127	200000	161713	600	1,48	91,6	5,4
10-12 cm	28.10.2018	30.12.2018	59,1	329-349	4153	124	200000	145708	600	1,55	86,1	5,1
12-14 cm	28.10.2018	07.01.2019	57,2	329-349	3958	130	255804	160342	600	1,49	63,4	3,8
14-16 cm	28.10.2018	08.01.2019	56,8	329-349	998	70	80378	153574	600	1,52	51,9	4,5
16-18 cm	28.10.2018	09.01.2019	53,2	329-349	726	69	83572	173083	600	1,44	36,4	4,0

Table D10: Pb-210 measurements and correction for self absorption in core 2/2 from the Vefsnfjord (CTD1123-2).

Sample-id: 1123-2												
Sample				Measuring sample				Measuring sample with Pb-210 point-source on top			Results	
Layer	Sampling date	Date of measurement	Sample weight (g)	Mark peak channel	Net counts in 46,5keV roi	s(Net counts in 46,5keV	Counting time (sec)	Net counts in 46,5keV roi	Counting time (sec)	Correction factor for self-absoption	Pb-210 (Bq/kg d.w.)	Uncertainty (Bq/kg d.w.)
0-1 cm	28.10.2018	05.12.2018	52,3	327-347	8215	135	80256	260266	600	1,53	272,3	14,5
1-2 cm	28.10.2018	06.12.2018	54,7	327-347	6269	120	76616	252935	600	1,55	210,5	11,4
2-3 cm	28.10.2018	07.12.2018	56,4	327-347	6405	124	87658	248306	600	1,56	183,6	10,0
3-4 cm	28.10.2018	10.12.2018	53,3	327-347	14423	197	250185	265655	600	1,52	148,9	7,8
4-5 cm	28.10.2018	11.12.2018	56,6	327-347	3422	106	79350	246105	600	1,57	108,1	6,4
5-6 cm	28.10.2018	12.12.2018	56,8	327-347	3294	106	84514	250481	600	1,56	96,6	5,8
6-7 cm	28.10.2018	13.12.2018	54,1	327-347	3240	106	87779	265084	600	1,52	93,7	5,7
7-8 cm	28.10.2018	18.12.2018	54,4	327-347	3090	104	80091	262846	600	1,52	97,9	6,0
8-9 cm	28.10.2018	19.12.2018	57,2	327-347	3099	108	82704	245077	600	1,57	93,1	5,7
9-10 cm	28.10.2018	30.12.2018	58,1	327-347	6277	159	200000	239114	600	1,59	77,5	4,4
10-12 cm	28.10.2018	03.01.2019	58,4	327-347	2321	102	95477	237619	600	1,59	59,7	4,0
12-14 cm	28.10.2018	04.01.2019	57,9	327-347	1489	86	76733	239925	600	1,58	47,7	3,7
14-16 cm	28.10.2018	07.01.2019	58,1	327-347	3908	151	254578	239503	600	1,58	37,5	2,4

Table D11: Pb-210 measurements and correction for self absorption in core 1/2 from the Vefsnfjord (CTD1124-1).

Sample-id: 1124-1												
Sample				Measuring sample				Measuring sample with Pb-210 point-source on top			Results	
Layer	Sampling date	Date of measurement	Sample weight (g)	Mark peak channel	Net counts in 46,5keV roi	s(Net counts in 46,5keV	Counting time (sec)	Net counts in 46,5keV roi	Counting time (sec)	Correction factor for self-absoption	Pb-210 (Bq/kg d.w.)	Uncertainty (Bq/kg d.w.)
0-1 cm	28.10.2018	25.01.2019	56,5	329-349	4447	102	85360	162279	600	1,48	218,3	12,1
1-2 cm	28.10.2018	28.01.2019	58,7	329-349	12616	173	260578	158384	600	1,50	197,3	10,3
2-3 cm	28.10.2018	29.01.2019	63,6	329-349	3149	90	71073	140809	600	1,57	175,0	10,2
3-4 cm	28.10.2018	30.01.2019	65,4	329-349	3050	88	74005	136506	600	1,59	160,3	9,3
4-5 cm	28.10.2018	31.01.2019	67,2	329-349	3106	94	89392	134503	600	1,60	132,2	7,8
5-6 cm	28.10.2018	05.02.2019	67,9	329-349	2098	86	78231	137021	600	1,59	100,0	6,5
6-7 cm	28.10.2018	06.02.2019	65,3	329-349	1876	84	84327	147924	600	1,54	83,3	5,6
7-8 cm	28.10.2018	07.02.2019	65,5	329-349	1933	84	86035	143225	600	1,56	85,1	5,7
8-9 cm	28.10.2018	08.02.2019	63,2	329-349	1745	85	91938	170293	600	1,45	69,0	4,9
9-10 cm	28.10.2018	11.02.2019	62,1	329-349	4544	139	260200	156054	600	1,50	67,0	4,0
10-12 cm	28.10.2018	12.02.2019	64,5	329-349	1518	78	84861	144257	600	1,56	68,3	4,9

Table D12: Pb-210 measurements and correction for self absorption in core 2/2 from the Vefsnfjord (CTD1124-2).

Sample-id: 1124-2												
Sample				Measuring sample				Measuring sample with Pb-210 point-source on top			Results	
Layer	Sampling date	Date of measurement	Sample weight (g)	Mark peak channel	Net counts in 46,5keV roi	s(Net counts in 46,5keV	Counting time (sec)	Net counts in 46,5keV roi	Counting time (sec)	Correction factor for self-absoption	Pb-210 (Bq/kg d.w.)	Uncertainty (Bq/kg d.w.)
0-1 cm	28.10.2018	08.01.2019	58,1	327-347	7129	127	80850	236855	600	1,59	220,2	11,8
1-2 cm	28.10.2018	09.01.2019	61,3	327-347	7127	130	83467	221486	600	1,64	207,8	11,2
2-3 cm	28.10.2018	10.01.2019	62,0	327-347	5884	118	79303	223905	600	1,63	177,6	9,7
3-4 cm	28.10.2018	11.01.2019	64,5	327-347	5221	116	80985	219535	600	1,64	149,5	8,3
4-5 cm	28.10.2018	25.02.2019	65,2	327-347	12848	194	249132	220311	600	1,64	118,4	6,2
5-6 cm	28.10.2018	14.01.2019	67,0	327-347	11764	198	259714	209538	600	1,67	102,9	5,5
6-7 cm	28.10.2018	15.01.2019	69,3	327-347	3660	112	87032	199569	600	1,71	94,1	5,6
7-8 cm	28.10.2018	17.01.2019	70,7	327-347	6311	154	170962	193595	600	1,73	81,9	4,6
8-9 cm	28.10.2018	18.01.2019	65,2	327-347	2826	102	83640	218964	600	1,64	77,3	4,8
9-10 cm	28.10.2018	21.01.2019	66,0	327-347	7772	176	252508	215786	600	1,65	69,9	3,9
10-12 cm	28.10.2018	22.01.2019	69,6	327-347	2014	94	77195	198854	600	1,71	58,0	4,0
12-13 cm	28.10.2018	23.01.2019	63,0	327-347	2021	94	83698	224684	600	1,63	56,4	3,9

Appendix E: Pb-210 data for calculating correction factors and ^{210}Pb activity concentration.

Table E1: Pb-210 standard calibration.

	Masuring Pb-210 standard: R-cal (Cps) in 46.5 keV						
Detector	Date	Net area	±	Mark peak ch-ch	Counting time (sec)	R-cal (Cps)	Uncertainty (Cps)
RAD12	13.09.2018	129225	394	329-349	5002	25,83	0,08
RAD14	27.03.2019	2739847	1793	327-347	63968	42,83	0,03

Table E2: Activity concentration in Pb-210 standard at calibration date.

A_0	7460 Bq
$T_{1/2}$	8145 days
Ref. date	01.07.2008
Uncertainty	5 %

Detector	Region of interest, Roi (ch-ch)	Calibration date	Ref. date	Days decayed	Activity on counting day (Bq)	Uncertainty (Bq)
RAD12	329-349	13.09.2018	01.07.2008	3726	5433	278
RAD14	327-347	27.03.2019	01.07.2008	3921	5343	273

Table E3: Geometry facor, g(Pb-210).

Detector	Region of interest, Roi (ch-ch)	g(Pb-210) (Bq/Cps)	Uncertainty (Bq/Cps)
RAD12	329-349	210,3	10,5
RAD14	327-347	124,8	6,2

Table E4: Point source on top of Pb-210 standard (Rcal+).

Detector	Region of interest, Roi (ch-ch)	Net area	±	Counting time (sec)	Cps (Rcal+)	Uncertainty (Cps)
RAD12	329-349	378125	719	1000	378,1	0.7
RAD14	327-347	359852	697	600	599,8	1.2

Tabel E5: Measurements of an empty container with a point source on top (Rs).

Detector	Region of interest, Roi (ch-ch)	Net area	±	Counting time (sec)	Cps (Rs)	Uncertainty (Cps)
RAD12	329-349	376842	671	600	628,1	1.1
RAD14	327-347	653539	874	600	1089,2	1.5

Table E6: Geometry factor, G.

Detector	Region of interest, Roi (ch-ch)	KF (Pb-210)	Uncertainty	G (Pb-210)	Uncertainty (Bq/Cps)
RAD12	329-349	1,32	0,01	159,7	8,1
RAD14	327-347	1,37	0,01	90,9	4,6